NASA Tech Briefs

National Aeronautics and
Space Administration

Electronic Components and Circuits

Electronic Systems

Physical Sciences

Materials

Computer Programs

Mechanics

Machinery

Fabrication Technology

Mathematics and Information Sciences

Life Sciences

95-10

October 1995

INTRODUCTION

Tech Briefs are short announcements of new technology derived from the research and development activities of the National Aeronautics and Space Administration. These Briefs emphasize information considered likely to be transferable across industrial, regional, or disciplinary lines and are issued to encourage commercial application.

Availability of NASA Tech Briefs and TSP's

Distribution of NASA Tech Briefs, a monthly periodical publication, is limited to engineers in U.S. Industry and to other domestic technology transfer agents. Requests for individual Tech Briefs or for Technical Support Packages (TSP's) announced herein should be addressed to

NASA Center for AeroSpace Information
Technology Transfer Office
800 Elkridge Landing Rd.
Linthicum Heights, MD 21090-2934
Telephone No. (301) 621-0245

Please reference the three-letter, five-digit control number located at the end of each Tech Brief. Information on NASA's Technology Utilization Program, its documents, and services is also available at the same facility.

Technology Utilization Officers and Patent Counsels are located at NASA field installations to provide technology-transfer access to industrial users. Inquiries can be made by writing to NASA field installations listed below.

Technology Utilization Officers and Patent Counsels

Ames Research Center
Technology Utilization Officer
Mail Code 223-3
Moffett Field, CA 94035

Patent Counsel
Mail Code 200-11
Moffett Field, CA 94035

Goddard Space Flight Center
Technology Utilization Officer
Mail Code 702-1
Greenbelt, MD 20771

Patent Counsel
Mail Code 204
Greenbelt, MD 20771

Lyndon B. Johnson Space Center
Technology Utilization Officer
Mail Code IC-4
Houston, TX 77058

Patent Counsel
Mail Code AL3
Houston, TX 77058

John F. Kennedy Space Center
Technology Utilization Officer
Mail Stop PT-PMO-A
Kennedy Space Center, FL 32899

Patent Counsel
Mail Code PT-PAT
Kennedy Space Center, FL 32899

Langley Research Center
Technology Utilization Officer
Mail Stop 143
Hampton, VA 23665

Patent Counsel
Mail Code 279
Hampton, VA 23665

Lewis Research Center
Technology Utilization Officer
Mail Stop 7-3
21000 Brookpark Road
Cleveland, OH 44135

Patent Counsel
Mail Code LE-LAW
21000 Brookpark Road
Cleveland, OH 44135

Jet Propulsion Laboratory
Technology Utilization Officer
Mail Stop 156-211
4800 Oak Grove Drive
Pasadena, CA 91109

NASA Resident Office-JPL
Technology Utilization Officer
Mail Stop 180-801
4800 Oak Grove Drive
Pasadena, CA 91109

Patent Counsel
Mail Code 180-801
4800 Oak Grove Drive
Pasadena, CA 91109

George C. Marshall Space Flight Center
Technology Utilization Officer
Code AT01
Marshall Space Flight Center,
AL 35812

Patent Counsel
Mail Code CC01
Marshall Space Flight Center,
AL 35812

John C. Stennis Space Center
Technology Utilization Officer
Code HA-30
Stennis Space Center, MS 39529

NASA Headquarters
Technology Utilization Officer
Code CU
Washington, DC 20546

Assistant General Counsel for Patent Matters
Code GP
Washington, DC 20546

Dryden Flight Research Center
Technology Utilization Officer
M/S D21-31
Bldg. 4832 Whse 7
Lilly Dr.
Edwards, CA 93523

NASA Tech Briefs

National Aeronautics and Space Administration

October 1995
05710

BLANK PAGE

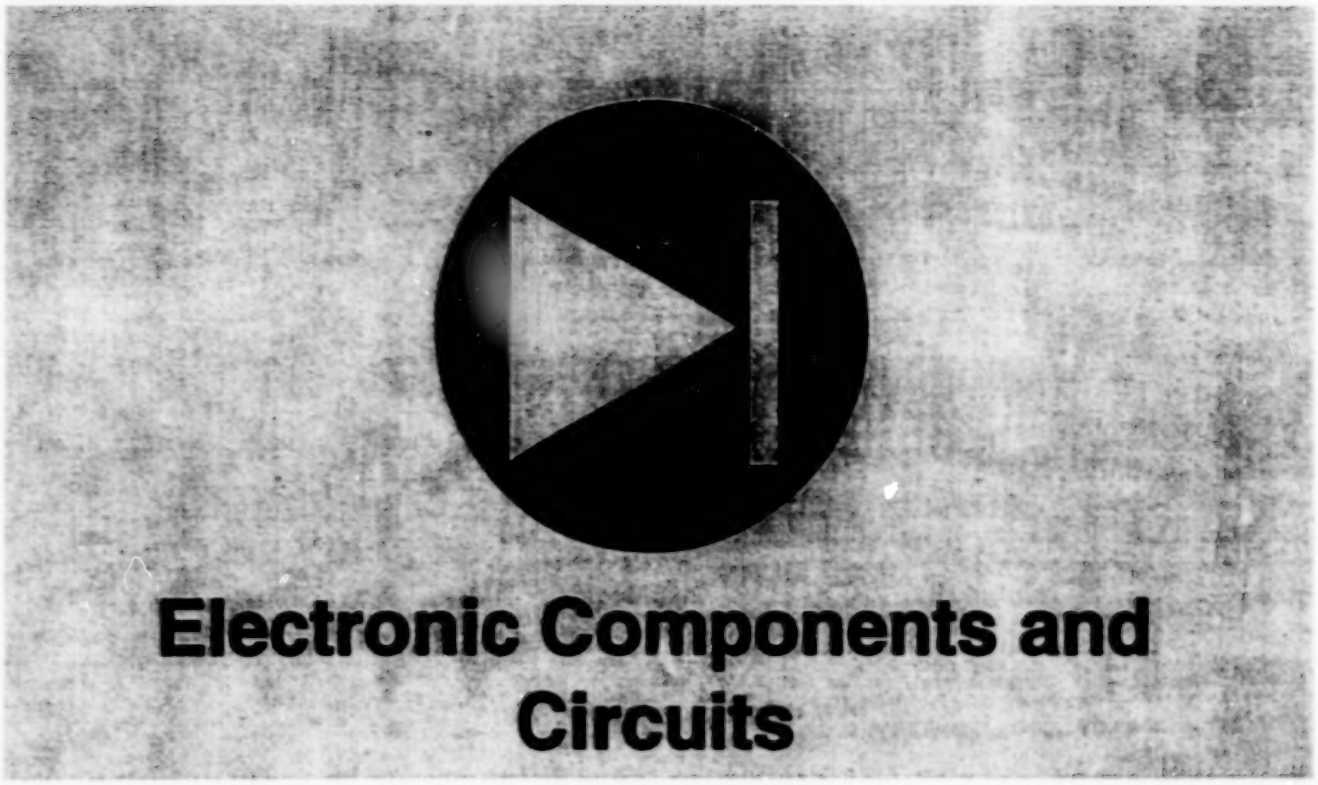

Electronic Components and Circuits

Hardware, Techniques, and Processes

Books and Reports

BLANK PAGE

CCD/CID Processors Would Offer Greater Precision

Each cell would contain 1 bit of the binary representation of a matrix element.

NASA's Jet Propulsion Laboratory, Pasadena, California

Charge-coupled-device/charge-injection-device (CCD/CID) data processors of a proposed type would offer the advantages of massively parallel computational architecture and high computational speed typical of older CCD/CID data processors, but with increased precision. Typically, the precision of an older CCD/CID processor is limited to about 8 bits. The proposed devices could be made precise to an arbitrarily large number of bits. CCD/CID processors are especially useful in performing matrix-vector multiplications in a variety of applications, including solving partial differential equations, processing signal and image data, control computations, and neural-network simulations. The greater precision of the proposed devices could help to ensure accuracy in CCD/CID implementations of pseudospectral neural networks — a particular class of artificial neural networks that are especially well-suited to solving nonlinear differential equations.

Figure 1 is a simplified schematic diagram of a typical older CCD/CID array. Each cell in the array is connected to an input column line and an output row line via a column gate and a row gate, respectively. These gates acting together hold, in a silicon substrate underneath them, a charge that represents an analog matrix element. In a default mode of operation, the matrix charges sit under the column gates.

In the basic matrix-vector multiplication mode of operation, with a binary input vector, the column gates serve as binary-analog multipliers by transferring the matrix charges toward the row gates only where the input bits of the columns indicate binary "ones." The charge transferred under the row gates is summed capacitively on the output line of each row, yielding an analog output vector that is the product of the binary input vector with the analog charge matrix. By virtue of the principle of operation of the CCD, the charges are sensed nondestructively, and the charge matrix is restored to its original state simply by pushing the charges back under the column gates.

A bit-serial digital-analog matrix-vector multiplication can be obtained from a sequence of binary-analog matrix-vector multiplications, by feeding in vector input bits sequentially, and adding the corresponding output contributions after scaling them with the appropriate powers of 2. A simple parallel array of divide-by-2 circuits at the output accomplishes this task. Further extensions of the basic matrix-vector multiplication scheme support full digital outputs by parallel analog-to-digital conversion at the outputs, and four-quadrant operation by use of differential-circuit techniques.

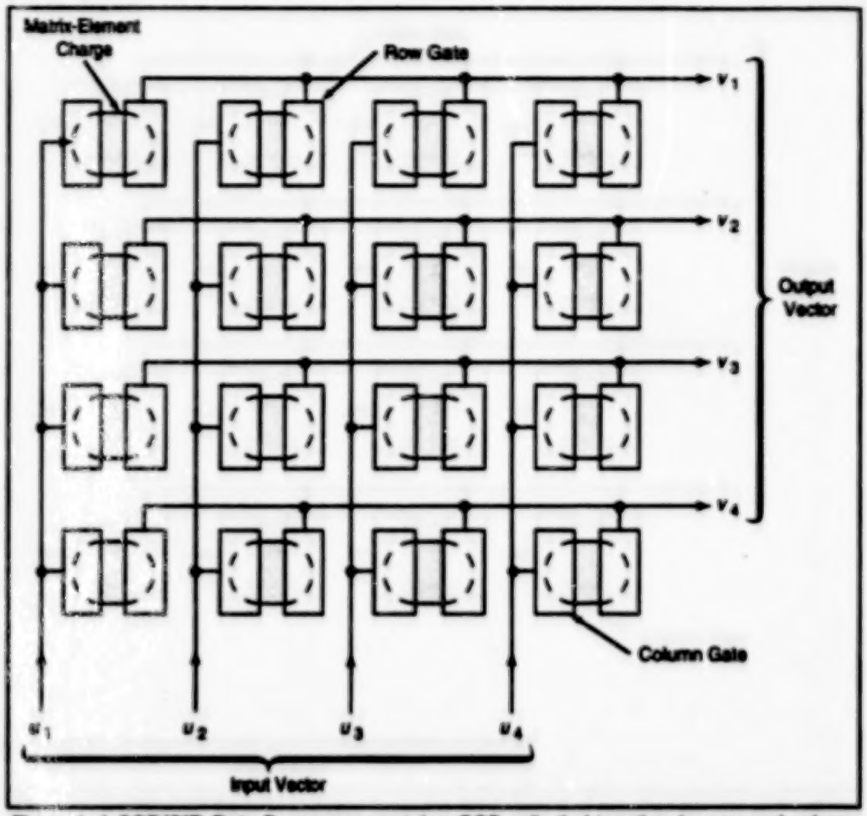

Figure 1. A CCD/CID Data Processor contains CCD cells tied together by row and column electrodes. Matrix elements are represented by packets of electric charge. Computation involves transfers of charges from column gates to row gates.

The key innovation in the proposed CD/CID processors is to encode 1 bit of the binary representation of each matrix element in one cell. Thus, as shown in Figure 2, if a matrix **A** were to be specified with b bits of precision, an element A_{ij} would be located in cells

$$[b(i-1)+\ell, j], \text{ for } \ell = 1, \ldots, b;$$

these bits would be denoted

$$A_{ij}^0, \ldots A_{ij}^{b-1}$$

Thus, the price of increased precision would be increased size (each matrix element being spread over b rows). One added benefit would be a reduction in refresh time, inasmuch as each packet of charge would represent only a binary quantity.

Computation would proceed as follows: At clock cycle one, the matrix **A**, in its binary representation, would be multiplied by the binary vector

$$\left(u_1^0 \ldots u_N^0\right),$$

which would contain the least significant bits of vector $(u_1, \ldots u_N)$. By virtue of the charge-transfer mechanism, analog voltage

$$^{(0)}v_1^0 \ldots {}^{(0)}v_N^{b-1}$$

would be sensed at the output end of each row. At clock cycle two, these voltages would be fed into a pipelined analog-to-digital converter having d bits of precision (where $d = \log_2 N$, and N denotes the number of columns of **A**), while simultaneously **A** would be multiplied by

$$\left(u_1^1, \ldots u_N^1\right)$$

[which would contain the next more significant bits of $(u_1, \ldots u_N)$], yielding $^{(1)}\mathbf{v}$.

At clock cycle three, the digital representations of

$$^{(0)}\vec{v}_1^{\,0} \ldots {}^{(0)}\vec{v}_N^{\,b-1}$$

would be bit-mapped into a register with an appropriate offset (in general, ik bits of offset at clock cycle k for element $\vec{v}_i$), each offset pointer would be incremented by one, the voltages $^{(1)}\mathbf{v}$ would be fed into the analog-to-digital converter, and **A** would be multiplied by vector

$$\left(1, u_1^2, \ldots u_N^2\right)$$

to obtain $^{(2)}\mathbf{v}$. Elements

$$^{(k)}\vec{v}_i$$

index i would then be fed into cascaded sum circuits, in parallel for all i, pipelined over k. Thus, the components v_i of the product $\mathbf{v} = \mathbf{Au}$ would be obtained after $\log_2 b$ cycles, and the overall latency would be $b + \log_2 b + 3$. If one needed to multiply a set of vectors **u** by the same matrix **A**, this pipelined architecture would result in an output vector every clock cycle.

This work was done by Jacob Barhen, Nikzad Toomarian, and Amir Fijany of Caltech for **NASA's Jet Propulsion Laboratory.** *Further information is contained in a TSP [see page 1].*

In accordance with Public Law 96-517, the contractor has elected to retain title to this invention. Inquiries concerning rights for its commercial use should be addressed to

William T. Callaghan, Manager
Technology Commercialization
JPL-301-350
4800 Oak Grove Drive
Pasadena, CA 91109

Refer to NPO-18972 volume and number of this NASA Tech Briefs *issue, and the page number.*

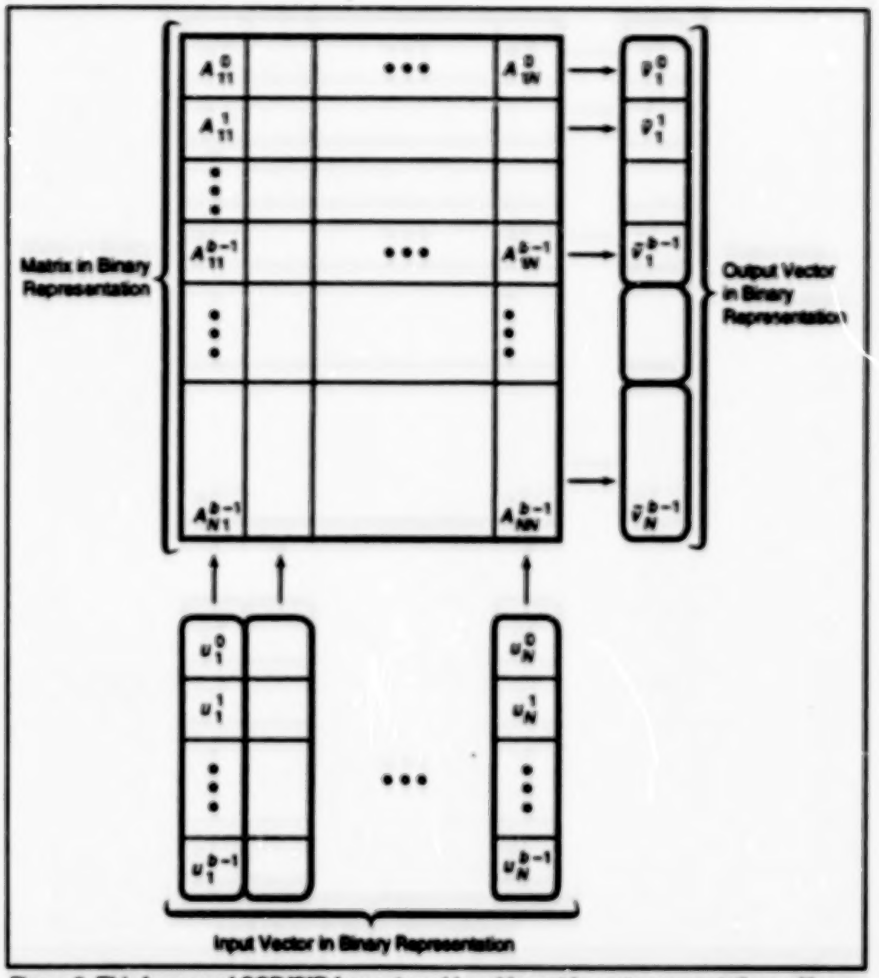

Figure 2. This Improved CCD/CID Layout would enable matrix-vector computations with precision of b bits.

Media Controller for Receiving Data From a TAXI™ Link

This circuit buffers data signals and detects some abnormalities in the signals.

Lyndon B. Johnson Space Center, Houston, Texas

The TAXI™ media controller (TMC) is an interface circuit that supports the operation of test equipment in diagnosis of a telemetry system in which data are communicated via TAXI™ links. The TMC is designed specifically for use with a TAXI™ test adapter for monitoring and testing telemetry data signals generated by payloads and other subsystems of the Space Station Freedom. The TMC can also be used with other data-communication test equipment for testing TAXI™ links or other links that generate signals according to the same protocols.

"TAXI" as used here means "transparent asynchronous xmitter/receiver interface" (using "xmitter" for "transmitter" as is occasionally done in the electronics industry). A unidirectional high-speed serial data link can be constructed with TAXI™ transmitting and receiving integrated-circuit chips: At the source of data, a TAXI™ transmitting chip implements a 4-bit/5-bit coding scheme for serial transmission in which extra bits (beyond those needed to communicate data) are added for command symbols. At the receiving end of the link, a TAXI™ receiving chip decodes the signal and deserializes the data stream.

The test equipment in the original application is required to receive the data output of the TAXI™ receiver, verify the applicable data-packet protocol, and verify that the data rate does not exceed the data-buffering capabilities of the high-rate frame multiplexer which is used to receive the telemetry in the real system. The TMC helps the test adapter to perform these functions. Overall, the TMC can be characterized as providing an interface between the output port of a TAXI™ receiving chip and the input port of a memory system in the test adapter (see figure).

The output of the TAXI™ receiving chip consists of decoded parallel data and command symbols, which could, in principle, be clocked into compatible test-adapter logic circuits by use of a receiving clock signal derived from the serial data signal. However, because the phase and frequency of this clock signal vary with the data stream, this clock sig-

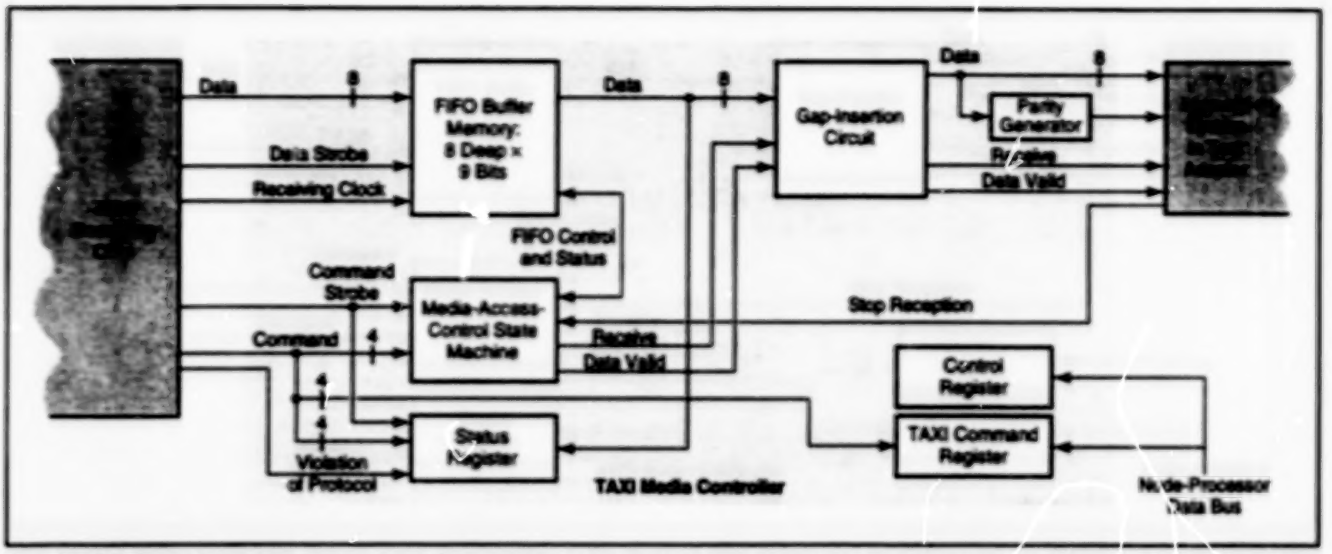

The TAXI™ Media Controller detects some abnormalities in the received data stream and resynchronizes the stream to a locally generated clock signal.

nal is not suitable for clocking logic circuits in the test adapter that depend on steady clock signals. Therefore the TMC performs the initial clocking in of the data signal, stores the data in a first-in/first-out (FIFO) buffer memory, and resynchronizes the stored data by transferring them from the FIFO buffer memory to the memory in the test adapter under control of a steady local clock.

As an integral part of the resynchronization and readout from the FIFO buffer memory, the TMC inserts gaps between packets of data that have been received too close together for the memory system in the test adapter to manage without loss of data. When command symbols in the data stream are used to implement a low-level protocol (for example, encapsulating packets of data between "start" and "stop" delimiters), there is also a need for a media-access-control state machine to detect these protocol elements and respond accordingly. The TMC includes such a state machine, which supports two low-level protocols used in the original application. The TMC includes logic circuits and a status register for detection of three abnormal phenomena: data packets without end delimiters, data packets received too close together, and command symbols not defined by the low-level protocol.

* "TAXI" is a registered trademark of Advanced Micro Devices, Inc.

This work was done by David R. Stauffer and Rebecca Stempski McMahon of International Business Machines, Inc., for **Johnson Space Center**. *Further information is contained in a TSP [see page 1].*
MSC-22418

Miniature X-Ray Tubes

Micromachined field emitters would be used instead of thermionic emitters.

NASA's Jet Propulsion Laboratory, Pasadena, California

Miniature x-ray tubes have been proposed for use in portable instruments used to analyze minerals. Instead of the thermionic emitters (hot filaments or cathodes heated by hot filaments) of conventional x-ray tubes, micromachined field emitters (see figure) would serve as the sources of electrons in the proposed x-ray tubes. Filaments are subject to breakage, their lifetimes are limited, and they are sensitive to operation in vacuum and near-vacuum environments. Fabricated from silicon wafers, the micromachined field emitters (MFEs) would not be subject to breakage or restrictions on lifetimes, and can tolerate vacuums that filaments cannot. MFEs use low voltage (≤ +100V) to obtain field emission across a micron-size gap. Thus, they are small and use little power.

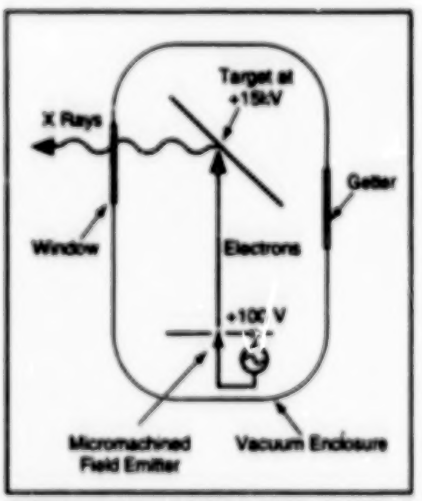

Electrons From a Field Emitter (instead of a thermionic emitter) would be accelerated to a target to generate x rays.

The miniature x-ray tubes would be very robust, immune to shock and vibration, and could be permanently sealed with a getter for continued pumping. They could be combined with solid-state x-ray detectors for analysis of x-ray fluorescence. For protective redundancy, a single tube could contain an array of field emitters. Because of the smallness of the field emitters (~1μm), the x-ray tubes could be made quite small. Very little power would be needed to cause emission of electrons, and the tubes could be operated in a flash mode, so that the overall power demand of such a tube would be so low that it could be satisfied by a trickle-charged battery.

This work was done by Gregory H. Bearman of Caltech for **NASA's Jet Propulsion Laboratory**. *Further information is contained in a TSP [see page 1].*
NPO-19364

Multiband Frequency-Selective Microwave Reflectors

Double-loop patch and slot elements are used in two different frequency-multiplexing designs.

NASA's Jet Propulsion Laboratory, Pasadena, California

Two different frequency-selective reflectors have been studied for use in multiplexing signals at selected frequencies in the S, X, K_u, and K_a frequency bands in a microwave communication system. One reflector is designed to be highly transmissive at frequencies of 2.3 GHz (in the S band) and 13.8 GHz (in the K_u band); at the same time, it is highly reflective at frequencies of 7.2 and 8.4 GHz (in the X band) and 32 and 34.5 GHz (in the K_a band). The other reflector is designed to be highly transmissive in the K_a band and highly reflective in the S, X, and K_u bands.

These frequency-selective reflectors are closely related to the ones described in several previous articles in *NASA Tech Briefs*, including "Frequency-Selective Microwave Reflectors" (NPO-18701), Vol. 18, No. 1, (January, 1994), page 32; "Improved Dichroics for Microwave Reflector Antenna Systems" (NPO-18664), Vol. 19, No. 8, (August, 1995), page 34; "Double-Square-Loop Dichroic Microwave Reflector" (NPO-18676), Vol. 18, No. 3, (March, 1994), page 38; "Triband Circular-Loop Dichroic Microwave Reflector" (NPO-18714), Vol. 18, No. 3, (March, 1994), page 41; "Making Curved Frequency-Selective Microwave Reflectors" (NPO-18755), Vol. 19, No. 8, (August, 1995), page 38; and "Circular-Loop-Element Microwave Frequency-Selective Reflectors" (NPO-18940), Vol. 19, No. 1, (January, 1995), page 42.

The first-mentioned reflector is designed according to a double screen approach. The double screens were bonded to the front and back surfaces of a foam- or honeycomb-core dielectric panel. In this case, the front surface consists of a K_a-band-reflective array of double-round-loop electrically conductive patches (see Figure 1) on a dielectric sheet of polyimide. The other surface is transmissive in the S and K_u bands and reflective in the X band.

The second-mentioned reflector is designed according to a single screen approach, in which only one surface of a dielectric panel supports a single array of antenna elements that provides the required frequency-selective characteristics. In this case, the array consists of double-square-loop slot elements etched into a metal film on a polyimide sheet (see Figure 2).

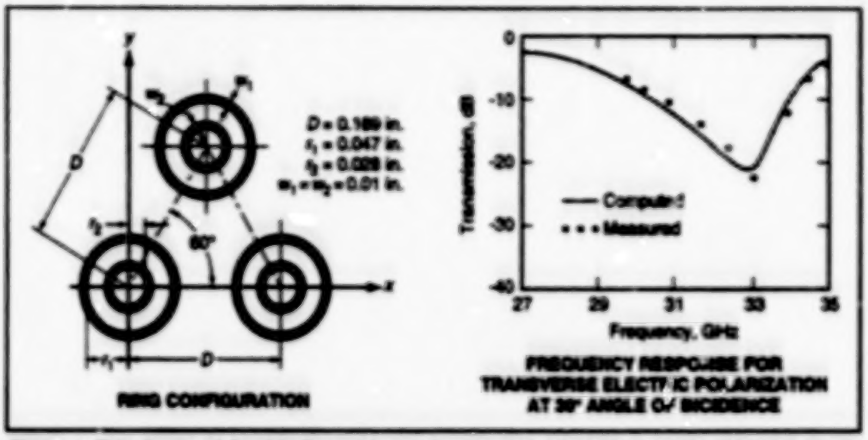

Figure 1. This Array of Double-Round-Loop Conductive Patches is highly reflective at frequencies around 33 GHz (in the K_a band).

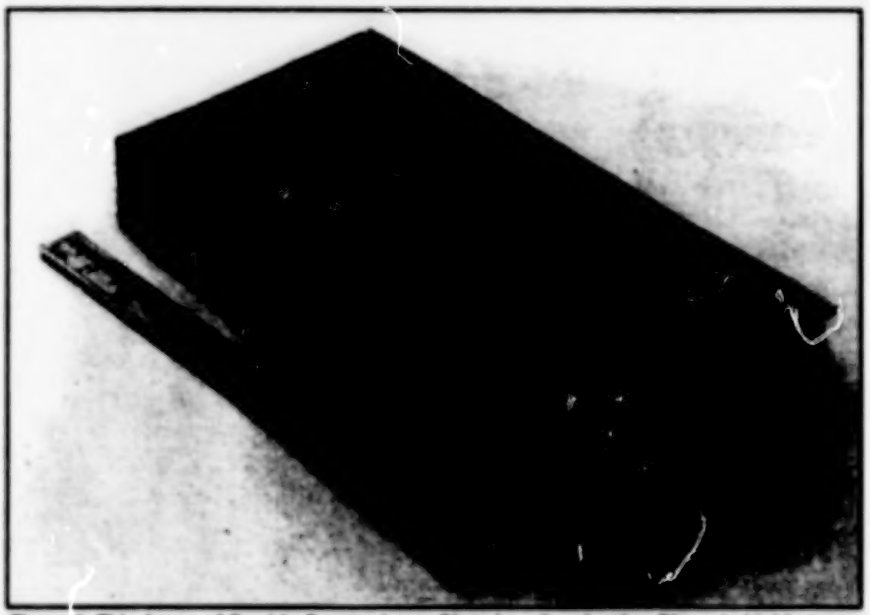

Figure 2. This Array of Double-Square-Loop Slots in a Conductive Plane is highly transmissive in the S and K_u bands and highly reflective in the X band.

The two designs have been tested by computer simulation and in experiments. The measured and computed performances were found to be in fairly good agreement. The S-band loss was found to be significantly smaller in the second-mentioned design.

This work was done by Te-Kao Wu of Caltech for **NASA's Jet Propulsion Laboratory.** *Further information is contained in a TSP [see page 1].*

NPO-19016

Wireless Infrared Data Link

The rate of repetition of infrared pulses indicates a measured physical quantity.

Lyndon B. Johnson Space Center, Houston, Texas

An infrared transmitter and receiver have been designed for wireless transmission of information on a measured physical quantity (for example, temperature) from a transducer device to a remote-acquisition system. In the transmitter, the output of a transducer (in this example, a thermocouple) is amplified and shifted with respect to a bias or reference level, then

fed to a voltage-to-frequency converter to control the frequency of repetition of current pulses applied to an infrared-light-emitting diode. In the receiver, the frequency of repetition of the pulses is converted back into a voltage indicative of the temperature or other measured quantity. This voltage is fed to the data-acquisition system.

In the original temperature-measurement application, the transducer is a type-T thermocouple. In the transmitter, the voltage output of the thermocouple is amplified, shifted with respect to a bias or reference level, and fed to a voltage-to-frequency converter to control the frequency of repetition of pulses applied to an infrared-light-emitting diode that radiates at a wavelength of 880 nm. The frequency is 3.6 kHz at a temperature of 20 °C and changes with temperature at a rate of 5.1 Hz/°C. The temperature resolution of the transmitter is about 0.1 °C.

An infrared-sensitive phototransistor in the receiver detects the modulated infrared signal. The electrical output of the phototransistor is processed by a waveform-conditioning amplifier, then by a frequency-to-voltage converter, then by an adjustable-gain, adjustable-offset amplifier. The final output voltage of the receiver varies with the thermocouple reading at a rate of 26 mV/°C; at this rate, the increment of voltage that corresponds to the temperature resolution of the transmitter (2.6 mV per 0.1 °C) matches the voltage resolution of most commercial data-acquisition systems.

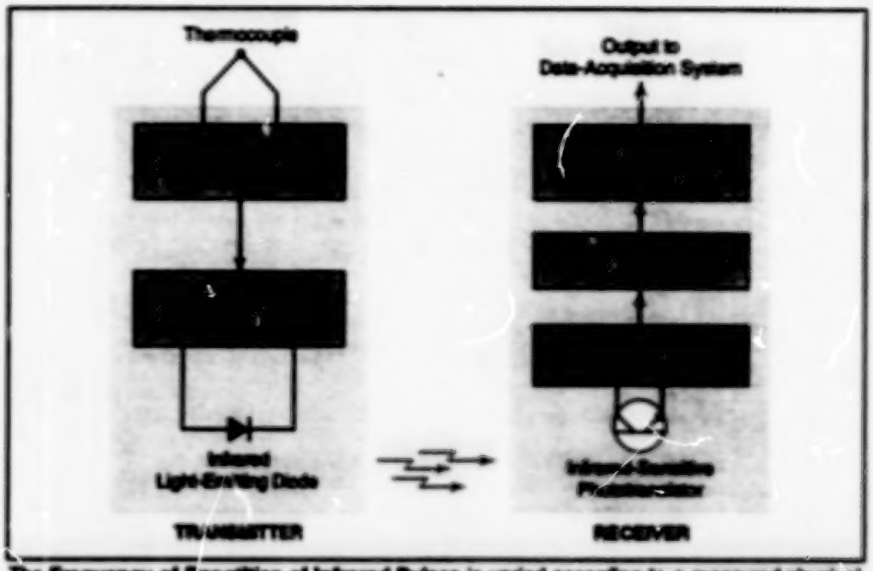

The Frequency of Repetition of Infrared Pulses is varied according to a measured physical parameter; in this case, temperature as sensed by the thermocouple. The receiver converts the pulse-repetition frequency back to a voltage, which is thus indicative of the sensed temperature.

The transmitter and receiver are small and light in weight, and they consume little power. Modified versions with suitable coding of signals could be used to transmit multiple measurements. Potential applications include logging data while drilling for oil, transmitting measurements from rotors in machines without using slip rings, remote monitoring of temperatures and pressures in hazardous locations, and remote continuous monitoring of temperatures and blood pressures in medical patients, who could thus remain mobile.

This work was done by Timothy E. Roth of Allied Signal Technical Services Corp. for Johnson Space Center. Further information is contained in a TSP [see page 1].
MSC-22567

Thin-Film Power Transformers

Layers of ferromagnetic, conductive, and insulating materials would be used.

NASA's Jet Propulsion Laboratory, Pasadena, California

Miniature power transformers would be made by thin-film microfabrication techniques, according to a proposal. The microstructures of these transformers would be built in multiple thin layers, which would typically consist, variously, of ferromagnetic, electrically conductive nonferromagnetic, and electrically insulating materials (see figure).

The proposed transformers could have geometric features finer than those of transformers made in the customary way by machining and mechanical pressing. In addition, some thin-film materials exhibit magnetic-flux-carrying capabilities superior to those of the customary bulk transformer materials. Taking advantage of the flexibility of design afforded by thin-film microfabrication techniques, one could choose the materials, shapes, thicknesses, and lateral dimensions of the thin layers to shape magnetic-flux paths, suppress eddy currents, obtain specified reluctances, and otherwise generally optimize designs and performance characteristics. Thin-film transformers might be suitable for low-cost, high-yield mass production.

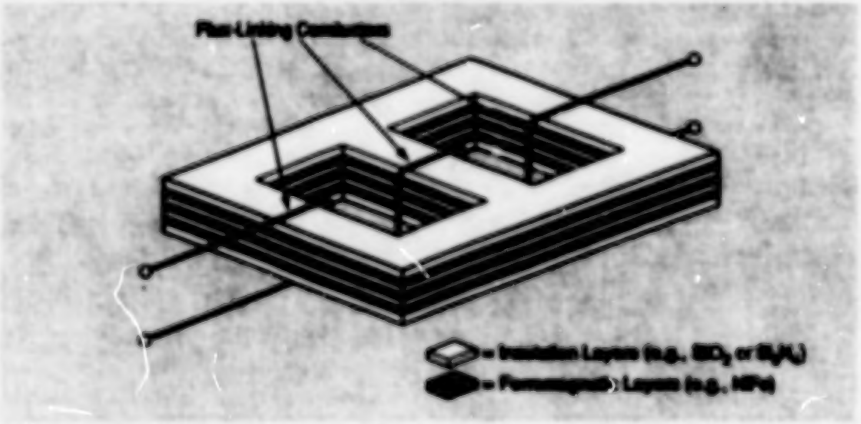

A Transformer Core would be made of thin layers of an insulating material interspersed with thin layers of a ferromagnetic material. Flux-linking conductors made of thinner nonferromagnetic-conductor/insulator multilayers could be wrapped around the core.

This work was done by Romney R. Katti of Caltech for NASA's Jet Propulsion Laboratory. Further information is contained in a TSP [see page 1].
NPO-19092

Multilayer Thin-Film Microcapacitors

These devices would be much smaller than state-of-the-art capacitors.

NASA's Jet Propulsion Laboratory, Pasadena, California

Miniature capacitors containing multiple alternating thin-film dielectric and metal layers have been proposed, especially for use in integrated and hybrid electronic circuits. Because capacitance is inversely proportional to the thickness of the dielectric layers, the use of thin, high-quality dielectric layers would afford capacitance and energy-storage densities much greater than are now available. The volumes and weights of the proposed capacitors could be made a hundred times less than those of equivalent state-of-the art capacitors — an important advantage in power- and signal-handling circuits, in which capacitors typically occupy 15 to 80 percent of the circuit-board area and contribute about 30 percent of the weight. In comparison with state-of-the art capacitors, the proposed capacitors could also be made more reliable.

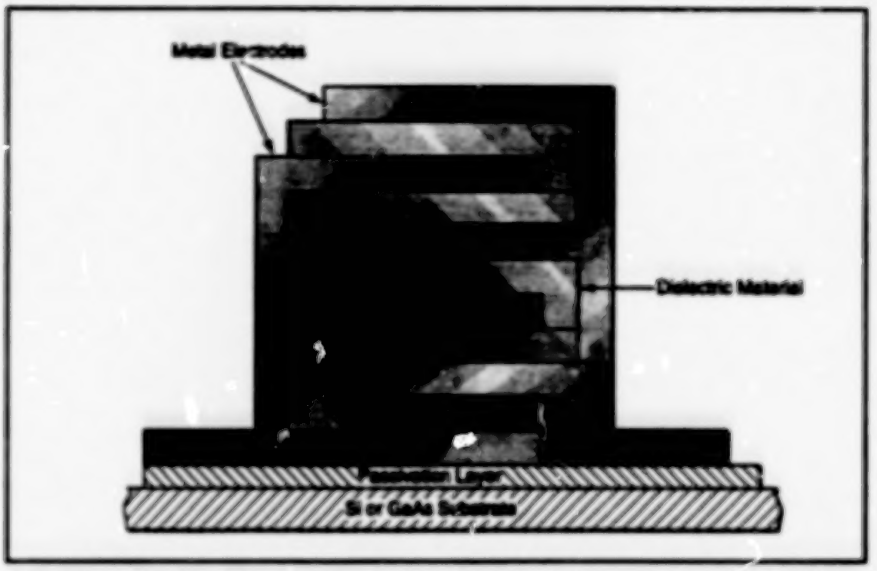

A Multilayer Thin-Film Microcapacitor would be fabricated by depositing layers of a high-permittivity dielectric material alternately with layers of metal, using two sets of masks in alternation.

The figure is a schematic cross section of a typical multilayer thin-film capacitor. Capacitors of this type could be formed on silicon and gallium arsenide substrates along with other integrated-circuit components by use of thin-film-deposition and masking techniques compatible with other integrated-circuit-fabrication techniques. One of the advantages of the configuration illustrated in the figure is that only two sets of deposition masks would be needed; the sets would be used alternately to obtain the desired serpentine winding of the dielectric layer between stacked metal layers connected alternately to external contacts to form two electrodes.

The thin-film dielectric materials in the proposed capacitors will likely be perovskite ceramics like lead magnesium niobate, lead lanthanum zirconate titanate, and barium strontium titanate. Multilayer ceramic capacitors, which are the most compact state-of-the-art capacitors, contain dielectric layers of these and similar materials in "bulk" form, made by screen printing, followed by sintering. Despite the high relative permittivities (500 to 20,000) and high breakdown electric fields (≈1,000 V/μm) inherently achievable in such crystalline ceramics, the dielectric layers in multilayer ceramic capacitors exhibit breakdown electric fields of only ≈10 V/μm. This disparity between the inherent and actual values is due to the defects, impurities and voids introduced during processing.

The use of these materials in conjunction with thin-film deposition techniques, as distinguished from sintered bulk forms of these and similar materials, would offer the potential for significantly better quality; in comparison with their sintered bulk counterparts, the thin-film materials would be denser and smoother, would contain fewer and smaller voids, and could be deposited with control over chemical compositions and grain sizes. Thin-film technology offers the option of selecting from among a wider variety of materials with high relative permittivity and high temperature stability.

It will be necessary to solve some practical problems in developing the proposed capacitors. One problem is to develop and refine deposition processes to obtain dielectric films with acceptably low densities of defects in thicknesses up to about 1 μm. Another problem is posed by the fact that depending on specific compositions, the crystalline structures of the candidate dielectric materials can exhibit piezoelectric, pyroelectric, and ferroelectric properties simultaneously. Pyroelectricity leads to large variations in the permittivity (and thus capacitance) with temperature, while piezoelectricity gives rise to mechanical stresses proportional to applied potentials. Piezoelectricity could be especially troublesome because the resultant mechanical stresses could crack the dielectric films. The choice of material for a specific application must be based partly on consideration of these effects, and the material and/or the specific configuration must be chosen to resist or compensate for these effects.

This work was done by Sarita Thakoor, Anil Thakoor, and Dan Karmon of Caltech for **NASA's Jet Propulsion Laboratory.** *Further information is contained in a TSP [see page 1].*

In accordance with Public Law 96-517, the contractor has elected to retain title to this invention. Inquiries concerning rights for its commercial use should be addressed to

William T. Callaghan, Manager
Technology Commercialization
JPL-301-350
4800 Oak Grove Drive
Pasadena, CA 91109

Refer to NPO-19403, volume and number of this NASA Tech Briefs *issue, and the page number.*

Reshaping Light-Emitting Diodes To Increase External Efficiency

Rays would be redirected to reduce trapping by total internal reflection.

Langley Research Center, Hampton, Virginia

Light-emitting diodes (LEDs) would be reshaped, according to a proposal, to increase the amount of light emitted by decreasing the fraction of light trapped via total internal reflection. Because the reshaping would utilize light that is generated in any event but is lost by trapping in present LEDs, the reshaping would result in greater luminous output power for the same electrical input power; in short, greater external efficiency. Furthermore, the light emitted by the reshaped LEDs would be more nearly collimated (less diffuse) than is the light from older LEDs.

Total internal reflection is a function of the geometry and indices of refraction of the component materials of the LED. The range of angles of incidence in which total internal reflection occurs increases with the indices of refraction. Most semiconductors exhibit high indices of refraction (in general, 3 or more), so that trapping by total internal reflection can be particularly severe in these materials.

One of the older ways to reduce trapping is to shape the semiconductor/air interface into a hemisphere, as shown in the top part of the figure. This approach is disadvantageous in that the hemisphere diffuses the light, thereby decreasing the intensity of emission in any given direction. It is also difficult and expensive to shape semiconducting material into a hemisphere.

The bottom part of the figure illustrates one of several proposed LED shapes that could reduce trapping. The external side surface would be conical. The cone angle, α, would be chosen so that most of the light incident on the conical surface would be redirected in such a way to avoid total internal reflection at the top of the LED (upper part of figure).

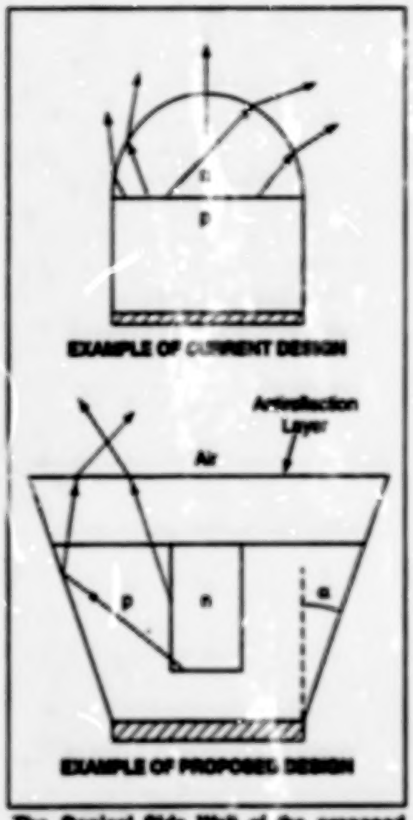

The Conical Side Wall of the proposed design would reduce trapping, as does the hemisphere in the current design, but the proposed design would be easier to implement and would concentrate more light in the forward direction.

The value of α, or the range of acceptable values of α, would be calculated from the applicable equations of geometric optics, using the indices of refraction and geometric parameters of the LED materials. Theoretical geometrical-optics calculations have shown that it should be possible to choose a value of α to untrap all of the light that would otherwise be trapped. To increase efficiency even more, one could reduce Fresnel reflection losses at the front face by covering the front face with an antireflection layer of transparent material that has an index of refraction lower than the indices of refraction of the LED materials.

This reshaping concept is potentially advantageous for conventional red-emitting LEDs. It is even more advantageous — even critical — for the new "blue" LEDs, because the luminous outputs and efficiencies of these devices are very low. Yet another advantage is that the proposed conical shapes could be achieved relatively easily by chemical etching of semiconductor surfaces.

This work was done by Robert Rogowski of Langley Research Center and Claudio Egalon of Analytical Services and Materials, Inc. No further documentation is available.

Inquiries concerning rights for the commercial use of this invention should be addressed to the Patent Counsel, Langley Research Center [see page 1]. Refer to LAR-15184.

Semiconductor/High-T_C-Superconductor Hybrid ICs

Sapphire substrates help to prevent diffusion of Cu from superconductors into semiconductors.

Lewis Research Center, Cleveland, Ohio

Hybrid integrated circuits (ICs) that contain both Si-based semiconducting and $YBa_2Cu_3O_{7-x}$ superconducting circuit elements on sapphire substrates are being developed. [$YBa_2Cu_3O_{7-x}$ is called a high-temperature or high-T_C superconductor because its critical temperature for transition to superconductivity (T_C) is above the temperature of liquid nitrogen (77 K) — higher than that of previously known superconductors.] These hybrid ICs can combine superconducting and semiconducting features that are unavailable in superconducting or semiconducting circuitry alone — for example, complementary metal oxide/semiconductor (CMOS) readout and memory devices integrated with fast-switching Josephson-junction superconducting logic devices and zero-resistance interconnections.

Previous attempts to integrate high-T_C superconductors with Si or GaAs devices have been thwarted by major obstacles. High-T_C superconductors are oxides that are chemically very weakly bound and hence are decomposed (often into elemental copper and other metals) by direct contact with semiconductors. Elemental copper diffuses through Si, GaAs, and Ge faster than does any element except hydrogen; at typical processing temperatures, Cu can move centimeters in a few hours. Copper forms deep electronic traps in Si, Ge, and GaAs and hence destroys those semiconducting properties that make these materials useful in transistors and integrated circuits. Although simple high-T_C films can be grown on buffered silicon, they have never been demonstrated to be useful for making Josephson junctions (the superconducting equivalent of a transistor).

The use of sapphire (Al_2O_3) substrates for both the semiconducting and superconducting circuit elements in the devel-

opmental hybrid ICs helps to overcome these obstacles because high-T_C materials are relatively chemically stable on sapphire, and copper does not diffuse through sapphire. Thus, the paths for diffusion of copper through a substrate from the superconductor devices to the semiconductor devices are eliminated, and the fraction of the total IC area that must be protected against diffusion is reduced. As an additional benefit in cases in which silicon-based devices are not connected to each other by direct silicon paths, (as is often true of CMOS devices) even if Cu does contaminate a transistor, it cannot diffuse to another. The developmental hybrid ICs also include protective layers of Si_3N_4, which are deposited on the silicon-based devices to act as barriers to the diffusion of Cu during subsequent fabrication of the high-T_C devices.

A representative hybrid IC of this type is fabricated in a four-stage process. In the first stage, CMOS devices are fabricated on a silicon-on-sapphire substrate, and reactive-ion etching is used to strip the Si, down to the bare sapphire substrate, from areas where high-T_C-superconductor interconnections are to be formed subsequently. In the second stage, the CMOS devices are encapsulated by the diffusion-barrier layers; these layers are formed by plasma-enhanced chemical vapor deposition of low-stress Si_3N_4 to a typical thickness of 200 nm. By use of standard photolithographic techniques, the Si_3N_4 is patterned so that it covers only the silicon islands that contain the CMOS devices. In the third stage, the $YBa_2Cu_3O_{7-x}$ structures are fabricated. In the fourth stage, holes are made in the diffusion barriers to provide access to the electrical-contact parts of the CMOS devices.

This fabrication sequence — in particular, doing the Si processing before the $YBa_2Cu_3O_{7-x}$ processing — is dictated by the phase stability of the $YBa_2Cu_3O_{7-x}$. The Si processing involves depositions, diffusions, and annealing at temperatures of the order of 1,100 °C. $YBa_2Cu_3O_{7-x}$ is deposited at about 750 °C and irreversibly decomposes into various copper yttrium and barium oxides at temperatures above approximately 950 °C. The processing temperature for the $YBa_2Cu_3O_{7-x}$ and associated buffer layers never exceeds 800 °C, at which the CMOS structures are quite stable.

This work was done by Michael J. Burns of Conductus, Inc., for Lewis Research Center. Further information is contained in a TSP (see page 1).
LEW-15762

Lightweight Solar Photovoltaic Blankets

Efficient arrays of stacked cells are integrated into laminated sheets.

Lewis Research Center, Cleveland, Ohio

Lightweight, flexible sheets that contain arrays of stacked solar photovoltaic cells are being developed to supply electric power aboard spacecraft. Solar batteries that satisfy the stringent requirements for operation in outer space should also be readily adaptable to the terrestrial environment. These flexible solar batteries could be especially attractive for use as long-lived, portable photovoltaic power sources.

The cells are based on amorphous silicon instead of crystalline silicon, which until now has been the major solar-cell material. The reason for this choice is that the unique combination of physical and chemical properties of amorphous silicon offer potential for order-of-magnitude increases in power per unit weight, power per unit volume, and endurance in the presence of ionizing radiation. In addition, technology for manufacturing amorphous silicon cells and arrays of cells has now matured.

The basic unit cell is of the p/i/n type: it comprises an undoped (intrinsic; i) layer sandwiched between an electron-acceptor-doped (p) layer and an electron-donor-doped (n) layer. For reasons grounded in the basic physics of photovoltaic devices, it is necessary to make the intrinsic layer thin (typically, no thicker than a few thousand Å) to maximize the efficiency of conversion of intercepted photons and to minimize the degradation of efficiency with continued exposure to both light and ionizing radiation.

Unfortunately, thinning a cell reduces the fraction of incident photons that the cell can intercept and thereby imposes a fundamental limitation on overall energy-conversion efficiency. The stacked-cell configuration (see figure) of the developmental solar photovoltaic blankets helps to overcome this limitation by providing subsequent cell layers that can intercept photons that have passed through previous cell layers. One can increase the utilization of the solar spectrum and thus the overall energy-conversion efficiency by making the intrinsic layers of the stacked cells out of materials that have different bandgaps, so that each cell in the stack captures predominantly photons in a different wavelength range.

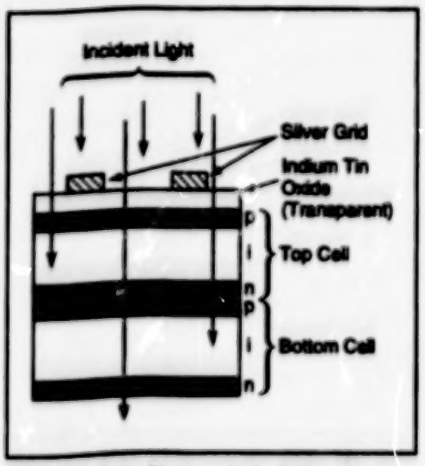

Stacked Thin Photovoltaic Cells can convert light to electricity more efficiently than can a single thick cell. Each cell in the stack can be designed to intercept photons in a different wavelength range.

The design of an optimum stacked-cell structure is a complex task that requires consideration of numerous physical effects and physical properties of materials, including those mentioned above. Theoretical calculations have shown that a stack of three cells that have intrinsic layers with bandgaps of 1.7, 1.4, and 1.1 eV, respectively, should operate at an efficiency between 20 and 24 percent. Amorphous silicon alone has a bandgap of about 1.7 eV, and materials with various bandgaps can be made by alloying amorphous silicon with other elements; bandgaps can be decreased by alloying with germanium or tin, or increased by alloying with carbon, nitrogen, or oxygen.

A sheet array of stacked cells can be manufactured in a complex, multiple-step process in a roll-to-roll deposition facility. The cells are formed on a substrate of Kapton (or equivalent) polyimide, with a reflective back layer of alternating sublayers of aluminum and zinc oxide to increase the utilization of light. The front-surface electrical contact to each stack is made with a transparent, electrically conductive layer of indium tin oxide. The stacks are connected together into modular subarrays and arrays by screen-printed silver grids. The entire sheet is covered with an ultraviolet-resistant polymeric coat and with a silicon oxide top coat.

This work was done by R. Ceragioli and R. Himmler of Energy Conversion Devices, Inc., and P. Nath, C. Vogeli, and S. Guha of United Solar Systems Corp. for Lewis Research Center. Further information is contained in a TSP (see page 1).
LEW-15545

Data-Logger Interface and Test Controller

A data-logger interface and test controller (hereafter "the controller" for short) has been developed to enable the automation of tests in conjunction with data-acquisition functions performed by data loggers that have output-switching capabilities. The controller includes relay logic circuits that remain deenergized until an out-of-tolerance condition on any data channel is discovered. The controller is designed to be connected to a Fluke model 2286A (or equivalent) data-logger system, which features 3 control channels with 6 data inputs per channel. The controller includes an elapsed-time counter that keeps track of power outages.

This work was done by Donnie R. Burch for **Marshall Space Flight Center.** *Further information is contained in a TSP [see page 1].*

Inquiries concerning rights for the commercial use of this invention should be addressed to the Patent Counsel, Marshall Space Flight Center [see page 1]. Refer to MFS-28978.

Sinterless Formation of Contacts on Indium Phosphide

Heat is unnecessary to achieve low contact resistance.

An improved technique makes it possible to form low-resistivity ($\approx 10^{-6}$ Ω-cm^2) electrical contacts on indium phosphide semiconductor devices without damaging the devices. Previously, metal contacts were deposited on n-doped InP and sintered to reduce the contact resistivity. The sintering process caused intermixing of the metal and semiconductor, destroying all but the deepest junctions under the contacts. In the improved technique, a layer of AgP_2 40 Å thick is deposited on the InP before depositing a metal contact. The AgP_2 interlayer sharply reduces the contact resistance, without need for sintering.

This work was done by Victor G. Weizer and Navid S. Fatemi of Sverdrup Technology Corp. for **Lewis Research Center.** *Further information is contained in a TSP [see page 1].*
LEW-15814

Books and Reports

Fundamental Limitations of Passive Power Dividers

Passivity and geometrical factors limit achievable performance even when ideal materials are used.

A report presents a novel theoretical analysis of the performance of passive, multiport power dividers like those used to distribute power to the radiating elements of array antennas. Typically, a unit cell of a power-divider network is a three- or four-port subnetwork with one port terminated, and the subnetworks of a network are cascaded in multiple layers, so that insertion losses are of major concern. Starting with general equations for a passive power divider, the report derives a Hermitian dissipation matrix, **Q**, that can be expressed in terms of the traditional scattering matrix, **S**. Each eigenvalue of **Q** represents the fraction of power dissipated in the network when the network is excited by an incident wave represented by the corresponding eigenvector. The general properties of Hermitian matrices and the more specific mathematical properties that represent passivity are used to draw conclusions about these eigenvalues and eigenvectors and the corresponding implications for power-division performance. The effects of geometrical factors in conductors with dimensions that are appreciable fractions of wavelengths, and thus cannot be accurately modeled as lumped circuit elements, are also considered. It is shown that passivity and geometrical factors impose fundamental limits on performance, beyond the limits imposed by losses in dielectrics and in the resistances of conductors.

This work was done by Dimitrios Antsos of Caltech for **NASA's Jet Propulsion Laboratory.** *To obtain a copy of the report, "Implications of Passivity on Power Division," see TSP's [page 1].*
NPO-19600

Study of Corrosion of Lead-Sheathed Cables

A report presents a statistical analysis of corrosion failures of the lead-sheathed cables that serve as the primary communication links at Kennedy Space Center. Most of these cables were installed during the years 1962 through 1964, and cathodic protection was added to some parts of the cable network in 1971 and to other parts of the network in 1980. However, corrosion failures continued to occur. In the study, corrosion-failure data were analyzed by use of the Weibull distribution in the effort to assess the effectiveness of cathodic protection and to predict future failures.

This work was done by Rupert U. Lee of **Kennedy Space Center.** *To obtain a copy of the report, "Statistical Analysis of Corrosion Failures of Lead-Sheathed Cables," see TSP's [page 1].*
KSC-11627

BLANK PAGE

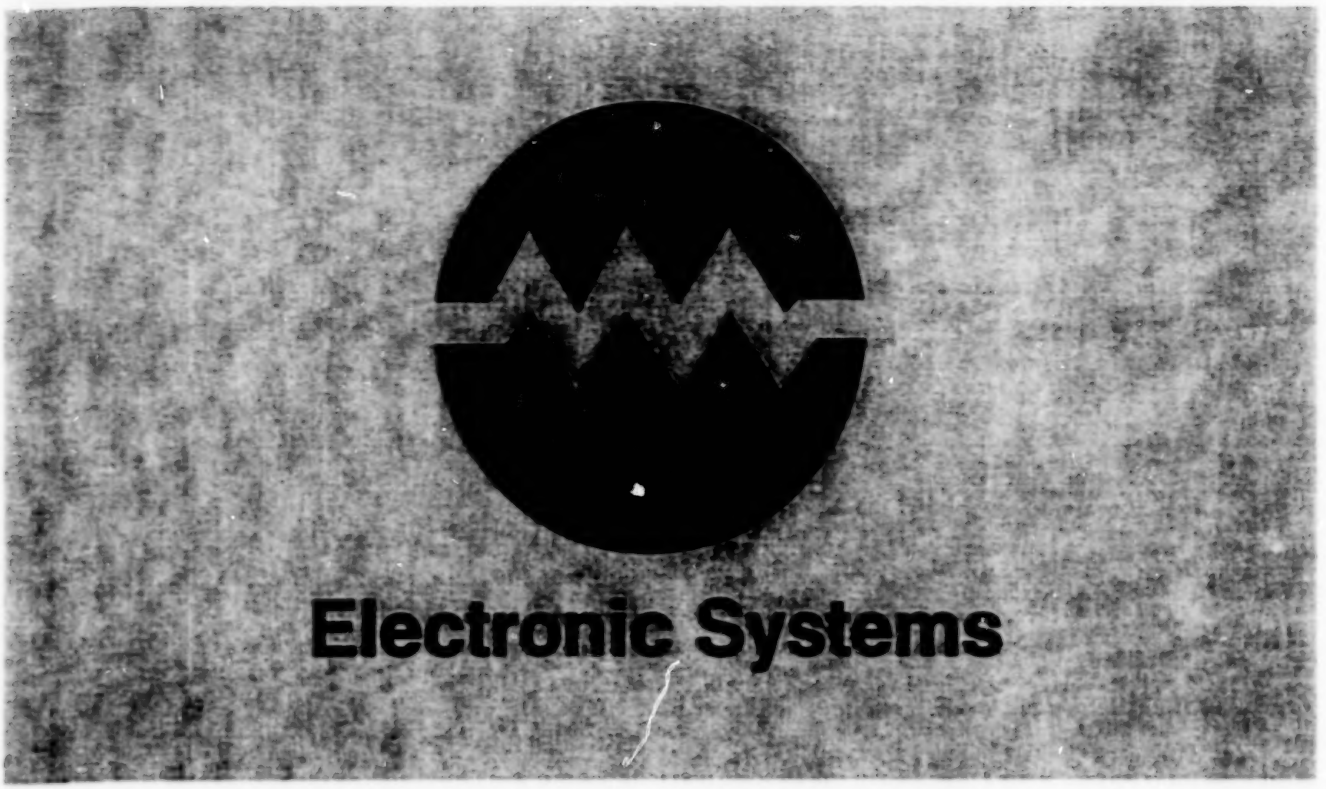

Hardware, Techniques, and Processes

Systolic Processor Array for Recognition of Spectra

Spectral signatures of materials would be detected and identified quickly.

NASA's Jet Propulsion Laboratory, Pasadena, California

A proposed systolic array of digital data processors would quickly detect and identify spectral signatures of materials of interest that appear in images produced by advanced imaging spectrometers of high spectral resolution. Called the Spectral Analysis Systolic Processor Array (SPA^2), this array would be relatively inexpensive and would satisfy the need to analyze the large, complex volume of multispectral data generated by imaging spectrometers to extract the desired information: the computational performance needed to do this in real time exceeds that of current supercomputers.

The SPA^2 would be able to locate highly similar segments or contiguous subsegments in two different spectra at a time. Exploiting this capability, the SPA^2 could compare sampled spectra from instruments with a data base of spectral signatures of known materials. The SPA^2 would compute and report scores that would express the degrees of similarity between the sampled and data-base spectra. Higher scores would be deemed to indicate that the material(s) of interest had been detected at the sampling locations in the spectral images.

The building block of the SPA^2 would be a 400,000-transistor complementary metal oxide/semiconductor very-large-scale integrated circuit chip called the "Biological Information Signal Processor" (BISP). This chip (see figure) contains 16 processing elements that operate at a clock frequency of 12.5 MHz. It can compare spectral images as long as 4,194,304 elements.

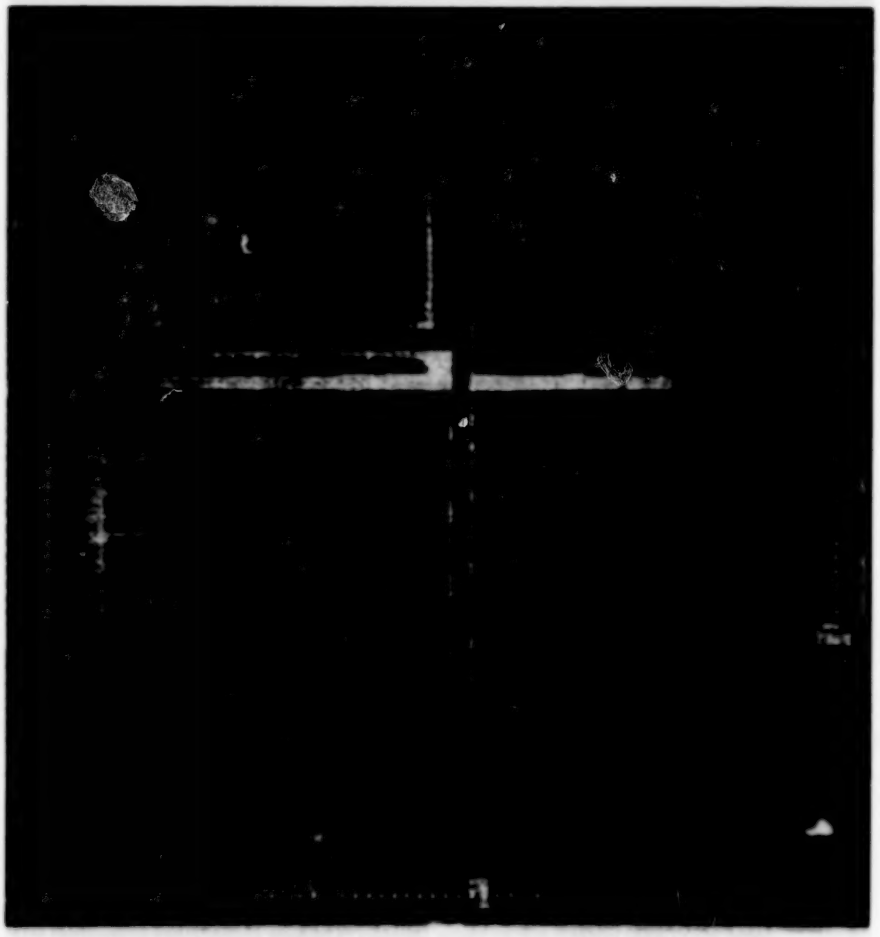

The Biological Information Signal Processor would be the building block of the SPA^2.

The SPA^2 composed of BISPs could operate orders of magnitude faster than does a CRAY-2 computer, yet it would fit in a package smaller than 20 cm^3.

This work was done by Edward T. Chow and John C. Peterson of Caltech for **NASA's Jet Propulsion Laboratory.** *Further information is contained in a TSP [see page 1].*

NPO-18808

Multilayer Active Control for Structural Damping and Optical-Path Regulation

Two control concepts are combined.

NASA's Jet Propulsion Laboratory, Pasadena, California

Two active-control concepts have been incorporated into a system for suppression of vibrations in a truss structure and regulation of the length of an optical path on the structure to the nanometer level. In the original intended application, the structure would be a lightweight truss structure supporting a stellar interferometer in zero gravitation. However, the control concepts should also be applicable wherever there is a need to maintain high precision and make a lightweight structure behave as

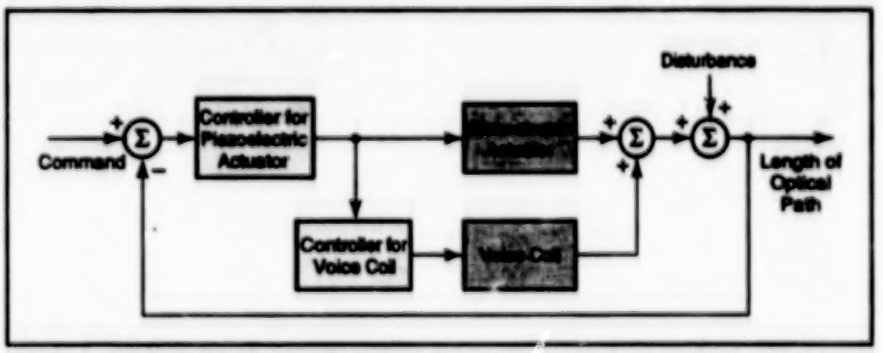

Figure 1. The Optical-Path-Length-Control Subsystem contains two feedback control loops to obtain active damping in a wide amplitude-and-frequency range.

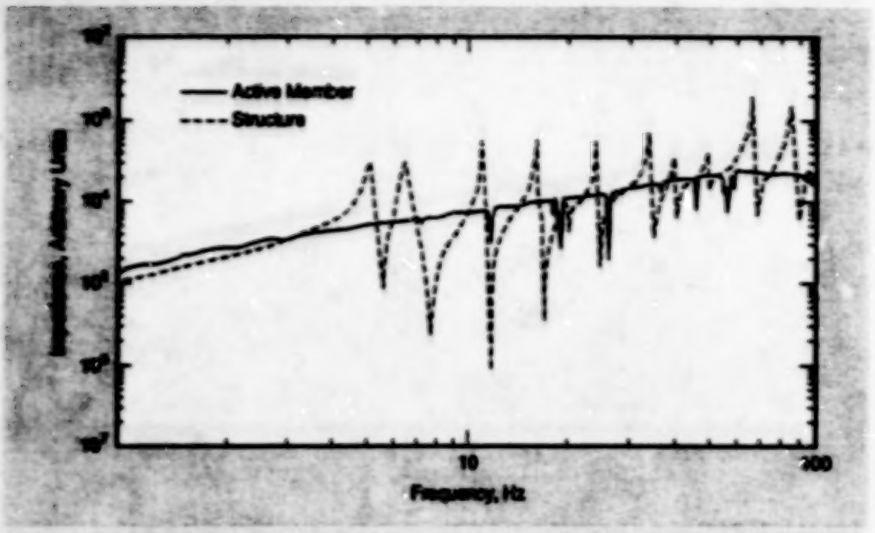

Figure 2. The Impedance-vs.-Frequency response of an experimental actively controlled structural member was adjusted to a smooth approximation of the impedance of the rest of the structure.

though it had the stiffness of a much heavier structure.

One of the active-control concepts involves direct control of the length of the optical path, one end of which lies within a retroreflective optical assembly. In an experimental version, the optical assembly is mounted on a trolley, attached via flexures and a low-frequency large-amplitude voice coil actuator to the free upper end of a tower-like cantilevered flexible structure. A lightweight mirror within the assembly is mounted on a high-frequency, small-amplitude piezoelectric actuator. The two actuators respond to measurements from optical-path-length sensors: the outputs of the sensors are processed into actuator commands by a feedback control subsystem (see Figure 1). This concept has been described in more detail in a number of previous articles, including "Stabilizing Optical-Path Length on a Vibrating Structure" (NPO-19040), *NASA Tech Briefs*, Vol. 19, No. 8 (August, 1995), page 48; "Controllable Optical Delay Line for Stellar Interferometry" (NPO-18686), *Laser Tech Briefs*, Vol. 1, No. 1 (September, 1993), page 44; and "Test Bed for Control of Optical-Path Lengths" (NPO-18487), *Laser Tech Briefs*, Vol. 2, No. 1 (Winter, 1994), page 61.

The other active-control concept, called "dial-a-strut", has also been discussed in previous articles, though not under its present name. In dial-a-strut control, one uses active structural members (struts that contain both sensors and actuators) in conjunction with active feedback control subsystems to achieve a form of active damping in which each active member acts like a passive damper in a frequency range of interest. Ideally, one would optimize damping by making the effective mechanical impedance of an actively controlled member equal to the complex conjugate of the mechanical impedance of the rest of the structure. In practice, this is not feasible, and instead one adjusts dials on the front panel of the control electronics (hence the name, "dial-a-strut") to adjust the effective stiffness and damping parameters of the controlled strut to match the magnitude of the impedance of the strut to a smoothed (in terms of frequency dependence) approximation of the magnitude of impedance of the rest of the structure (see Figure 2). The results of the experiments indicate that the combination of optical-path-length control and dial-a-strut control is effective for stellar interferometer applications.

This work was done by Zahidul H. Rahman, John T. Spanos, and James L. Fanson of Caltech for NASA's Jet Propulsion Laboratory. Further information is contained in a TSP [see page 1].
NPO-19041

Process-Information Display Panel for Welder's Visor

Information would be presented adjacent to the welder's usual field of view.

Marshall Space Flight Center, Alabama

A head-up display (HUD) unit would be mounted in a welder's visor or helmet (see Figure 1) to provide process information in real time, according to a proposal. Until now, success in manual welding has depended on the welder's training and intuition in judging the progress of a weld by interpreting sights and sounds. The proposed display would enable the welder to gain greater awareness of the effects of welding while controlling the welding process in the usual way(s) by use of a foot pedal, voice command, and/or manipulation of the welding torch. Data obtained during the welding process could be used to compare welding performance with a guideline or model performance established through laboratory tests or through a data base compiled from experience, making it possible to avoid the need for every new welder on the job to solve the same problems that were previously solved by other welders.

Figure 1. A Compact Head-Mounted Display Unit like this commercial one developed for a different purpose would be mounted in a welder's visor or helmet.

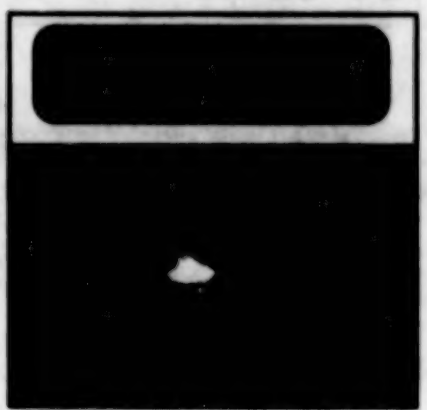

Figure 2. A Graphical Display would be presented to the welder, adjacent to the normal field of view through the visor.

One candidate design concept calls for a fully packaged HUD that would present computer-generated graphics adjacent to

the normal viewing window of the welder's visor or helmet (see Figure 2). The virtual-reality industry has created a new generation of such devices, with color and with resolutions of as much as 640 × 480 pixels and with higher-resolution units expected to come to market. Some modifications may be necessary to mount the display unit in the visor or helmet.

The HUD could be used, for example, to inform the welder of binary parameters like the states of solenoid-actuated switches and valves. Such continuously varying parameters as the rate of travel of the torch along the workpiece could be depicted by use of arrows, the lengths of which would be proportional to the deviations of the parameters from desired values or ranges of values. Colors could also play a key role; for example, the color of an arrow could be made to change from yellow to red as the error increased to an intolerable level. Such symbolic representation of the data would favor quick, intuitive interpretation.

In many cases, manual arc welding (as contrasted with automated arc welding) still offers the best balance of setup time, production volume, capital investment, and quality. Display devices of the proposed type could be especially beneficial in supporting and enhancing the continued practice of manual arc welding in such cases; even NASA and its contractors continue to use manual arc welding for fabrication and repair of much flight hardware and ground support equipment. The proposed display devices could also be of value in industries that invest millions of technician-hours each year in manual arc welding for a variety of products.

This work was done by Carolyn Russell of **Marshall Space Flight Center** *and Ken Gangl of Advanced Welding Concepts, Inc. No further documentation is available.*

Inquiries concerning rights for the commercial use of this invention should be addressed to the Patent Counsel, Marshall Space Flight Center [see page 1]. Refer to MFS-26322.

Neural Networks Analyze Data in Particle-Impact-Noise Tests

Interpretation of test data is more objective and accurate.

Lewis Research Center, Cleveland, Ohio

Electronic neural networks and computers have been put to use in analyzing data acquired in particle-impact-noise-detection (PIND) tests of packaged electronic components. PIND tests are performed to detect loose particles in the packages that could cause failures during subsequent operation of the packages in the presence of accelerations or other effects — for example, loose electrically conductive particles that could bounce into positions in which they would cause short circuits.

A PIND test is an instrumented and systematic version of the intuitive "shake-and-rattle" test. In a PIND test, the part in question is vibrated in a controlled manner by use of a shaker, while a microphone picks up the noise emitted by the shaken part. The output of the microphone is recorded, yielding a history of noise that is subsequently analyzed.

Previously, data from PIND tests were analyzed in a labor-intensive and error-prone process of subjective human interpretation. The average accuracy of such interpretation has been found to be about 44 percent. Accordingly, the neural-network computerized method was introduced to automate the analysis and to increase its accuracy by reducing human subjectivity and error.

In this method, the recorded noise signal is first processed by a computer-controlled analog-to-digital converter. The digitized noise-signal data (see figure) are then processed into voltage data bins, the contents of which serve as inputs to a neural network. The neural network then analyzes the data, deciding whether or not the tested package contained loose particles.

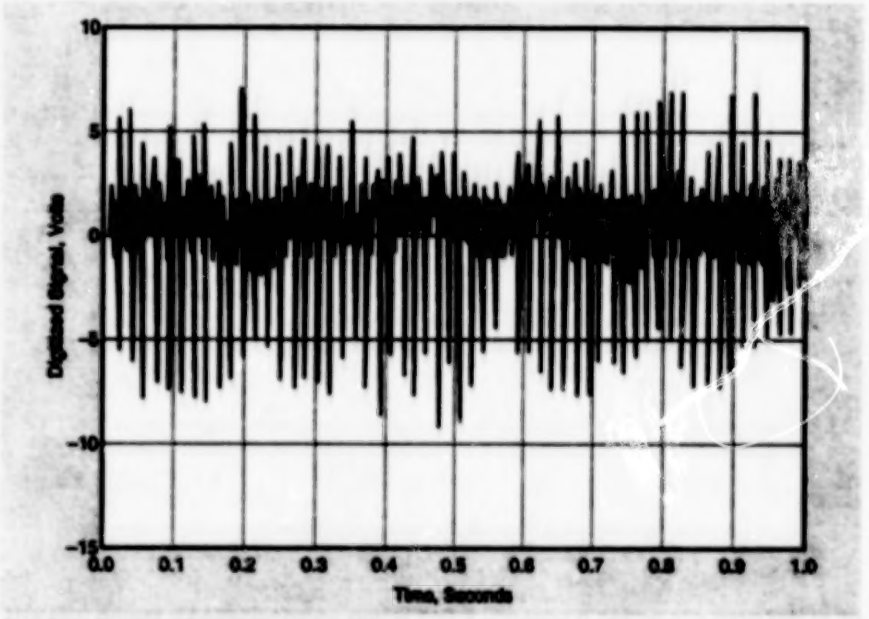

This Plot Shows a Digitized Noise Signal from a one-second interval of a PIND test of an electronic part that contained loose particles.

Neural networks of both the back-propagation and the self-organizing-map types have been successfully trained and tested on PIND data. Preliminary results suggest that the use of neural networks will result in significant improvement in the quality and reliability and decrease in the cost of PIND testing.

This work was done by Lois J. Scaglione of **Lewis Research Center.** *Further information is contained in a TSP [see page 1].*
LEW-16077

Computer-Aided Air-Traffic Control in the Terminal Area

A developmental computer-aided system for the automated management and control of arrival traffic at a large airport would include three integrated subsystems. One subsystem, called the Traffic Management Advisor, establishes optimized landing sequences and landing times for aircraft arriving in designated airspace several hundred miles from the airport. Another subsystem, called the Descent Advisor, generates advisory data for fuel-efficient and conflict-free descents

of aircraft assigned to available terminal gates. The third subsystem, called the Final Approach Spacing Tool, provides heading and speed clearances that produce an accurately spaced flow of aircraft on their final approaches. A data base that includes current wind measurements and mathematical models of performances of types of aircraft contributes to effective operation of the system.

This work was done by Heinz Erzberger of Ames Research Center. Further information is contained in a TSP [see page 1].
ARC-13332

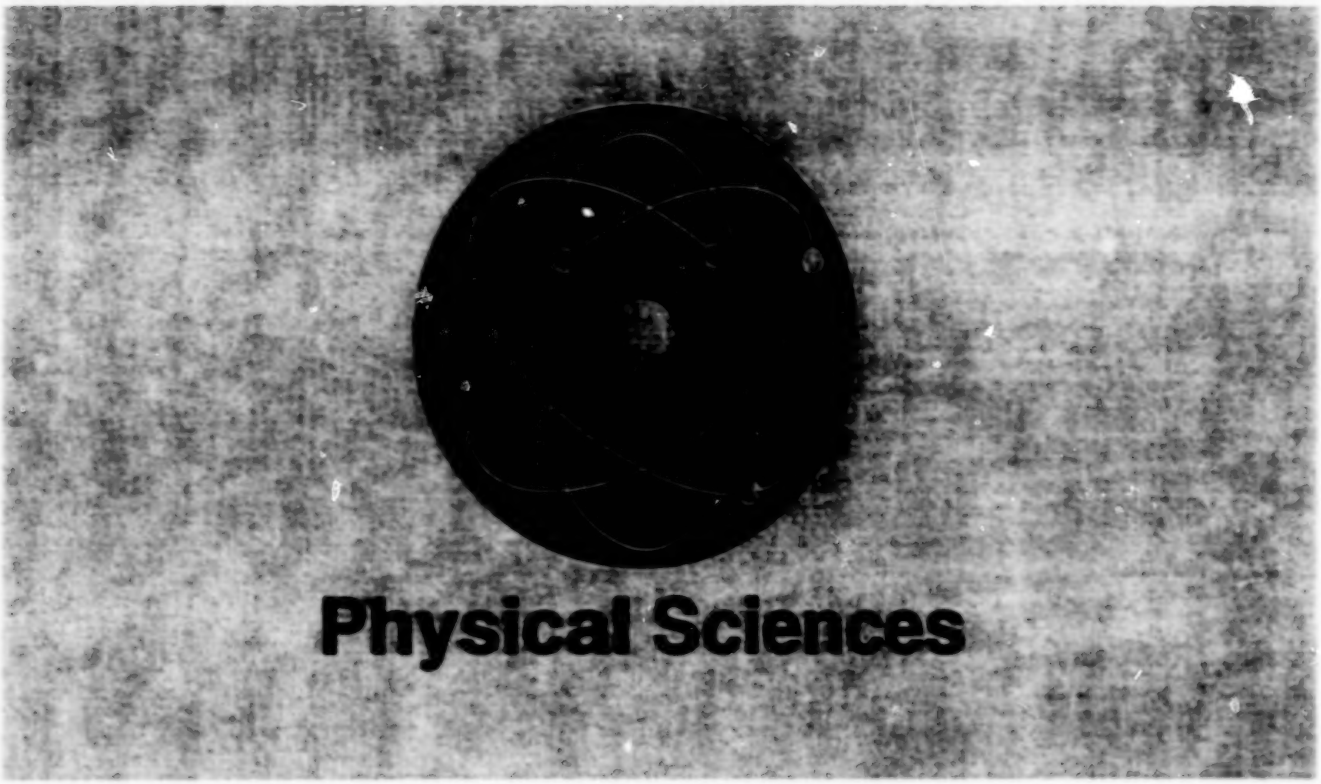

Physical Sciences

Hardware, Techniques, and Processes

Books and Reports

BLANK PAGE

Magnetic or Optical Surface Layer Would Indicate Strain

The surface layer would be deformed along with the substrate.

Langley Research Center, Hampton, Virginia

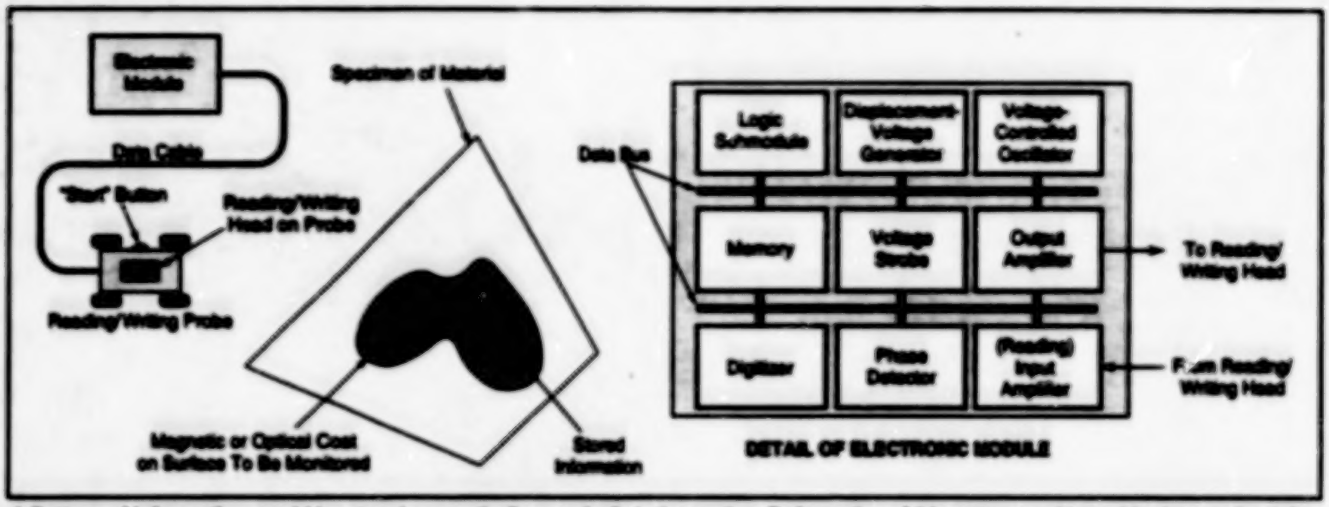

A Pattern of Information would be stored magnetically or optically in the coating. Deformation of this pattern would provide data on the deformation of the underlying material. The electronic module would process the stored information.

In a proposed method of obtaining information on strain at a surface of a material specimen, a magnetic coat (like that on magnetic tape) or an optical coat (like that on a compact disk) would be applied to all or part of the surface to be monitored. The coat would contain a record of its initial geometrical condition and would be read to determine changes in its condition, which changes would correspond to changes in the monitored surface.

The coating layer and the associated measuring equipment, taken together, would constitute a system called a "material strain monitor" (MSM). The system (see figure) would include an electronic module connected to a reading/writing probe via a data cable. The reading/writing probe would include wheels or other means of determining displacement of the probe along the surface. The probe would also include a reading/writing head, which would read and write information in the coating layer. A technician would press a "start" button on the probe to initiate the strain-monitoring procedure. The probe would then move over the surface to be monitored, writing or reading information in the coating layer.

In coating the surface to be monitored, magnetic particles could be mixed with a bonding agent and the mixture could be applied to the surface as a paint or spray. The resulting thin surface film would resemble the coating layer on a magnetic recording tape. The reading/writing probe used with such a film would be a standard magnetic reading/writing head capable of aligning the random magnetic domains in the film.

Alternatively, the coating layer could be a photographic emulsion applied in the dark. In this case, the reading/writing head could be connected to the electronic module via a fiber-optic cable and would include a lens to focus light onto the photographically treated surface. The fiber-optic cable could be used to both write in (expose) the emulsion and read from (measure the reflectance of) the emulsion.

The electronic module would include a logic submodule, a data bus, and a displacement-voltage generator, which together would measure the motion of the reading/writing probe over the monitored surface by use of rate-of-change-of-voltage (dV/dt) processing. The output of the displacement-voltage generator would govern the rate of generation of pulses by a voltage-controlled oscillator. These pulses would drive an output amplifier that would be connected to the reading/writing probe during writing. During reading, an input amplifier would be connected to the reading/writing head and a phase detector would compare the phase of the input (reading) signal with the phase of the signal from the displacement-voltage generator. The output of the phase detector would be digitized and stored in memory along with the position calculated by the logic submodule, which would integrate the signal from the displacement-voltage generator to calculate the distance (measured via rotation of the wheels) traveled along the surface.

Information would be written into the surface layer prior to deformation. The information pattern would remain embedded in the material and would suffer the same deformation as that of the material. Therefore, it would provide quantitative data on plastic deformation of the material. The data could be vectorized by writing the information in orthogonal tracks. Inasmuch as magnetic or optical lines can be read at densities of more than 10^6/in. (about 4×10^4/cm), the MSM could measure plastic deformations at high data densities anywhere a surface could be suitably coated. In contrast, conventional strain gauges can measure at single locations only, are vulnerable to mechanical disturbances, and cannot achieve high densities of data. The MSM will likely be very important in research in materials and mechanics; in particular, it is expected to compete strongly with systems based on image-analysis and laser techniques now being developed to obtain information on strain fields.

This work was done by Joseph S. Heyman of **Langley Research Center.** *No further documentation is available.*

Inquiries concerning rights for the commercial use of this invention should be addressed to the Patent Counsel, Langley Research Center [see page 1]. Refer to LAR-14510.

Five-Channel Polychromator Head

This device is part of a Raman-scattering temperature-measuring system.

Marshall Space Flight Center, Alabama

Figure 1 illustrates the five-channel polychromator head of a laser Raman polychromator that is being developed for use in measuring the rotational temperatures of H_2 molecules in subscale combustors. Each channel consists of a 1-mm fiber-optic cable that is individually translatable along the dispersion axis of a spectrometer to provide both flexibility and fine-tuning capability.

The basic idea is to measure the temperature in terms of the temperature dependence of Raman scattering of a laser beam from hydrogen molecules in the Q branch of the vibrational ground state. The Raman-scattered light can be resolved into a small number of spectral lines, the relative intensities of which indicate the population distribution of the hydrogen molecules in various rotational states. These spectral lines are denoted by their rotational quantum numbers, J, and the ratio between the intensities of any two of these spectral lines is related in a known way to the temperature at the point of measurement.

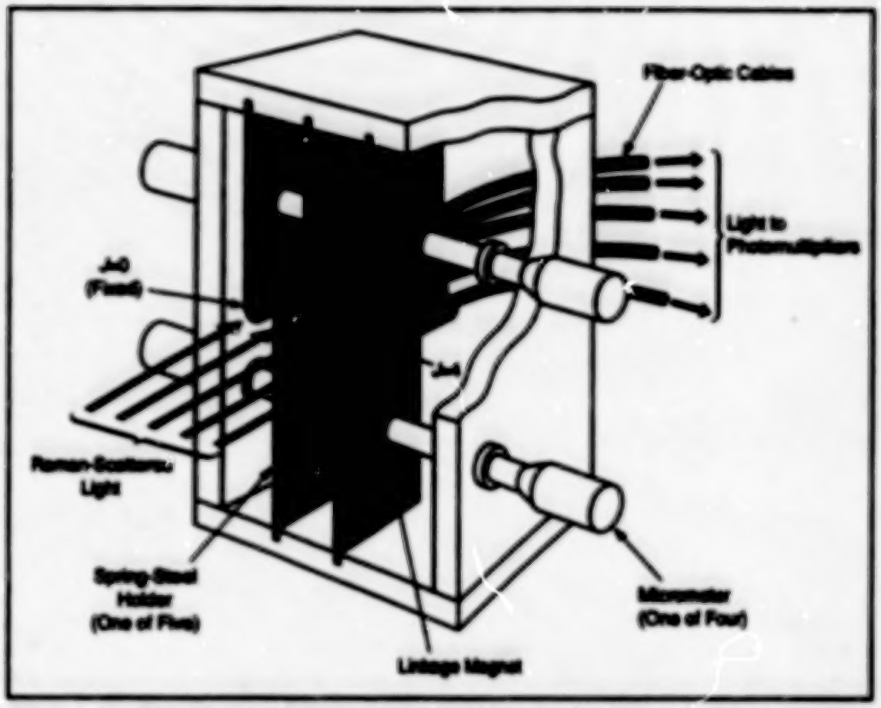

Figure 1. The Five-Channel Polychromator Head samples the Raman-scattering spectrum simultaneously at five wavelengths.

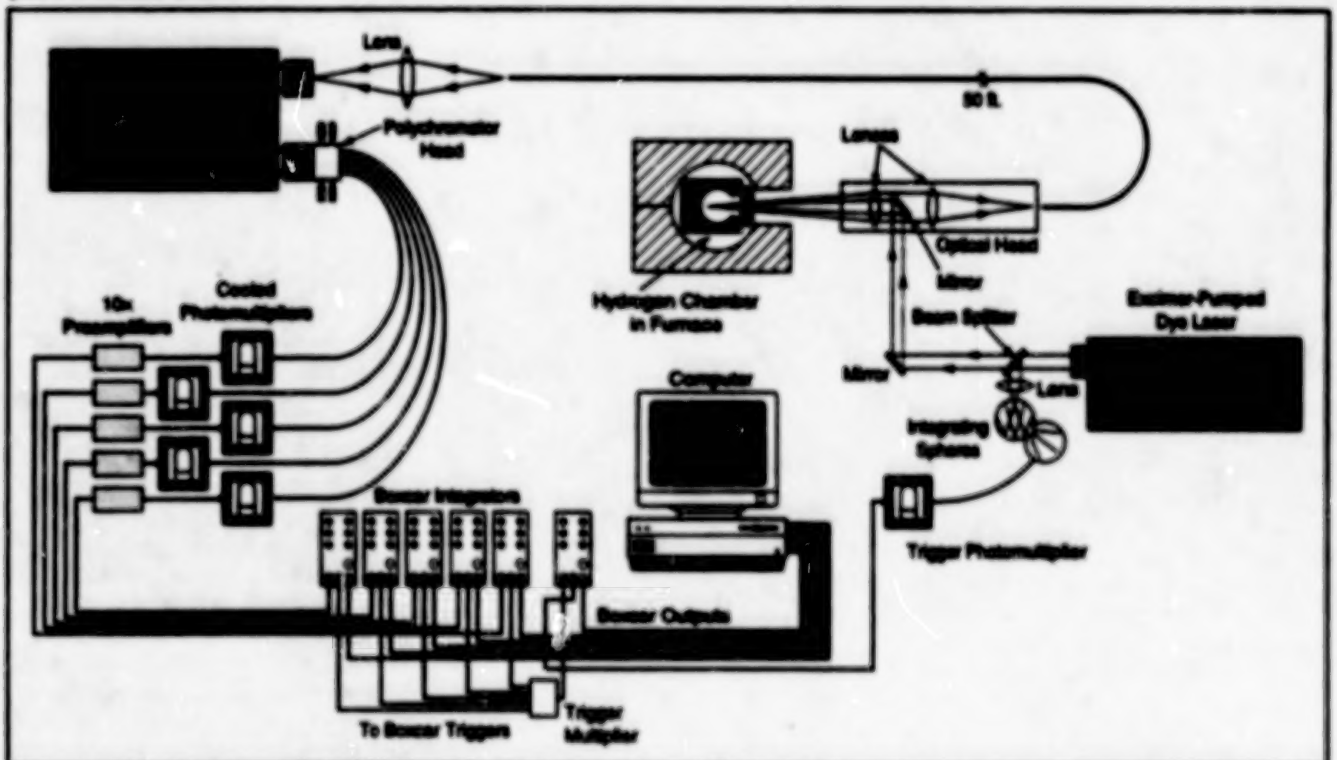

Figure 2. The Laser Raman Thermometer is not a thermometer in the usual sense of the word, but a noncontact spectrometer that measures temperature indirectly in terms of the relative intensities of selected Raman-scattering spectral lines.

The five-channel polychromator is used in conjunction with five photomultipliers (one photomultiplier for each channel) for simultaneous measurement of the $J = 0$ through $J = 4$ transitions of the $v = 0 \rightarrow v = 1$ Q branch. The photomultipliers offer high sensitivity and dynamic range, and the multiple channels eliminate the need for time-consuming scanning.

Figure 2 illustrates the laboratory configuration of the Raman thermometer in which the five-channel polychromator

head is installed. The head is mounted on the exit plane of a double monochromator (spectrometer) with plane holographic gratings of 2,400 grooves/mm. The reciprocal linear dispersion at the middle of the spectrum (wavelength of 538 nm) is 0.14 nm/mm. The output signal of each individual fiber-optic cable is sent to a separate photomultiplier, the output of which is sent to a signal-conditioning amplifier. The outputs of the amplifiers are gated and boxcar-averaged. A computer digitizes, stores, and analyzes the boxcar-averaged data via real-time algorithms.

This work was done by Richard Eskridge, Chris Dobson, Mike Lee, and Tony Robertson of Marshall Space Flight Center. Further information is contained in a TSP [see page 1].

Inquiries concerning rights for the commercial use of this invention should be addressed to the Patent Counsel, Marshall Space Flight Center [see page 1]. Refer to MFS-28646.

Improved Bakeout Chambers Within Vacuum Chambers

Heated enclaves reduce contamination further.

NASA's Jet Propulsion Laboratory, Pasadena, California

The figure illustrates schematically one of several vacuum-bakeout chambers that have been redesigned to reduce contamination. When operated according to a revised bakeout procedure, they yield measurements of contamination on vacuum-bake test articles more accurate than were available previously, and the potential for postbake recontamination of the vacuum-baked articles is reduced.

These chambers are improved versions of the one described in "Bakeout Chamber Within Vacuum Chamber" (NPO-18656), *NASA Tech Briefs*, Vol. 19, No. 5 (May, 1995), page 52. As before, each of the present vacuum-bakeout chambers includes an inner heated chamber surrounded by an insulating blanket that is, in turn, surrounded by a cold shroud, all mounted within a conventional vacuum chamber. The heated inner chamber, previously called a "bakeout chamber," is now called an "enclave." The cold shroud is cooled by flowing liquid nitrogen; the cold shroud is used to reduce background pressure in the vacuum chamber and thereby reduce the deposition of background contamination on contamination detectors located near the bakeout chamber.

The improvements in design and bakeout procedure were made to satisfy the following three criteria: (1) A test article must not become contaminated by outgassed volatile materials at any time during bakeout, contamination-level testing, or post-test warmup of the cold shroud; (2) The background rate of outgassing by the chamber hardware must be negligibly small in comparison with that of the test article; and (3) the method used to measure contamination must positively verify that the required degree of cleanliness has been achieved.

The enclave consists mostly of a can and cover made of stainless steel and electropolished to remove contamination embedded in their surfaces. Contamination detectors of several different

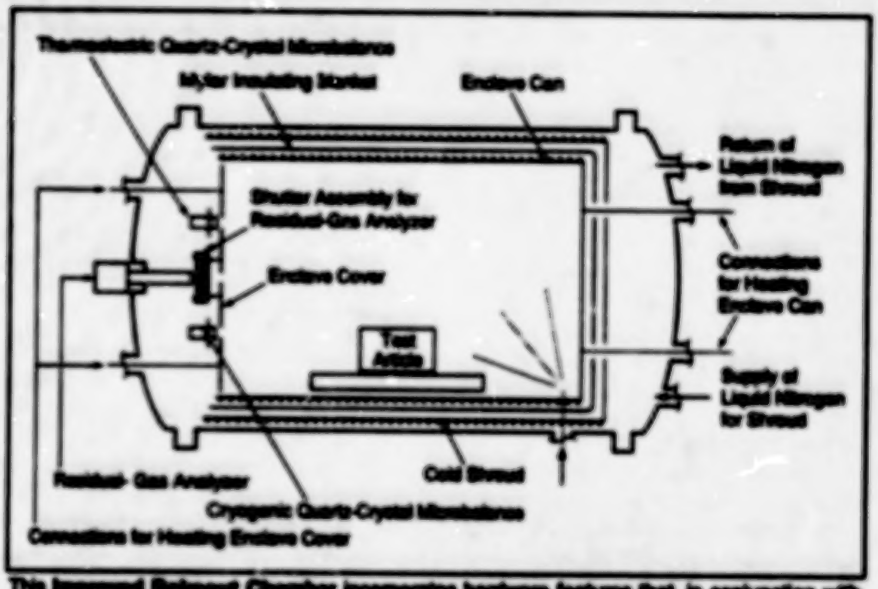

This Improved Bakeout Chamber incorporates hardware features that, in conjunction with an improved bakeout procedure, reduce spurious contamination and increase the accuracy of contamination measurements.

types (residual-gas analyzer, thermoelectric quartz-crystal microbalance, and cryogenic quartz-crystal microbalance) are mounted facing orifices in the cover, so that their directional sensitivity patterns cause them to measure predominantly the outgassed contaminants that stream from the enclave through the orifices. The measurement of contamination involves a multistep procedure in which the various detectors are operated at various temperatures and pressures.

By enclosing the test article in the enclave and keeping the walls of the enclave hotter than the test article during bakeout, one prevents condensation of contaminants on the inner walls of the enclave. In preparation for measurement of contamination of the test article, the background rate of outgassing by the chamber hardware is minimized by baking the enclave at a temperature greater than the maximum expected operating temperature of the test article. During bakeout, contaminants leave the enclave through the orifices and are removed from the vacuum chamber — some by the vacuum-chamber pump, others by condensing onto the cold shroud.

After bakeout is complete and before a post-bakeout test of cleanliness of the test article, the enclave is cooled slowly enough to prevent the condensation of volatile contaminants that are still being emitted from the test article (contaminants are still being emitted because the temperature of the test article lags behind the temperature of the enclave; that is, the test article is still hot at this phase of operation). After the post-bakeout test, the shroud is warmed slowly enough to limit the flux of desorption from the shroud to an acceptably low level, while the enclave is purged with high-purity gaseous nitrogen to minimize backstreaming of contaminants into the enclave.

This work was done by Kenneth R. Johnson, Daniel M. Taylor, Robert W. Lane, Maximo G. Cortez, and Mark R. Anderson of Caltech for NASA's Jet Propulsion Laboratory. Further information is contained in a TSP [see page 1].

NPO-19015

Techniques for Topographical Mapping via Interferometric SAR

Data-processing techniques combined with advanced navigational capabilities yield terrain-height maps.

NASA's Jet Propulsion Laboratory, Pasadena, California

Two techniques for processing data acquired by an airborne interferometric synthetic-aperture-radar (SAR) system yield terrain-height maps. The techniques are predicated on the availability of an accurate navigational system that yields data on the motion and orientation of the airplane that carries the SAR system and, thus, also effectively gives the orientation of the baseline between the two radar antennas of the system.

The figure presents a simplified view of the broadside-looking interferometric-SAR geometry. For an SAR system operating at a wavelength $\lambda = c/f$ (where c = the speed of light and f = the radar carrier frequency), the phase shift, ϕ, between the radar returns received at the two antennas is given by

$$\frac{\phi\lambda}{2\pi} = |r_{21}|\cos(\theta - \theta_{21})$$

where r_{21} is the baseline vector between the two antennas and θ_{21} is the angle of this baseline above the nadir direction. This angle can be computed from the navigational data. The other quantities indicated in the figure are given by

$$\theta = \theta_{21} + \arccos\left(\frac{\phi\lambda}{2\pi|r_{21}|}\right)$$

$$h = H - r\cos\theta, \text{ and } y = r\sin\theta.$$

Thus, in principle, the three-dimensional coordinates of a target point on the terrain can be determined from (1) the position and orientation of the airplane as given by the navigational system and (2) the slant range r and phase shift ϕ as measured by the SAR system.

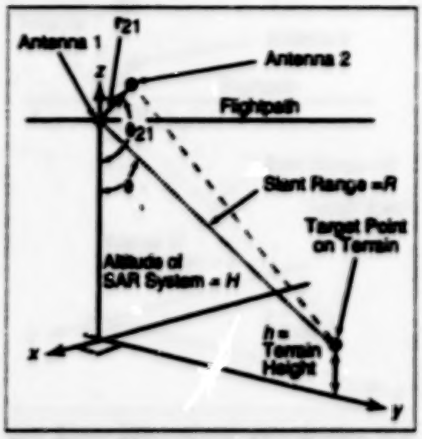

The Three-Dimensional Coordinates of a target point can be computed if the position along the flightpath, the angle θ of the line of sight, and the slant range are known.

One of the two techniques resolves the $2\pi N$ ambiguity (where N is an integer) in the measured value of ϕ, enabling an absolute determination of the terrain height h. In an older technique, this ambiguity was resolved by use of a reference terrain point of known elevation. In the present technique, no a priori elevational information is needed: Instead, this technique involves the construction of a differential SAR interferogram within which the maximum variation of phase is less than 2π.

First, SAR data are acquired at two slightly different frequencies f_u and f_l, which could be, for example, sidebands of the carrier frequency f. Then the difference $\Delta\phi$ between the phase shifts at the two frequencies is computed. In principle, $\Delta\phi = f_u\phi/f - f_l\phi/f$; thus, by choosing f_u and f_l sufficiently close, one can restrict the range of $\Delta\phi$ to less than 2π. Also in principle, one can then compute an unambiguous value of ϕ from $\phi = f\Delta\phi/f_u - f_l$. In practice, this computation amplifies the phase noise in the differential interferogram, and it is necessary to average the noisy computed phase over an image patch containing a large number of pixels to determine N.

The other technique is an algorithm for efficient computation of the three-dimensional coordinates of a target point. The algorithm computes the unit vector along the slant range from ϕ, r_{21}, and the velocity of the airplane (which affects the Doppler centroid frequency). It computes the position of the target point, relative to the airplane, as the product of the slant range and the unit vector along the slant range. Then it adds this relative-position vector to the position vector of the airplane to obtain the position vector of the target point.

This work was done by Soren N. Madsen, Howard A. Zebker, and Jan M. Martin of Caltech for NASA's Jet Propulsion Laboratory. Further information is contained in a TSP [see page 1].

NPO-18840

Simple Magnetic Device Indicates Thickness of Alloy 903

Relative strength of attraction shows whether an alloy overlay is thinner than allowable.

Marshall Space Flight Center, Alabama

The figure illustrates a simple, hand-held, magnetic device that can be used to determine whether an overlay of alloy 903 on a body of alloy 718 is thinner than allowable in a specific application. The device is called a "ferrite indicator" and was originally designed to be used in determining the ferrite content of a specimen of steel. It is placed in contact with the specimen and functions by indicating whether a magnet that it contains is attracted more strongly to the specimen or to a calibrated reference sample.

An experiment showed that the magnetic characteristics of alloy 903 make it suitable for inspection of overlays of this material by the ferrite-indicator technique. In the application that motivated the experiment, there was a need to ensure that the overlay of alloy 903 was at least 0.020 in. (about 0.5 mm) thick. In the experiment, one of the available reference samples gave an indication of 0.025 in. (about 0.6 mm). [The extra 0.005 in. (about 0.1 mm) can be used to advantage as a margin of safety.]

The Ferrite Indicator is shown here with several reference samples.

This work was done by Pin Jeng Long, Sergio Rodriguez, and Mark L. Bright of Rockwell International Corp. for **Marshall Space Flight Center**. *Further information is contained in a TSP [see page 1].*

MFS-29980

Verifying Dissolution of Wax From Hardware Surfaces

Wax removed by cleaning solvent is revealed by cooling the solution with liquid nitrogen.

Marshall Space Flight Center, Alabama

An improved solvent cleaning procedure and associated cleanliness test have been devised for removing wax that previously coated a piece of hardware and for verifying that the wax has been removed. Such a procedure and test are needed in the case of hardware that must be protected by wax during machining or plating but is required to be free of wax during subsequent use. In a previous solvent cleaning procedure and cleanliness test, carbon tetrachloride (which is highly toxic) was used as the solvent, and infrared spectroscopy was used to detect wax in the solvent flushings. A typical infrared analysis took as long as 2 1/2 hours.

The improved cleaning procedure and test take less than 5 minutes. Unlike the previous infrared-analysis cleanliness test, the improved test does not require special skill or equipment and can be performed at the cleaning site. In addition, the improved procedure and test enable recovery of all the cleaning solvent.

In the improved cleaning procedure, one uses 1,1,1-trichloroethane or perchloroethylene as the solvent. In the improved cleanliness test, liquid nitrogen, in a proportion of up to 40 volume percent, is mixed into the solvent flushings to cool them. The same proportion of liquid nitrogen is mixed into an equal amount of solvent known to be pure. If the solvent flushings contain a significant quantity of wax, a separate waxy phase collects on top of the flushing solution and can be identified by visual comparison with the clean solution.

This work was done by Benjamina G. Montoya of Rockwell International Corp. for **Marshall Space Flight Center**. *Further information is contained in a TSP [see page 1].*

MFS-29978

Slide Rule for Calculating Curing Schedules

A special-purpose slide rule has been devised for calculating schedules for storing and curing adhesives, sealants, and other materials that are characterized by known curing times and shelf lives. The use of the slide rule can prevent mistakes that are commonly made in determining storage and curing schedules. The slide rule is calibrated in days and hours. In using the slide rule, one simply selects the curing time and the starting calendar day and time; the slide rule indicates the number of days of curing and the hour when cure will be completed on the final day. It is, however, necessary to account separately for the number of days when the cure extends into the following month.

This work was done by Don Hester of Thiokol Corp. for **Marshall Space Flight Center**. *Further information is contained in a TSP [see page 1].*

MFS-28938

Books and Reports

Scattering of Nonplanar Acoustic Waves

A report presents a theoretical study of scattering of nonplanar acoustic waves by rigid bodies. The study was performed as part of an effort to develop means of predicting scattering, from aircraft fuselages, of noise made by rotating blades. The basic approach taken in the study was to model acoustic scattering by use of a boundary integral equation to solve the equation by the Galerkin method. This approach was followed in solving example problems that involved point acoustic sources. The computations by the present approach were found to converge on the exact solutions much faster than would computations performed with infinite series according to the method of separation of variables.

This work was done by Judith M. Gilman of **Ames Research Center**, *F. Farassat of Langley Research Center, and M. K. Myers of George Washington University. To obtain a copy of the report, "A Boundary Integral Approach to the Scattering of Nonplanar Acoustic Waves by Rigid Bodies," see Tsp's [page 1].*

Inquiries concerning rights for the commercial use of this invention should be addressed to the Patent Counsel, Ames Research Center [see page 1]. Refer to ARC-12837.

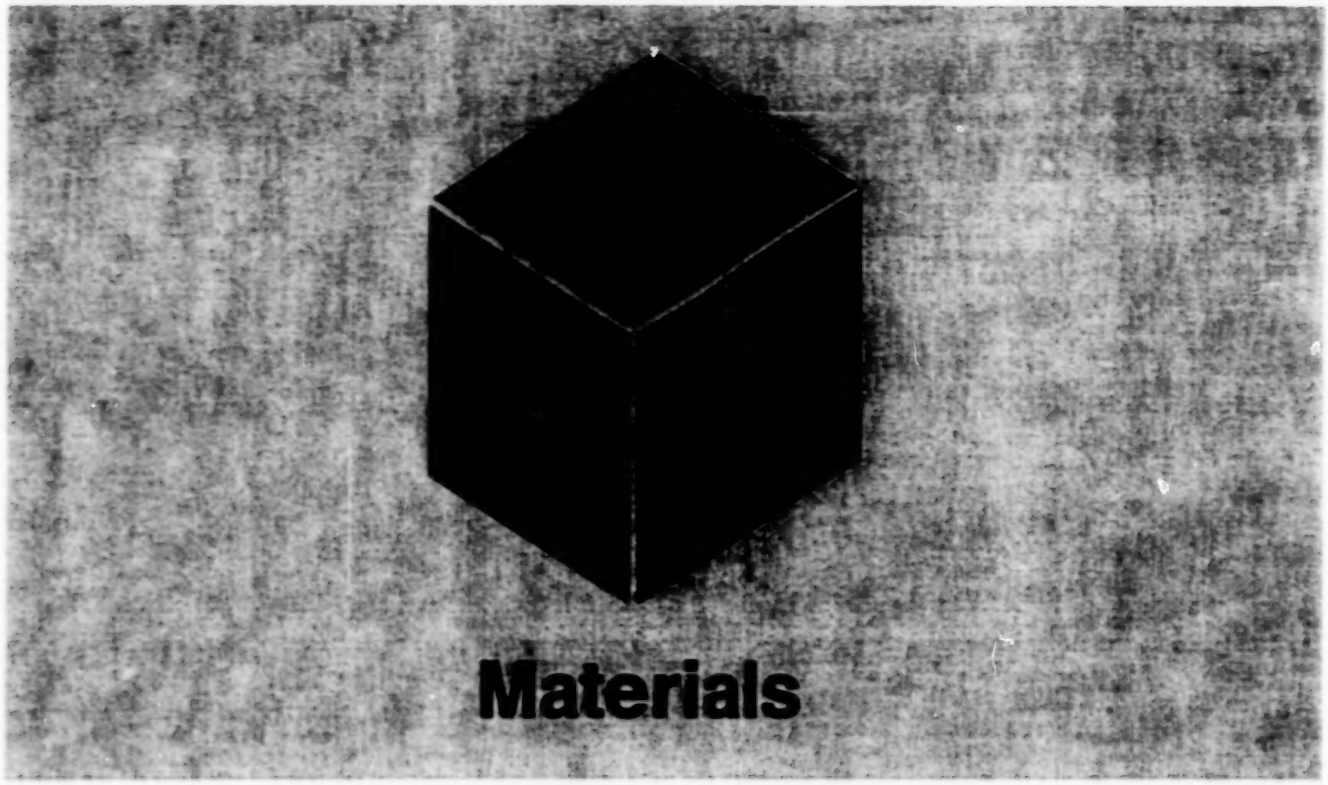

Materials

Hardware, Techniques, and Processes

BLANK PAGE

Trimethoxymethane: a Fuel for Direct-Oxidation Fuel Cells

Trimethoxymethane can be oxidized to CO_2 and H_2O at high rates, without poisoning electrodes.

NASA's Jet Propulsion Laboratory, Pasadena, California

Trimethoxymethane (TMM) has been identified as a high-energy fuel for direct-oxidation fuel cells. TMM can be synthesized from natural gas (methane) and can be handled easily because it is a non-toxic, low-vapor-pressure liquid. Data obtained from both half-cell and full-cell tests indicate that TMM can be oxidized at very high rates. Thus, TMM is considered to be an excellent candidate for use in direct-oxidation fuel cells in vehicles and portable power supplies.

The electrochemical oxidation of TMM, represented by

$$(CH_3O)_3CH + 5H_2O \rightarrow 4CO_2 + 20H^+ + 20e^-,$$

has been studied in experiments in half cells in which the electrolyte was 0.5 M sulfuric acid and the electrocatalysts were Pt/Sn and Pt/Ru electrodes. It was found that TMM can be oxidized at potentials considerably more negative than those of methanol. As shown by the data plotted in Figure 1, increasing the concentration of TMM increases the kinetics of its oxidation. The kinetics are also increased by increasing the temperature: at temperatures as high as 60 °C, the rate of oxidation is twice that at 25 °C.

Experiments on the direct oxidation of TMM were carried out in a liquid-feed-type fuel cell developed previously for direct oxidation of methanol. In this cell, Nafion 117, a commercial proton-conducting solid-polymer membrane, was used as the electrolyte. The membrane electrode assembly included a specially constructed fuel-oxidation electrode made of an unsupported Pt/Ru catalyst layer (4 mg/cm^2) and a gas-diffusion-type unsupported platinum electrode (4 mg/cm^2) for the reduction of oxygen. A fuel solution of 2 M TMM was circulated past the anode of the cell, while oxygen at a pressure of 20 psi (≈140 kPa) was applied to the cathode. The CO_2 produced by the oxidation of TMM was easily separated from the fuel solution in a tall glass column.

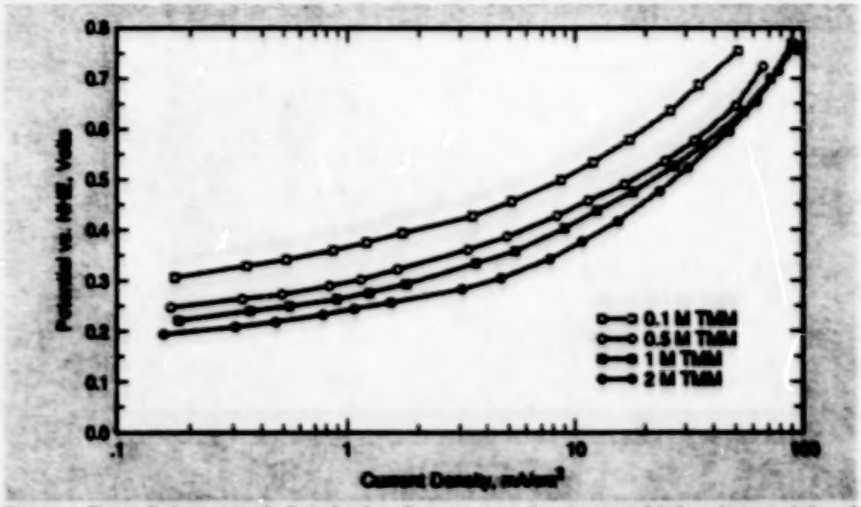

Figure 1. These Galvanostatic Polarization Curves show the electro-oxidation characteristics of several concentrations of TMM at Pt/Sn electrodes of the gas-diffusion type, at room temperature, in a solution with 0.5 M H_2SO_4 and 0.01 M perfluorooctanesulfonic acid (C_8 acid) at 25 °C.

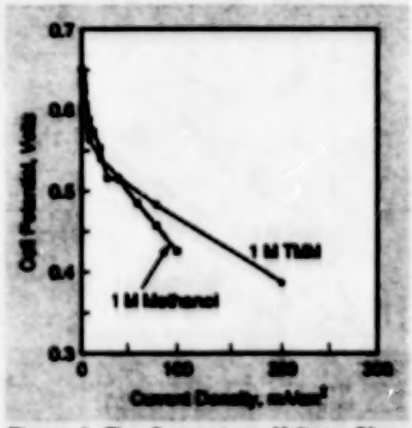

Figure 2. The Current-vs.-Voltage Characteristics of a liquid-feed direct-oxidation fuel were measured with TMM and with methanol as the fuel at 60 °C.

Analysis revealed no oxidation products other than methanol, which may be an intermediate product in the process of oxidation of TMM to carbon dioxide and water. Inasmuch as the particular fuel cell was designed to handle methanol in the first place, the presence of methanol is no cause for concern. Figure 2 shows current-vs.-voltage characteristics of the cell in an experiment using TMM and in another experiment using methanol as the fuel.

This work was done by George A. Olah, Surya G. Prakash, Sekharipuram R. Narayanan, Eugene Vamos, and Subbarao Surampudi of Caltech for NASA's Jet Propulsion Laboratory. Further information is contained in a TSP [see page 1].

In accordance with Public Law 96-517, the contractor has elected to retain title to this invention. Inquiries concerning rights for its commercial use should be addressed to

William T. Callaghan, Manager
Technology Commercialization
JPL-301-350
4800 Oak Grove Drive
Pasadena, CA 91109

Refer to NPO-19228, volume and number of this NASA Tech Briefs *issue, and the page number.*

Dimethoxymethane: a Fuel for Direct-Oxidation Fuel Cells

This fuel can be electro-oxidized at sustained high rates without poisoning electrodes.

NASA's Jet Propulsion Laboratory, Pasadena, California

Dimethoxymethane (also called methylal), is a nontoxic liquid that has been identified as one of several high-energy fuels for direct-oxidation fuel cells. DMM has been found to undergo facile electro-oxidation to carbon dioxide and water, with methanol as a possible intermediate product. The electro-oxidation is catalyzed at Pt/Sn and Pt/Ru electrodes. The high rates of oxidation sustained by DMM make it possible to operate liquid-feed cells at significant power densities at temperatures close to ambient. The performance of DMM is superior to that of methanol at the same temperature. DMM

can be synthesized from natural gas (methane) and is thus a viable alternative to methanol in direct-oxidation fuel cells.

The electro-oxidation of DMM involves a series of dissociative adsorption steps followed by a surface reaction to form carbon dioxide and water. The electro-oxidation reaction is represented by

$$(CH_3O)_2CH_2 + 4\,H_2O \rightarrow 3\,CO_2 + 16\,H^+ + 16\,e^-$$

Experiments on the electro-oxidation of DMM were carried out in half cells in which the electrolyte was 0.5 M sulfuric acid and the electrocatalysts were gas-diffusion-type Pt/Sn and Pt/Ru electrodes. It was found that DMM can be oxidized at potentials considerably more negative than those of methanol. Although increasing the temperature was found to increase the rate of oxidation significantly, the low boiling temperature of DMM (41 °C) made it impractical to use temperatures greater than 37 °C in the half-cell experiments. As shown in Figure 1, increasing the concentration of DMM increases the rate of its oxidation.

Experiments on the direct oxidation of DMM were carried out in a liquid-feed-type fuel cell developed previously for direct oxidation of methanol. In this cell, the electrolyte was a membrane of Nafion 117, which is a commercial proton-conducting solid polymer. The membrane electrode assembly included a specially constructed fuel-oxidizing electrode made of an unsupported Pt/Ru catalyst layer (4 mg/cm^2) and a gas-diffusion-type unsupported platinum electrode (4 mg/cm^2) for the reduction of oxygen. A fuel solution of 1 M DMM was circulated past the fuel-oxidizing (anode) side of the cell, while oxygen was supplied to the cathode at a pressure of 20 psi (≈140 kPa). The carbon dioxide produced by the oxidation of DMM was easily separated from the fuel solution in a tall glass column.

Analysis revealed no oxidation products other than methanol, which may be an intermediate product of the process

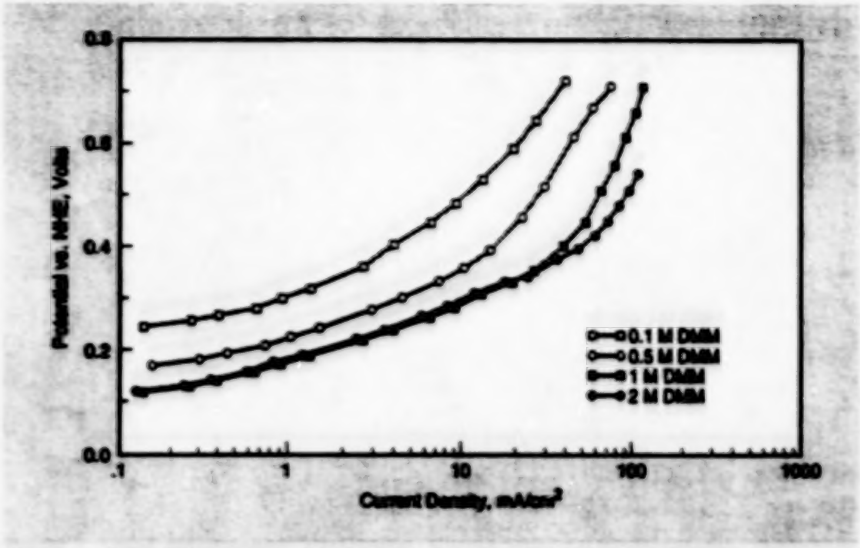

Figure 1. These Galvanostatic Polarization Curves show the electro-oxidation characteristics of several concentrations of DMM at Pt/Sn electrodes of the gas-diffusion type, at room temperature, in a solution with 0.5 M H_2SO_4 and 0.01 M perfluorooctanesulfonic acid (C_8 acid).

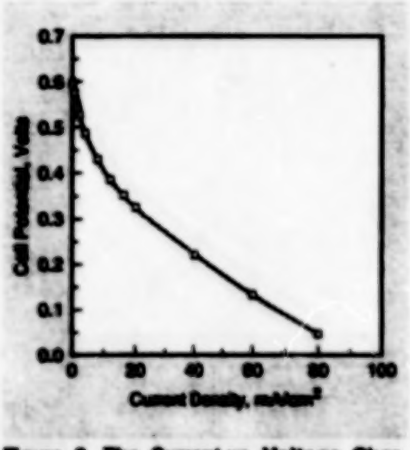

Figure 2. The Current-vs.-Voltage Characteristics of a liquid-feed direct-oxidation fuel were measured with DMM at 37 °C.

of oxidation of DMM to CO_2 and H_2O. The presence of methanol is not a cause for concern because the fuel cell was designed for use with methanol and the methanol is ultimately oxidized to carbon dioxide and water.

Figure 2 shows the current-vs.-voltage characteristic of the cell at 37 °C. The cell potential was 0.20 V at a current density of 50 mA/cm^2; this performance was comparable to that obtained using methanol as the fuel. Better performance is expected at higher temperature and by use of Pt/Sn catalyst. Alternatively, the low boiling temperature of DMM also makes it a candidate for a gas-feed operation.

This work was done by George A. Olah, Surya G. Prakash, Sekharipuram R. Narayanan, Eugene Vamos, and Gerald Halpert of Caltech for NASA's Jet Propulsion Laboratory. Further information is contained in a TSP [see page 1].

In accordance with Public Law 96-517, the contractor has elected to retain title to this invention. Inquiries concerning rights for its commercial use should be addressed to

William T. Callaghan, Manager
Technology Commercialization
JPL-301-350
4800 Oak Grove Drive
Pasadena, CA 91109

Refer to NPO-19229, volume and number of this NASA Tech Briefs issue, and the page number.

Trioxane: a Fuel for Direct-Oxidation Fuel Cells

Trioxane can be used as a substitute for formaldehyde.

NASA's Jet Propulsion Laboratory, Pasadena, California

Trioxane has been identified as a high-energy, nontoxic, solid substitute for formaldehyde as a water-soluble fuel for use in direct-oxidation fuel cells. Trioxane has been found to undergo facile electrochemical oxidation to water and carbon dioxide at platinum and platinum-alloy electrodes in liquid-feed-type fuel cells that contain acid electrolytes or solid proton-exchange membrane electrolytes. Trioxane exhibits less crossover than do such conventional fuels as methanol and formaldehyde. Being a solid at ambient temperature, trioxane offers significant advantages in handling and transportation. Trioxane can be synthesized from natural gas with relative ease.

The electro-oxidation of trioxane to carbon dioxide and water is believed to occur according to the reaction

$$(CH_2O)_3 + 6H_2O \rightarrow 3CO_2 + 12H^+ + 12e^-$$

Experiments on the electro-oxidation

characteristics of trioxane were performed in half cells with temperature control. The electrolyte was sulfuric acid at various concentrations between 0.5 and 2.0 M. The cells contained gas-diffusion-type electrodes consisting of platinum/tin at an areal density of 0.5 mg/cm^2 on a high-surface-area carbon. The data in Figure 1 indicate that increasing the concentration of trioxane results in an increased rate of oxidation. Current densities as high as 100 mA/cm^2 were realized at potentials of 0.4 V — comparable to the performance realized with formaldehyde.

Cyclic voltammetry showed that the mechanism of oxidation of trioxane does not involve a breakdown to formaldehyde before electro-oxidation. Increasing the concentration of acid was also found to result in increased rates of electro-oxidation. Therefore, it was projected that very high rates of electro-oxidation would occur when using a solid electrolyte of Nafion™ (a commercial perfluorinated, hydrophilic, proton-exchange polymer), which exhibits an acidity equivalent to that of 10 M sulfuric acid.

Experiments on the direct oxidation of trioxane were carried out in a liquid-feed-type fuel cell developed previously for direct oxidation of methanol. In this cell, a Nafion proton-conducting solid-polymer membrane was used as the electrolyte. The membrane electrode assembly included a specially constructed fuel-oxidation electrode made of an unsupported Pt/Ru catalyst layer and a gas-diffusion-type unsupported platinum catalyst for the reduction of oxygen. A fuel solution of trioxane at a concentration of 1 M was circulated past the anode of the cell, while oxygen at a pressure of 20 psi (~140 kPa) was applied to the cathode. The CO_2 produced by the oxidation of trioxane was separated from the fuel solution in a tall glass column.

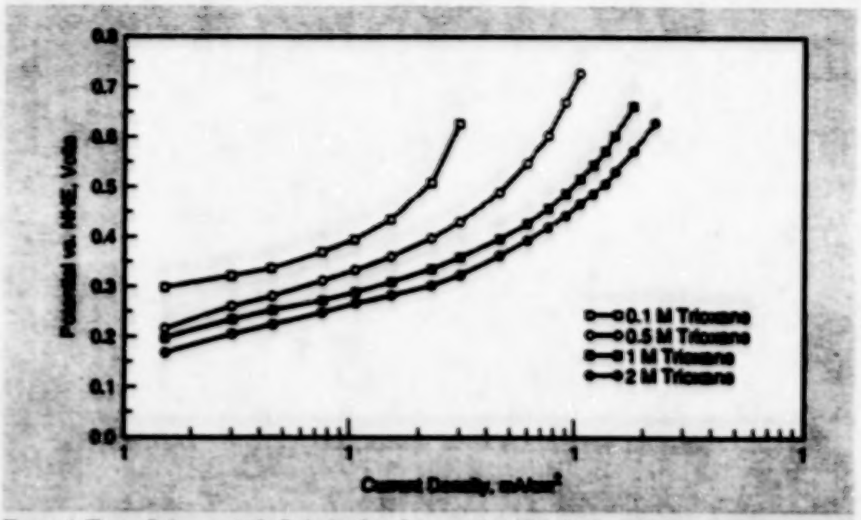

Figure 1. These Galvanostatic Polarization Curves show the electro-oxidation characteristics of several concentrations of trioxane at Pt/Sn electrodes of the gas-diffusion type, at a temperature of 55 °C, in a solution with 0.5 M H_2SO_4 and 0.01 M perfluorooctanesulfonic acid (C_8 acid).

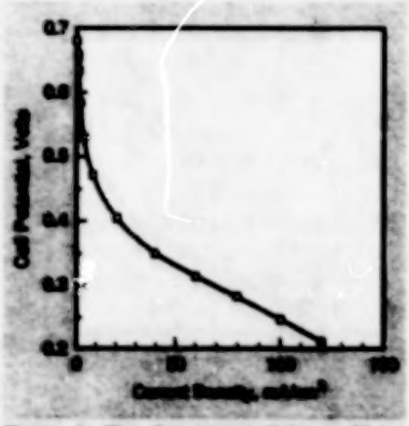

Figure 2. The Current-vs.-Voltage Characteristics of a liquid-feed direct-oxidation fuel cell were measured with a 1 M solution of trioxane as the fuel, at a temperature of 60 °C.

Figure 2 shows the current-vs.-voltage characteristics of trioxane in this fuel cell. This performance can be improved considerably by use of platinum/tin electrodes. The measured rate of crossover was found to be no more than 1/5 that in a comparable methanol fuel cell. Decreased rates of crossover are extremely desirable, inasmuch as crossover reduces the efficiency and performance.

This work was done by George A. Olah, Surya G. Prakash, Sekharipuram R. Narayanan, Eugene Vamos, and Subbarao Surampudi of Caltech for NASA's Jet Propulsion Laboratory. Further information is contained in a TSP [see page 1].

In accordance with Public Law 96-517, the contractor has elected to retain title to this invention. Inquiries concerning rights for its commercial use should be addressed to

William T. Callaghan, Manager
Technology Commercialization
JPL-301-350
4800 Oak Grove Drive
Pasadena, CA 91109

Refer to NPO-19230, volume and number of this NASA Tech Briefs *issue, and the page number.*

Electrochemical Deposition of Thiolate Monolayers on Metals

The degree of coverage can be controlled with relative ease.

NASA's Jet Propulsion Laboratory, Pasadena, California

An electrochemical method has been devised for coating metal (usually, gold) surfaces with adherent thiolate monolayers. In comparison with older, nonelectrical chemical solution methods, the present electrochemical method affords greater control over the location and amount of material deposited and makes it easier to control the chemical composition of the deposits. One important potential use for this method lies in the fabrication of chemically selective thin-film resonators for microwave oscillators used to detect pollutants: a monolayer can be formulated to bind selectively the pollutant chemical species of interest, causing an increase in mass of the monolayer and a corresponding decrease in the frequency of resonance. Another important potential use lies in selective chemical derivatization for purposes of improving adhesion, lubrication, protection against corrosion, electrocatalysis, and electroanalysis.

A compound used in this method is denoted by the general chemical formula *XRSY*. "*S*" is used here in the standard sense to denote sulfur, which is the component that bonds to the metal substrate. *Y* denotes a group that is lost during deposition, partly because it bonds to *S* less strongly than does the metal substrate; *Y* can represent hydrogen (in which case *XRSY* is a thiol), a metal (in which case *XRSY* is a thiolate salt), or another organic group.

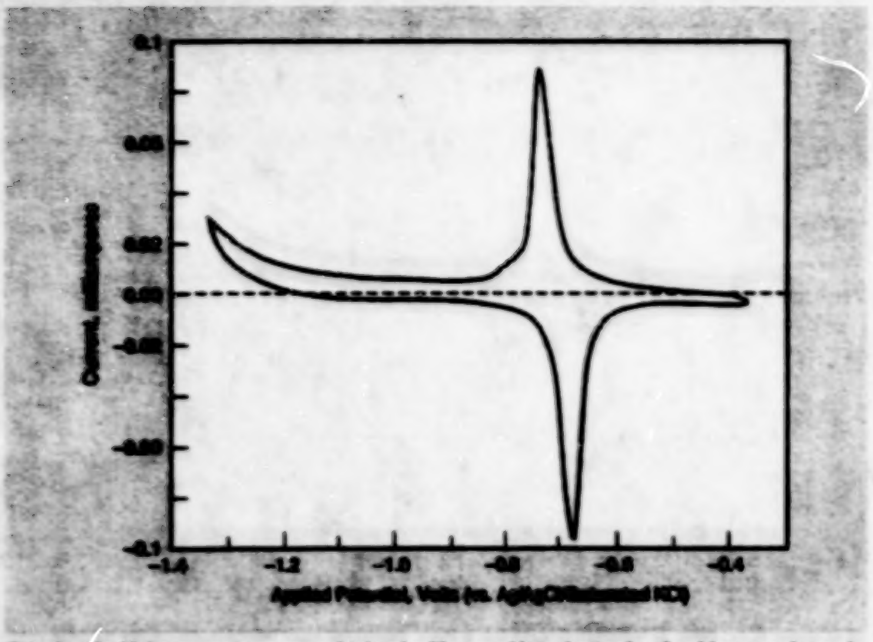

This Cyclic Voltammogram was obtained with a working electrode of gold on a mica substrate in a solution of 10 mM mercaptoethanol in an 0.5 M aqueous solution of LiOH.

R is a molecular group that forms somewhat of an isolation layer in that it lies between the *S* moiety attached to the metal and the *X* moiety at the outer end. *R* is chosen to obtain a desired packing density, stability, thickness, and/or other characteristics of the monolayer to suit a specific application. *R* can be any of a variety of organic groups; for example, a linear alkane chain $[(CH_2)_n]$, where *n* is an integer).

R and *X* together determine the characteristics of the deposit. The outer end group, *X*, is chosen to provide the end functionality required in a specific application. *X* end groups that have proven useful include CH_3, $CF_3(CF_2)_7$, COOH, and OH; other potentially useful end groups include inorganic complexes with thiol ligands, organometallic compounds, cyclodextrins, and crown ethers.

In preparation for the deposition process, *XRSY* is dissolved in any of a number of compatible electrolytes; typically, the electrolyte is an aqueous solution of KOH. The process can be carried out in any suitable electrochemical system that includes a voltammetric analyzer and cell assembly. The *XRSY*/electrolyte solution and the working, reference, and counter electrodes of the system are placed in the cell. (The working electrode is the metal substrate to be coated.) The cell is purged with a chemically inert gas to remove dissolved oxygen.

The electrodes are connected to the voltammetric analyzer. For the first 10 to 30 s, the applied voltage is set at a level at which any adsorbed compounds are desorbed so as to clean completely the working electrode, with stirring of the solution to facilitate transport of any desorbed impurities away from the substrate to prevent readsorption. The voltage is then stepped to the deposition voltage, which has been preselected from the anodic deposition wave, to establish a redox equilibrium, thus providing for the desired level of coverage. Typical deposition times range upward from about 1 min.

The figure shows a cyclic voltammogram that contains peaks showing the oxidative adsorption and reductive desorption of a layer of the thiolate $HOCH_2CH_2S^-$ on Au on a mica substrate. This plot shows that the adsorption and desorption processes are well-defined and reproducible.

This work was done by Marc D. Porter and Duane E. Weisshaar of Iowa State University for NASA's Jet Propulsion Laboratory. Further information is contained in a TSP [see page 1].

In accordance with Public Law 96-517, the contractor has elected to retain title to this invention. Inquiries concerning rights for its commercial use should be addressed to

Marc D. Porter, Director
Microanalytical Instrumentation Center
45 Spedding Hall
Iowa State University
Ames, IA 50014

Refer to NPO-19469, volume and number of this NASA Tech Briefs issue, and the page number.

Closed-Loop System Removes Contaminants From Inert Gas

The system can be used in place of a supply of purge gas.

NASA's Jet Propulsion Laboratory, Pasadena, California

A closed-loop system for the purification of an atmosphere of inert gas includes a bellows pump, a cartridge for removal of oxygen, a cartridge for removal of water vapor, and porous metal filters at the ends of the cartridges for removal of particles. These components are connected in series with each other and with a chamber in which the gas is to be used (see figure). In the specific application for which the system was devised, the chamber is one in which semiconducting materials are processed. By virtue of the closed-loop operation, a limited supply of inert gas is adequate to provide an atmosphere for industrial processing of semiconductors.

The rate of leakage of the bellows pump is less than 10^{-6} cm^3/s. All tubes in the system are electropolished and connected together by VCR fittings. Because the gas comes in contact with only metallic parts, the pump does not add new impurities to the gas.

The oxygen-removing cartridge contains a packed oxygen-sorbent material. The cartridge can be heated to a temperature as high as 300 °C for operation in the scrubbing mode or for regeneration of the spent sorbent. Four classes of oxygen sorbents have been developed at NASA's Jet Propulsion Laboratory, each class being best suited for operation in a specific temperature range. These classes of sorbents are (a) copper-exchanged zeolites (200 to 400 °C), (b) copper-modified carbon molecular sieves (room temperature to 250 °C), (c) copper-containing platinum zeolites (100 to 400 °C), and (d) cobalt-containing platinum-modified zeolites (400 to 800 °C).

All of these sorbents take in oxygen by catalytic oxidation of copper. The equilibrium level of oxygen after removal is well below 1 part per trillion at temperatures up to 400 °C. The oxygen-removing cartridge can be packed with

one or a mixture of the oxygen sorbents; the mixture can be tailored, along with the other design parameters, to help adapt the system to meet various design requirements, including temperature of operation, initial level of oxygen impurity, and the like.

The oxygen-removal capability of the system was tested in closed-loop operation, using copper-modified zeolite 13X as the oxygen sorbent. When the sorbent was heated to a temperature of 250 °C, and argon containing oxygen at a concentration of 100 parts per million was introduced, the concentration of oxygen fell, in less than 10 s, to a level below the sensitivity limit (100 parts per billion) of the oxygen-detecting instrument. The rapidity of the decrease in the oxygen level indicates that the ultimate attainable oxygen level is considerably lower than 100 parts per billion.

The water-vapor-removing cartridge was not included in the initial closed-loop tests. It is proposed to remove water vapor by use of pretreated zeolite. The pretreatment would consist in drying the zeolite for 48 h at a temperature of 300 °C. (The use of zeolite for removal of water vapor is well known.)

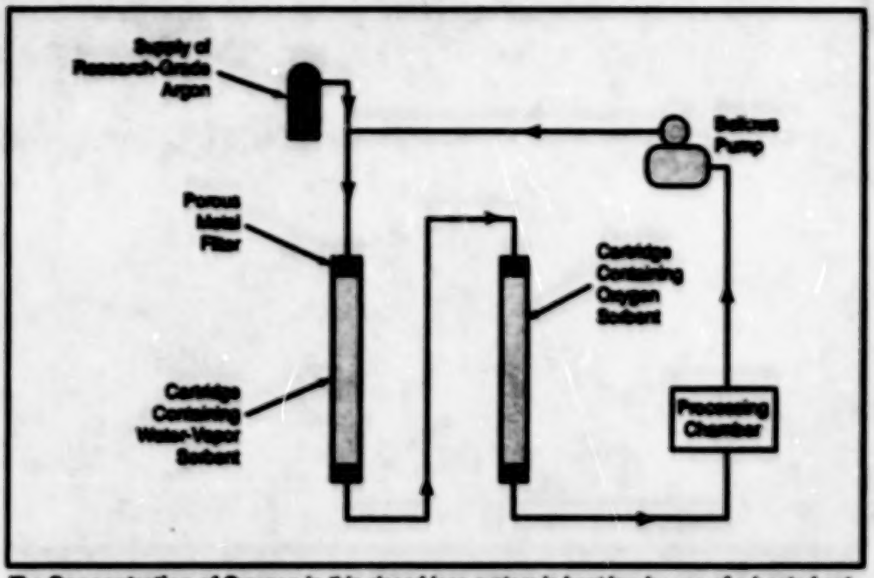

The Concentration of Oxygen in this closed-loop system is kept low by use of a heated catalytic sorbent bed in a cartridge. It is also proposed to keep the concentration of water vapor low by use of a predried zeolite sorbent bed in another cartridge, and to remove particles smaller than 0.1 μm by use of porous metal filters.

This work was done by Pramod K. Sharma of Caltech for NASA's Jet Propulsion Laboratory. Further information is contained in a TSP [see page 1].

NPO-18879

BLANK PAGE

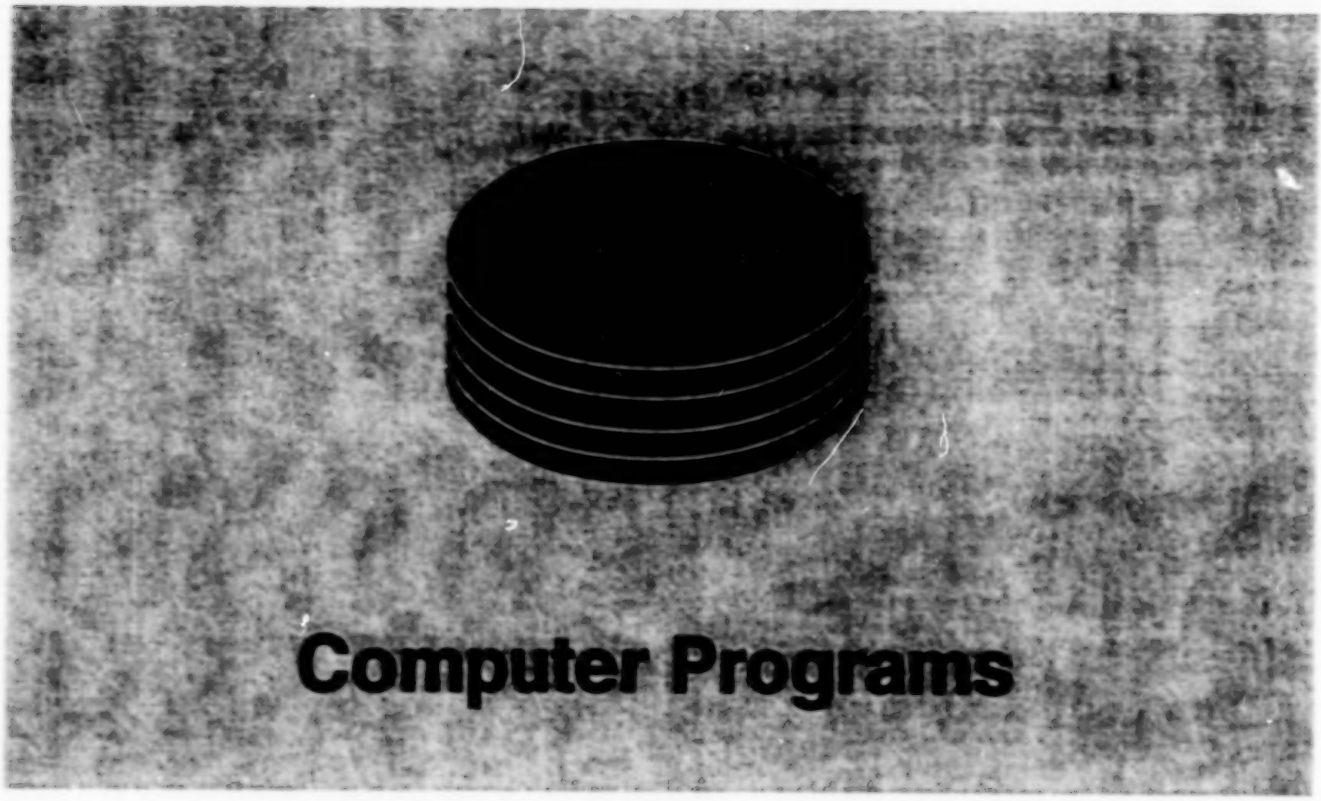

Mathematics and Information Sciences

BLANK PAGE

These programs may be obtained from COSMIC. Please contact

COSMIC®
Computer Services Annex
University of Georgia
Athens, GA 30602
Telephone No. (404) 542-3265.

Mathematics and Information Sciences

C-Language Integrated Production System, Version 6.0

CLIPS facilitates the development and delivery of expert-system software.

The C Language Integrated Production System (CLIPS) computer program provides a complete programming environment for developing expert system software — programs that are specifically intended to model human expertise or other knowledge. CLIPS is designed to enable research on, and the development and delivery of, artificial intelligence on conventional computers.

CLIPS 6.0 provides a cohesive software tool for handling a wide variety of knowledge with support for three different programming paradigms: rule-based, object-oriented, and procedural. Rule-based programming enables the representation of knowledge as heuristics — essentially, rules of thumb that specify a set of actions to be performed in a given situation. Object-oriented programming enables the modeling of complex systems comprised of modular components (which can be easily reused to model other systems or create new components). The procedural-programming capabilities provided by CLIPS 6.0 enable the representation of knowledge in ways similar to those of such languages as C, Pascal, Ada, and LISP. CLIPS 6.0 makes it possible to develop expert system software by use of rule-based programming only, object-oriented programming only, procedural programming only, or combinations of these three types of programming.

CLIPS provides extensive features to support the rule-based programming paradigm, including seven conflict-resolution strategies, dynamic rule priorities, and truth maintenance. CLIPS 6.0 supports more complex nesting of conditional elements in the "if" portion of a rule ("and", "or", and "not" conditional elements can be placed within a "not" conditional element). In addition, there is no longer a limitation on the number of multifield slots that a deftemplate can contain.

The CLIPS Object-Oriented Language (COOL) provides capabilities for object-oriented programming. Features supported by COOL include classes with multiple inheritance, abstraction, encapsulation, polymorphism, dynamic binding, and message passing. CLIPS 6.0 supports tight integration of the rule-based programming features of CLIPS with COOL (that is, a rule can pattern match on objects created by COOL).

CLIPS 6.0 provides the capability to define functions, overloaded functions, and global variables interactively. In addition, CLIPS can be embedded within procedural code, called as a subroutine, and integrated with such languages as C, FORTRAN, and Ada. CLIPS can be easily extended by use of several well-defined protocols. CLIPS provides several options for delivery of programs, including the ability to generate stand-alone executables or to load programs from text or binary files.

CLIPS 6.0 provides support for the modular development and execution of knowledge bases with the "defmodule" construct. CLIPS modules enable the grouping together of a set of constructs, such that explicit control can be maintained by restricting access to the constructs by other modules. This type of control is similar to global and local scoping used in such languages as C or Ada. By restricting access to deftemplate and defclass constructs, modules can function as blackboards, permitting only certain facts and instances to be seen by other modules. Modules are also used by rules to provide control over execution.

The CRSV (cross-reference, style, and verification) utility software included in previous versions of CLIPS is no longer included. The capabilities formerly provided by CRSV are now available directly within CLIPS 6.0 to aid in the development, debugging, and verification of large rule bases.

COSMIC offers four distribution versions of CLIPS 6.0: UNIX (MSC-22433), VMS (MSC-22434), Macintosh (MSC-22429), and IBM PC (MSC-22430). Executable files, source code, utility software, documentation, and examples are included on the program media. All distribution versions include identical source code for the command-line version of CLIPS 6.0. This source code should be compilable on any computer equipped with an ANSI C compiler. Each distribution version of CLIPS 6.0, except that for the Macintosh computer, includes an executable for the command-line version. For the UNIX version of CLIPS 6.0, the command-line interface has been successfully compiled on a Sun4 computer running SunOS, a DECstation computer running DEC RISC ULTRIX, an SGI Indigo Elan computer running IRIX, a DEC Alpha AXP computer running OSF/1, and an IBM RS/6000 computer running AIX. Command-line interface executables are included for Sun4 computers running SunOS 4.1.1 or later and for the DECstation computer running DEC RISC ULTRIX. The makefiles may have to be modified slightly to be used on other computers running UNIX.

The UNIX, Macintosh, and IBM PC versions of CLIPS 6.0 each include a platform-specific interface. Source code, a makefile, and an executable for the Windows 3.1 interface version of CLIPS 6.0 are provided only on the IBM PC distribution diskettes. Source code, a makefile, and an executable for the Macintosh interface version of CLIPS 6.0 are provided only on the Macintosh distribution diskettes. Likewise, for the UNIX version of CLIPS 6.0, only source code and a makefile for an X-Windows interface are provided. The X-Windows interface requires MIT's X Window System, Version 11, Release 4 (X11R4) or later, the Athena Widget Set, and the Xmu library. The source code for the Athena Widget Set is provided on the distribution medium. The X-Windows interface has been successfully compiled on a Sun4 computer running SunOS 4.1.2 with the MIT distribution of X11R4 (not OpenWindows), an SGI Indigo Elan computer running IRIX 4.0.5, and a DEC Alpha AXP computer running OSF/1 1.2.

The VAX version of CLIPS 6.0 comes only with the generic command line interface. ASCII makefiles for the com-

mand-line version of CLIPS are provided on all the distribution media for UNIX, VMS, Macintosh, and DOS.

Four executables are provided with the IBM PC version: a windowed interface executable for Windows 3.1 built by use of Borland C++ v3.1, an editor for use with the windowed interface, a command-line version of CLIPS for Windows 3.1, and a 386 command-line executable for DOS built by use of Zortech C++ v3.1. All four executables are capable of utilizing extended memory and require an 80386 or better central processing unit (CPU). Users who need executables on 8086/8088 or 80286 CPUs must recompile the CLIPS source code themselves. Users who wish to recompile the DOS executables by use of Borland C++ or Microsoft C must use a DOS extender program to produce an executable capable of using extended memory.

The version of CLIPS 6.0 for IBM PC-compatible computers requires DOS v3.3 or later and/or Windows 3.1 or later. It is distributed on a set of three 1.4-MB, 3.5-in. (8.89-cm) diskettes. A hard disk is necessary. The Macintosh version is distributed in compressed form on two 3.5-in. (8.89-cm), 1.4-MB Macintosh-format diskettes, and requires System 6.0.5 or higher, plus 1 MB of random-access memory. The version for DEC VAX/VMS is available in VAX BACKUP format on a 1,600-bit/in. (630-bit/cm), 9-track magnetic tape (standard distribution medium) or a TK50 tape cartridge. The UNIX version is distributed in UNIX tar format on a 0.25-in. (6.35-mm) streaming-magnetic-tape cartridge (Sun QIC-24). For the UNIX version, alternate distribution media and formats are available upon request.

The CLIPS 6.0 documentation includes a user's guide and a three-volume reference manual that consists of basic and advanced programming guides and an interfaces guide. An electronic version of the documentation is provided on the distribution medium for each version: in Microsoft Word format for the Macintosh and PC versions of CLIPS, and in both PostScript format and Microsoft Word for Macintosh format for the UNIX and DEC VAX versions of CLIPS. CLIPS was developed in 1986 and version 6.0 was released in 1993.

This program was written by Gary Riley, Brian Donnell, Huyen-Anh Bebe Ly, and Chris Ortiz of **Johnson Space Center.**

For further information on MSC-22429, see TSP's [page 1].

For further information on MSC-22430, see TSP's [page 1].

For further information on MSC-22433, see TSP's [page 1].

For further information on MSC-22434, see TSP's [page 1].

MSC-22429/MSC-22430/MSC-22433/MSC-22434.

Pairwise-Comparison Software

This program collects similarity data for psychometric scaling and cognitive research.

PWC (which stands for "pairwise comparison") is a computer program that collects data for psychometric scaling techniques now used in cognitive research. The cognitive tasks and processes of human operators of automated systems are considerations that now figure prominently in the process of defining requirements for such systems. Recent developments in cognitive research have emphasized the potential utility of such psychometric scaling techniques as multidimensional scaling for representing human knowledge and cognitive processing structures. Such techniques involve collecting measurements of stimulus-relatedness from human observers. When data are analyzed according to these scaling approaches, an *n*-dimensional representation of the stimuli is produced. This representation is said to describe the subject's cognitive or perceptual view of the stimuli.

PWC applies the technique of pairwise comparisons, which is one of the many techniques commonly used to acquire the data necessary for these types of analyses. PWC administers the task, collects the data from the test subject, and formats the data for analysis. It thereby addresses many of the limitations of the traditional "pen-and-paper" methods. By automating the data-collection process, PWC prevents subjects from going back to check previous responses, eliminates the possibility of erroneous transfer of data, and eases the burden of administering and taking the test in which the data are acquired. By use of randomization, PWC ensures that subjects see the stimuli pairs in random order, and that each subject sees pairs in a different random order.

PWC is written in Turbo Pascal v6.0 for IBM PC-compatible computers running MS-DOS. The program has also been successfully compiled with Turbo Pascal v7.0. A sample executable code is provided. PWC requires 30K of random-access memory for execution. The standard medium for distribution of this program is a 5.25-in. (13.335-cm), 360K MS-DOS-format diskette. Two electronic versions of the documentation are included on the diskette: one in ASCII format and one in MS Word for Windows format. PWC was developed in 1993.

This program was written by Wendell R. Parks of **Langley Research Center.** *Further information is contained in a TSP [see page 1].*

LAR-15143

Software for Computing Reliability of Other Software

Nonspecialists will likely prefer this program to others developed for the same purpose.

The Computer Aided Software Reliability Estimation (CASRE) computer program is a software tool developed for use in measuring the reliability of other software. CASRE is easier for nonspecialists in reliability to use than are many other currently available programs developed for the same purpose.

During the past 20 years, mathematical models of the reliability of software have been developed; these models can be used to predict the rates of failure of software systems. These models can be useful management tools during testing periods, enabling developers to (1) determine when the required reliabilities of software systems have been achieved, (2) estimate the times and efforts necessary to achieve required levels of reliability, and (3) quantitatively assess the effects of shortages of resources during testing periods.

CASRE incorporates the mathematical modeling capabilities of the public-domain Statistical Modeling and Estimation of Reliability Functions for Software (SMERFS) computer program and runs in a Windows software environment. CASRE provides a menu-driven command interface; the enabling and disabling of menu options guides the user through the (1) selection of a set of failure data, (2) execution of a

mathematical model, and (3) analysis of the results from the model.

Input to the models is simultaneously displayed as text and in a high-resolution form that can be controlled to enable the user to view the data in several different ways; for example, times between successive failures or cumulative numbers of failures. Predictions made by a model and statistical evaluations of the applicability of a model can be superimposed on a plot of data used as input to the model.

CASRE also incorporates earlier findings that the accuracy of prediction can be increased by combining the results of several models in a linear fashion. Users can define their own combinations of models, store them as part of the software configuration, and execute them in the same way as that of any other model.

This program would be particularly useful to software-development organizations searching for ways to manage their development resources more effectively. Inasmuch as CASRE was developed with the nonspecialist in mind, it should gain wider acceptance than do those software tools that require detailed knowledge of the models.

CASRE is written in C language for IBM PC-series and compatible computers running MS-DOS v5.0 or higher. This program requires 1MB of disk space for installation and up to 64KB of disk space for every failure-history file. The minimum required hardware and software required for running CASRE is the following: an 80386 processor with an 80387 coprocessor; Windows 3.1; 4MB of random-access memory (RAM); a mouse, trackball, or equivalent pointing device; a 16-in. (41-cm) or larger VGA monitor; and a video circuit card supported by Windows 3.1. Although CASRE can be executed on this minimum required hardware and software, the minimum combination of hardware and software recommended for execution of CASRE is the following: a 66-MHz 80486 DX/2 hardware system; Windows 3.1; at least 8MB of RAM; a mouse, trackball, or equivalent pointing device; a 19-in. (48-cm) VGA monitor; and a laser printer with a resolution of at least 300 dots per inch (12 dots per millimeter). CASRE may not function correctly on hardware based on the local bus architecture. The standard medium for distribution of CASRE is a 3.5-in. (8.89-cm), 1.44MB MS-DOS-format diskette. CASRE was developed in 1993 and is a copyrighted work with all copyright vested in NASA.

This program was written by Allen Nikora, Thomas M. Antczak, and Michael Lyu of Caltech for **NASA's Jet Propulsion Laboratory**. *Further information is contained in a TSP* *[see page 1]*.

NPO-19307

BLANK PAGE

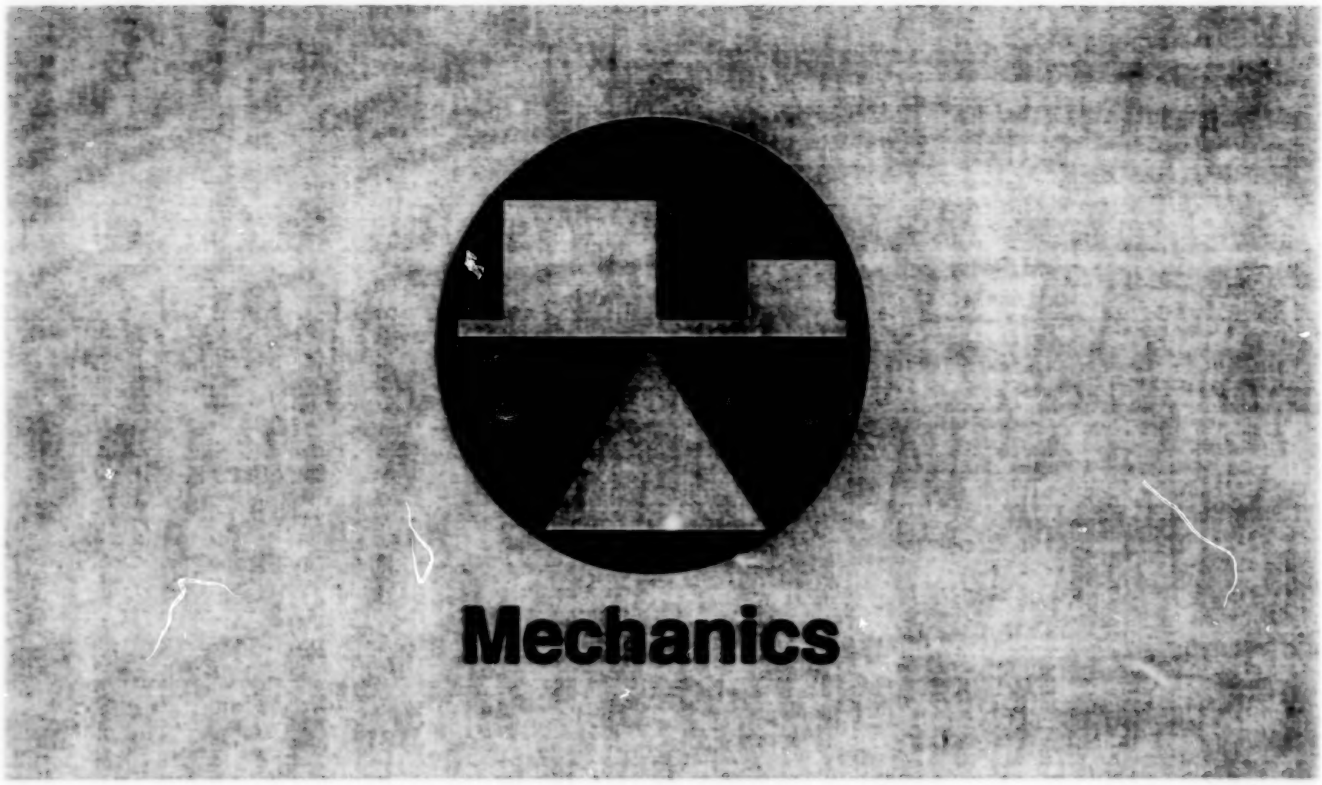

Mechanics

Hardware, Techniques, and Processes

Books and Reports

BLANK PAGE

Ceramic Replaces Metal in High-Performance Optomechanical Structures

Ceramic components feature dimensional stability, low cost, and ease of fabrication.

Langley Research Center, Hampton, Virginia

Recently developed ceramic materials and fabrication techniques have been integrated by Langley Research Center workers to produce superior optomechanical structures for spacecraft and aircraft instrumentation. The basic features of these novel supports, such as dimensional stability, low cost, and ease of fabrication, also make them ideal for many commercial optical systems as well.

Ceramic supports for optical components and benches offer important advantages over the usual metal parts. Ceramic materials expand and contract only slightly with changes in temperature. Moreover, they are relatively inexpensive and lightweight.

Nearly all optical components are mounted on supports and benches made of aluminum, stainless steel, or Invar (or equivalent) nickel/iron low-expansion alloy. Aluminum is lightweight, but expands and contracts significantly; its coefficient of thermal expansion at room temperature is 2.5×10^{-6}/°C. In optics, where precise alignments are essential, temperature-related dimensional changes can make a system inoperable. Stainless steel and Super Invar (or equivalent) have low coefficients of thermal expansion, about one-third and one-fifth, respectively, of that of aluminum; but they are heavy, expensive, and difficult to machine. In fact, much of the weight of optical systems is attributable to metal mounts.

Certain ceramics, on the other hand, have coefficients of thermal expansion lower than those of stainless steel and Invar, with density like that of aluminum, and they cost far less — about $10/lb ($22/kg) versus $1,000/lb ($2,200/kg) for Invar and $50/lb ($110/kg) for aluminum (1992 prices). Ceramics expand and contract only negligibly with changes in temperature and can thus be slip cast at Langley Research Center without temperature control.

Dimensionally stable optical mounts (far left of Fig. 1) and benches (Fig. 2), have been fabricated using a slip-casting technique. Slip casting is defined here as a process that consists of a slip (ceramic powders dispersed in an aqueous media) being poured into a porous mold, which extracts a large percent of the liquid from the slip leaving a semisolid part.

Figure 1. A Dimensionally Stable Optical Mount (left) is shown with a master pattern (right) and a silicone rubber mold (center).

Figure 2. This Ceramic Optical Bench was fabricated via slip-casting technique.

Developing a porous mold requires that a master pattern of required dimension be machined from aluminum, which is inexpensive, lightweight and easy to machine (far right of Fig. 1). Extreme importance was placed on design and preparation of the master, since it is the most important item in producing the mold.

The first step in producing a slip cast ceramic part is to fabricate a silicone rubber mold (middle of Fig. 1). Silicone rubber was used as the mold material because the silicon acted as a release agent for the molded parts. Hot wax was poured into the mold to produce a wax master. A quality inspection (dimensional and visually) is performed on the wax master upon its removal from the mold.

The wax master is encapsulated in a moisture-absorbing compound. The wax is burned out, leaving a dimensional cavity equal to that of the master. A ceramic slip is poured into the cavity and allowed to jell (1 to 2 h) before removing the mold. Because the mold becomes more plastic with increasing water absorption, it can be peeled off of the green ceramic body, regardless of the ceramic body shape.

A note of caution: If the ceramic part is placed in the furnace before final drying, the remaining moisture will turn to steam, and its volume will increase several hundred times. This steam will generate tremendous pressure within the ceramic part and explode or crack. To avoid explosions or cracks, the air around the piece must be totally saturated with water vapor as the temperature is raised to remove remaining moisture. No surface evaporation can then occur. After the piece has reached uniform temperature (below 100 °C), the relative humidity of the air around the piece can be slowly lowered to allow drying to occur.

Careful control of the temperature and humidity in the dryer is important. The dried piece is fired in a furnace, which can increase temperature at less than 1 °F/min (0.6 °C/min).

This work was done by Peter Vasquez, Robert L. Fox, and Stephen P. Sandford of **Langley Research Center**. *No further documentation is available.*
LAR-14948/LAR-14981

Optoelectronic Inclinometer

Tilt would be measured with respect to a vertical mirror.

Langley Research Center, Hampton, Virginia

A proposed optoelectronic instrument would measure the tilt of an object about a single horizontal axis by measuring the change of position and orientation of a laser beam reflected from a hanging mirror. The mirror would remain vertical while the rest of the instrument rotated with the object.

The instrument (see figure) would include a rectangular open frame mounted in the object, the tilt of which was to be measured. The mirror, made of heavy material or weighted, would be mounted in high-quality bearings in a gimbal that would, in turn, be held by a rod pivoted at its upper end. Thus, the rod, gimbal, and mirror taken together would constitute a pendulum. The frame or enclosure would be oriented so that the gimbal axis would be nominally parallel to the axis about which the tilt was to be measured, while the pivot axis of the pendulum would be nominally horizontal and perpendicular to the gimbal axis.

Acting via the combination of the pendulum and gimbal, gravitation would keep the mirror vertical when the frame tilted about either or both horizontal axes. A source of light (e.g., a laser diode or a light-emitting diode equipped with a collimating or focusing lens) would emit a beam that would be reflected from the mirror onto a linear array of photodetectors. The source of light would be oriented so that at zero tilt, both the beam of light from the source and the beam reflected by the mirror would lie in a horizontal plane, and the reflected beam would land at or near the midlength of the linear array of photodetectors. As the object and the instrument frame tilted about an axis parallel to the gimbal axis (pitch), the spot of light cast by the reflected beam would be translated along the array. Tilt of the object and instrument frame (about the pivot axis of the pendulum (roll)) would produce a small (second-order) change in the position of the spot with respect to the array, but this effect may be tolerable at small tilt angles. The maximum amount of tilt about the pivot axis of the pendulum that the instrument could tolerate would depend on the size of the mirror and the physical size of the linear array and the spacing of the components. A compensating lens could be included to correct for nonlinearity and to ensure that the beam continued to fall on the array throughout the desired angular range of the instrument.

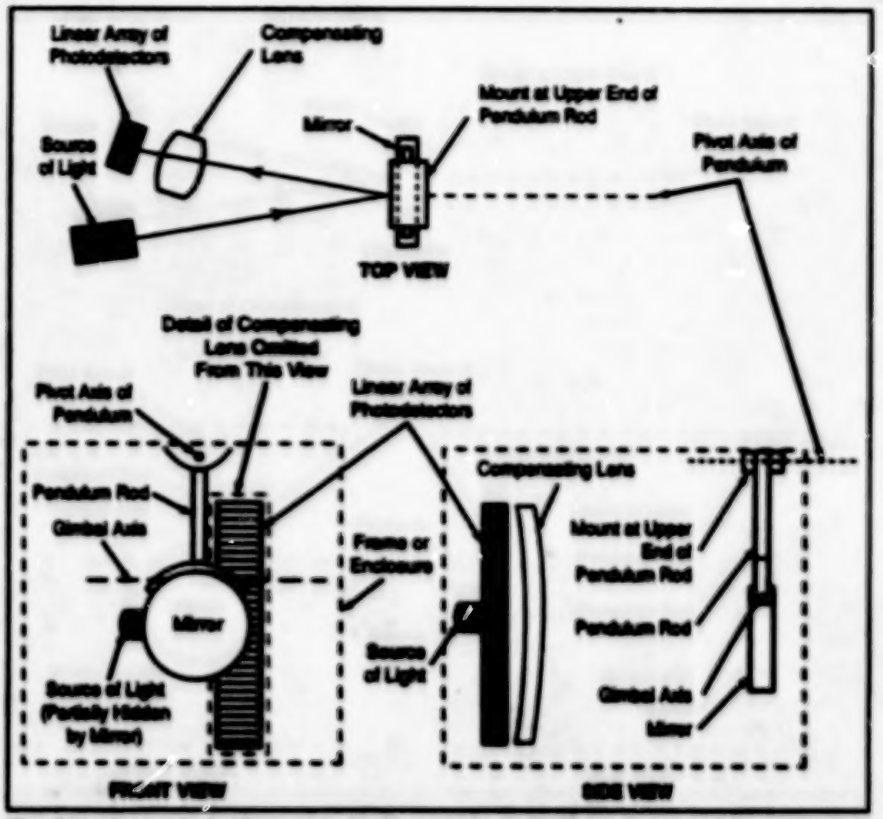

The Optoelectronic Inclinometer would measure tilt about the gimbal axis by measuring the change in position and orientation of the beam of light reflected from the mirror hanging in the gimbal.

This work was done by Timothy D. Schott of Langley Research Center. No further documentation is available.

Inquiries concerning rights for the commercial use of this invention should be addressed to the Patent Counsel, Langley Research Center [see page 1]. Refer to LAR-14728.

More About Pressure Probes for Turbulent Flows

An array of probes yields data on static and total pressures and cross-stream turbulence.

Ames Research Center, Moffett Field, California

The figure illustrates an array of pressure probes for use in a turbulent stream of inviscid, incompressible fluid. The measurements of the probes in this array can be processed into time-averaged values of the static pressure, the total pressure based on the entire velocity, the stagnation pressure based on the time-averaged streamwise component of velocity (along which the probe tubes are required to be aligned), and cross-stream turbulence.

The array is a combination of the separate pressure-probe arrays described in "Measuring Streamwise Momentum and Cross-Stream Turbulence" (ARC-11934), *NASA Tech Briefs*, Vol. 16, No. 8, (August 1992), page 53, and "Array of Probes To Measure Static Pressure and Turbulence" (ARC-12973), *NASA Tech Briefs*, Vol. 18, No. 9, (September 1995), page 108. To recapitulate: Each probe is designed by applying potential-flow theory to the flow field on and near its surface. An upstream-facing probe orifice can be shaped to sense the stagnation pressure based on the entire velocity or on one or

more components of velocity — in this case, the streamwise component. An orifice on the side of the probe tube downstream from the tip can be positioned to sense a combination of static pressure and pressure attributable to cross-stream turbulence. The cross-sectional shape of a probe tube can be made elliptical, and the probe orifices positioned around the circumference in such a way as to increase or decrease, by a known factor, its response to one of the components of cross-stream turbulence.

The equations that express the directional responses of the various probes in the array can be solved together to eliminate unknown quantities; this makes it possible to process the digitized time-averaged probe readings together to obtain the time-averaged static, stagnation, and cross-stream-turbulence pressures. In the case of the five-probe array shown in the figure, one obtains the time averages of the two stagnation pressures, plus redundant values of the time-averaged static pressure and the time-averaged cross-stream-turbulence pressures.

This work was done by Vernon J. Rossow of **Ames Research Center.** *Further information is contained in a TSP [see page 1].*

This invention is owned by NASA, and a patent application has been filed. Inquiries concerning nonexclusive or exclusive license for its commercial development should be addressed to the Patent Counsel, Ames Research Center [see page 1]. Refer to ARC-11935.

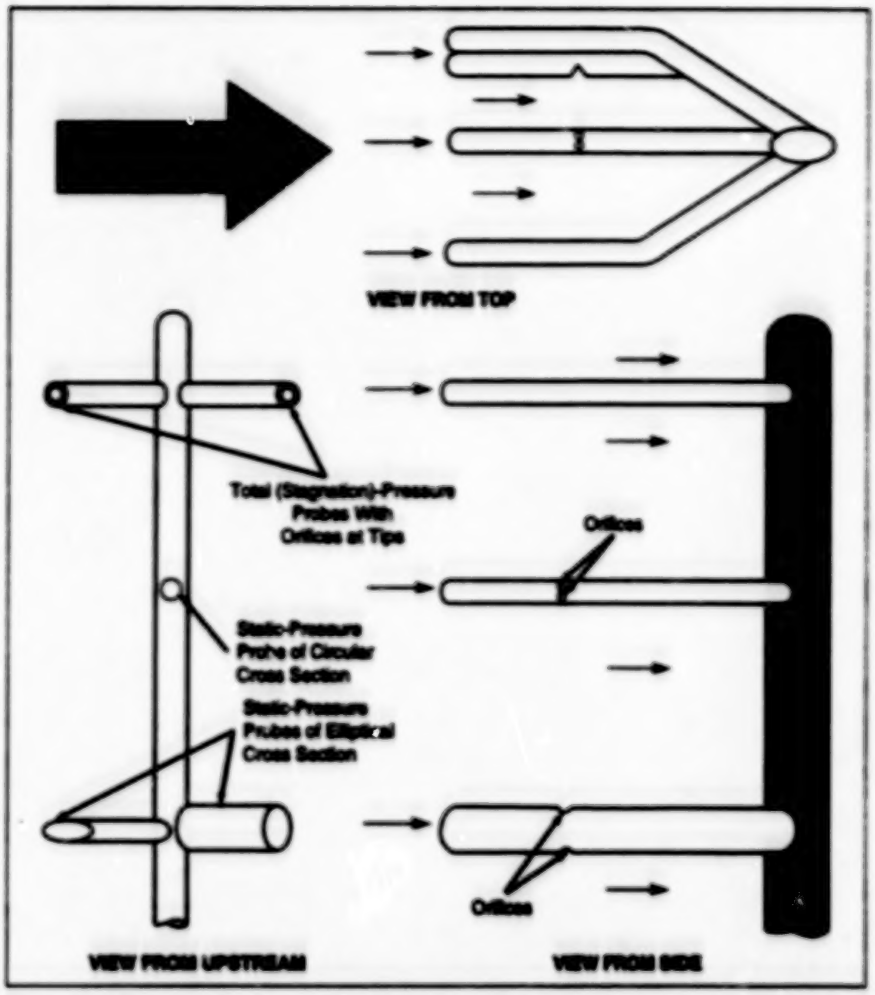

These Five Pressure Probes yield readings from which one can compute time averages of the entire and streamwise stagnation pressures, the static pressure, and the pressures associated with the two components of cross-stream turbulence. The three lower probes yield data that are redundant (in principle) and that could, therefore, be used to reduce errors.

Adaptive Force Control for Compliant Motion of a Robot

Performance is expected to be stable and uniform despite gross variations in environmental stiffnesses.

NASA's Jet Propulsion Laboratory, Pasadena, California

Two adaptive control schemes offer robust solutions to the problem of stable control of the forces of contact between a robotic manipulator and objects in its environment. These schemes were developed within the compliant-motion control framework, as were a number of other robot-control schemes reported previously in *NASA Tech Briefs*.

A control scheme that ensures stable and robust operation of a robotic manipulator in contact with objects in its environment is a basic requirement for the successful execution of many robotic tasks. The control problem is especially challenging in an environment in which the stiffnesses of objects with which the end effector of the robot can make contact ("environmental stiffnesses" for short) are unknown and/or subject to change. The present control schemes provide for automatic tuning of the force controller of the robot to compensate for unknown and/or changing environmental stiffnesses in order to yield stable, uniform, and acceptable performance.

The two control schemes (see figure) are called "adaptive admittance control" and "adaptive compliance control." Both schemes involve the use of force-and-torque sensors that indicate contact forces, **F**. The force-and-torque sensors can be replaced with proximity sensors, the outputs of which can be processed into virtual-contact-force signals, as though the end effector made contact with a nearby object via a spring. These virtual-contact-force signals are useful in preventing collisions with objects, following contours, and maintaining desired standoff distances.

Admittance control is an explicit force-control scheme in which a force set point, $\mathbf{F}_r$, is specified by the user and is tracked by a force compensator. This scheme is based partly on the concept of mechanical admittance, which relates the contact force to the resulting velocity perturbation. The end effector of the robot is commanded to deviate from its commanded position $\mathbf{X}_r$ by the amount $\mathbf{X}_f$ and to track the modified commanded trajectory $\mathbf{X}_c$. Two adaptive proportional-plus-integral-plus-derivative (PID) and proportional-plus-integral (PI) force compensators have been developed thus far and found to ensure robust tracking.

Compliance control is an implicit force-control scheme: this scheme establishes robot/environment-interaction dynamics specified by the user in terms of a contact

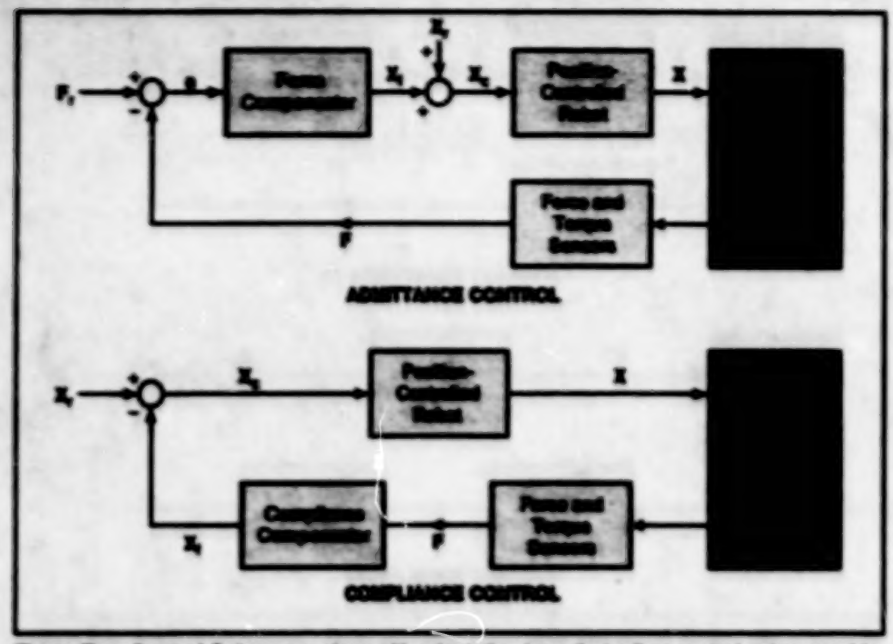

These Two Control Schemes, along with adaptation laws that adjust control gains, provide robust, stable control of a robot operating in the presence of unknown and/or changing environmental stiffnesses.

force as function of the difference between the actual position X and the desired position, X_c, of the end effector. Two adaptive lag-plus-feedforward compliance compensators have been developed. The compliance compensators and the PI force compensator do not require information on the rate of change of force. Both the admittance and compliance control schemes include adaptation laws that constantly adjust the compensator gains to drive tracking errors toward zero; this is the feature that helps to ensure stable and uniform performance despite large variations in environmental stiffnesses.

These schemes performed well when tested in computational simulations in which they were used to control a seven-degree-of-freedom robot arm in executing contact tasks. The admittance scheme offers (1) the advantage of robust tracking of force set points and rejection of constant disturbances and (2) the disadvantage of requiring switching between reference motion command trajectories for unconstrained tasks and force-set-point command trajectories for constrained tasks and possibly poor responses during transitions between them. The compliance scheme involves the use of reference motion commands in tasks of both types, so that it does not require switching of commands and therefore affords generally good responses during transitions. However, the compliance scheme offers the disadvantage of possibly less robust tracking of force commands and rejection of force disturbances. Therefore, the choice between admittance or compliance control is dictated by the requirements of the application at hand.

This work was done by Homayoun Seraji of Caltech for NASA's Jet Propulsion Laboratory. Further information is contained in a TSP (see page 1).
NPO-19507

Quick-Release Pin With Lever Action

The mechanism can be operated with a gloved hand. *Lyndon B. Johnson Space Center, Houston, Texas*

The figure illustrates original and modified versions of a quick-release ball-detent pin with a T-handle. The original version is a commercially available mechanism called a "pip pin," and is released by pressing the button on the handle. The original version is advantageous in that it resists inadvertent actuation. However, it is disadvantageous in that the operator must exert a force on the button, usually by pressing on the button with a thumb while simultaneously grasping the T-handle with at least two other fingers; this can be difficult to do, especially when wearing a heavy glove.

In the modified version, a lever has been added to the handle to facilitate actuation. The lever action reduces the actuation force. In addition, one is no longer limited to use of a thumb and at least two fingers to exert the reduced actuation force; the lever-action pin can also be operated by squeezing on any point of the movable ends of the lever and handle together between a thumb and forefinger or by simply grasping and squeezing the handle and lever with the entire hand in a more natural grasp. Tests showed that the modified release pin can be operated easily with a gloved hand.

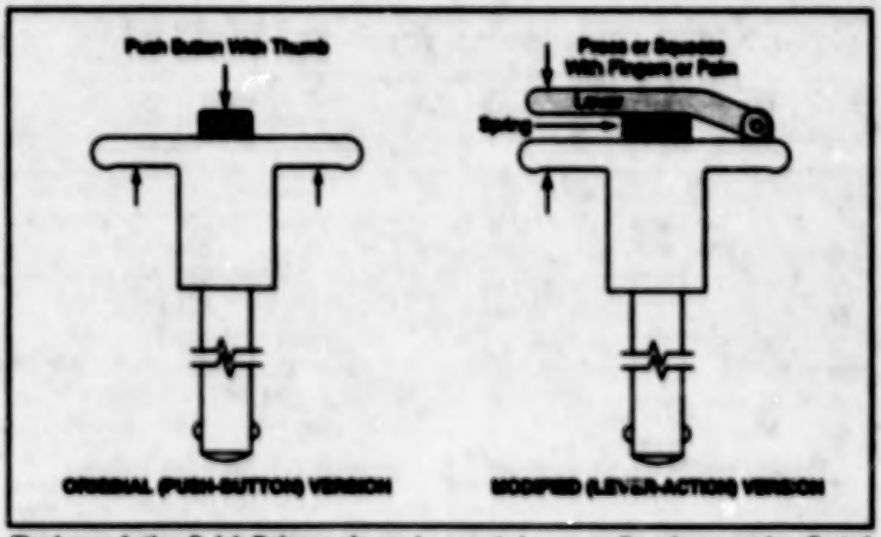

The Lever-Action Quick-Release pin can be operated more easily; release can be effected with less force and with simpler gripping configurations that are more suitable for gloved hands.

This work was done by Robert C. Trevino of Johnson Space Center. Further information is contained in a TSP (see page 1).
MSC-22398

Inversion of Dynamical Equations for Control of Attitude

Quaternion and direction-cosine formulations lead to direct inversion for linear feedback control.

Ames Research Center, Moffett Field, California

A method of inverting the nonlinear equations of the rotational dynamics of a rigid body could be used to design feedback control of the orientation of the body. The method is applicable to both direction-cosine and quaternion formulations, which are suitable for large-angle maneuvers. (These formulations are preferable to a Euler-angle formulation, which lends itself readily to inversion, but is not suitable for large-angle maneuvers.) Exploiting some apparently little-known properties of the direction cosine and quaternion formulations, the method leads to equations for a model-follower control system that exhibits exactly linear attitude-error dynamics.

Taking parallel approaches in both the direction-cosine and quaternion formulations, the method involves the simplification of the inversion of the equations for the angular accelerations as functions of the applied torques. The simplification is effected by transformations of coordinates that make it possible to express the angular velocity and angular acceleration in terms of the direction-cosine or quaternion elements and their derivatives with respect to time, the transformations being such that the resulting equations of state are linear.

Figure 1 depicts schematically the linearized attitude-control systems based on the two formulations. The direction-cosine system is limited to following roll-angle commands in the range of +180°, while the quaternion system can follow commands in the range of +360°.

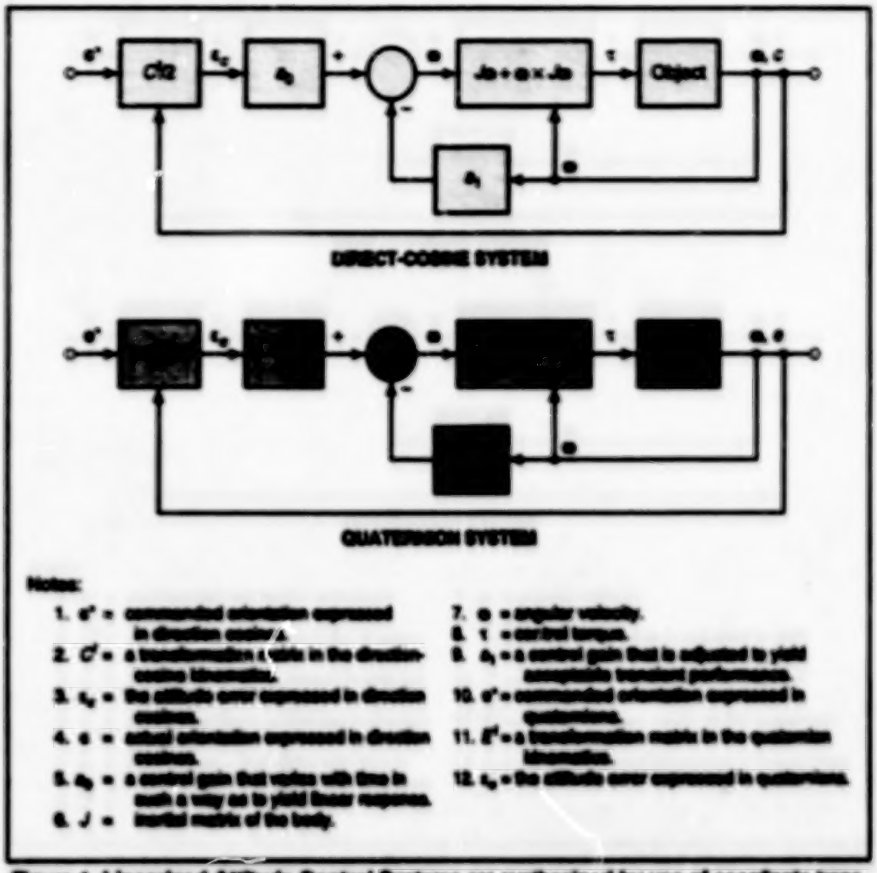

Notes:

1. C^c = commanded orientation expressed in direction cosines
2. C^t = a transformation matrix in the direction-cosine kinematics
3. ϵ_c = the attitude error expressed in direction cosines
4. C = actual orientation expressed in direction cosines
5. k_p = a control gain that varies with time in such a way as to yield linear response
6. J = inertial matrix of the body
7. ω = angular velocity
8. τ = control torque
9. k_v = a control gain that is adjusted to yield acceptable transient performance
10. q^c = commanded orientation expressed in quaternions
11. B^t = a transformation matrix in the quaternion kinematics
12. ϵ_q = the attitude error expressed in quaternions

Figure 1. Linearized Attitude-Control Systems are synthesized by use of coordinate transformations that simplify the inversion of the basic equations of motion of a rigid body.

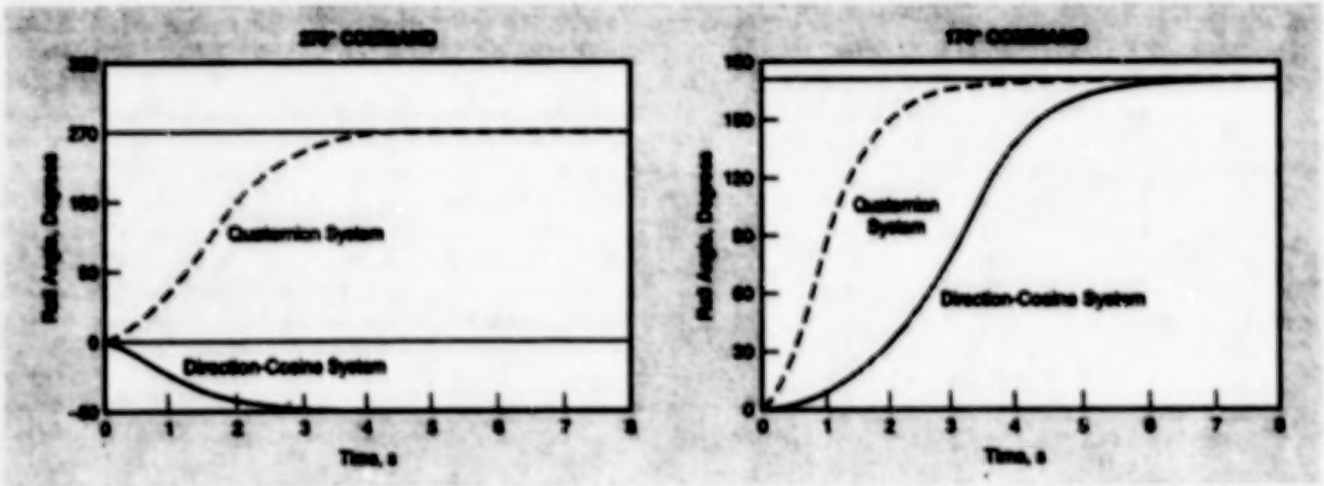

Figure 2. The Responses of Two Attitude-Control Systems to roll-angle commands were tested by computer simulation. The direction-cosine system cannot respond to commands outside the range of ±180°: it reacts to a command of 270° as though it were a command of −90°.

The error amplitude in the quaternion formulation is a maximum for commands of +180°, for which the error amplitude in the direction-cosine formulation is zero. Therefore, the quaternion system should be more robust in responding to large roll-angle commands, as demonstrated in Figure 2.

This work was done by Ralph Bach and Russell Paiell of Ames Research Center. Further information is contained in a TSP [see page 1].

Inquiries concerning rights for the commercial use of this invention should be addressed to the Patent Counsel, Ames Research Center [see page 1]. Refer to ARC-12769.

Unified Approach to Control of Motions of Mobile Robots

An updated configuration-control scheme incorporates a distinction between holonomic and nonholonomic constraints.

NASA's Jet Propulsion Laboratory, Pasadena, California

An improved computationally efficient scheme has been developed for on-line coordinated control of both manipulation and mobility of robots that include manipulator arms mounted on mobile bases. The present scheme is similar to the one described in "Coordinated Control of Mobile Robotic Manipulators" (NPO-19109), page 59, this issue. Both schemes are based on the configuration-control formalism. The major difference between the two schemes is that unlike the previous one, the present one incorporates an explicit distinction between holonomic and nonholonomic constraints (see figure). Both schemes are characterized by computational efficiency and flexibility, which are advantageous for on-line, real-time control.

In addition to the article cited above, several other prior articles in *NASA Tech Briefs* have discussed aspects of the configuration-control formalism. These include "Increasing the Dexterity of Redundant Robots" (NPO-17801), Vol. 14, No. 10 (October, 1990), page 88; "Redundant Robot Can Avoid Obstacles" (NPO-17852), Vol. 15, No. 10 (October, 1991), page 88; "Configuration-Control Scheme Copes With Singularities" (NPO-18556), Vol. 17, No. 2 (February, 1993), page 81; and "More Uses for Configuration Control of Robots" (NPO-18807/NPO-18808), Vol. 17, No. 10, (October, 1993), page 120. To recapitulate: A robot has n degrees of freedom. The basic task is to make the end effector (the hand at the tip of the manipulator arm) follow a prescribed trajectory in m-dimensional coordinates (where $m < n$). The $r = n-m$ redundant degrees of freedom are used simultaneously to perform an additional task.

The additional task can be specified by the user and can include (but is not limited to) reaching around obstacles, avoiding collisions with objects in the workspace, maintaining one or more links of the manipulator arm in a desired pose, and/or optimizing the overall kinematics in both the redundant and nonredundant degrees of freedom to enhance overall manipulability. The additional task is mathematically modeled by a set of kinematic functions that, in effect, define the trajectory in the redundant degrees of freedom. The user can assign weighting factors to individual degrees of mobility or manipulation as well as to each task specification. The user can also change task specifications and weighting factors during operation.

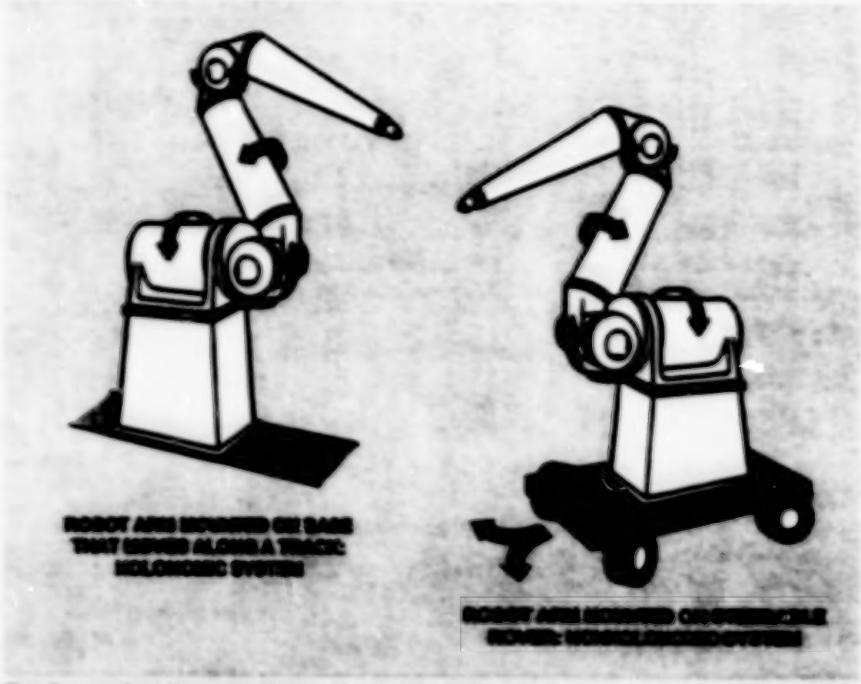

The Constraints Upon the Motion of a Mobile Base that supports a robot arm can be either holonomic (e.g., the kinematic constraints upon a mobile base that moves along a track) or nonholonomic (e.g., the kinematic constraints upon a mobile base with wheels like that of an ordinary highway vehicle).

In the present scheme, the degrees of mobility and the degrees of manipulation are treated within a common theoretical framework; to put it in slightly different terms, the mobile base and the manipulator arm are treated as closely interacting subsystems of the overall robotic system, rather than as two separate entities. Within this framework, the kinematic constraints upon the manipulator subsystem are holonomic, whereas those on the mobile base can be nonholonomic, depending on the type of mobile base. All degrees of freedom are treated on an equal footing according to the computationally efficient configuration-control formalism. The nonholonomic kinematic constraints (if any) fit naturally into the configuration-control formalism: the nonholonomic kinematic constraints, the desired motion of the end effector, and the additional task specified by the user are combined to form a set of augmented tasks. These tasks are then accomplished in a coordinated manner by use of the configuration-control equations to determine the motion in each mobility and manipulation degree of freedom.

This work was done by Hornayoun Seraji of Caltech for NASA's Jet Propulsion Laboratory. Further information is contained in a TSP [see page 1].

NPO-19508

Mechanism for Adjustment of Commutation of Brushless Motor

The adjustment can be performed while the motor is running.

Marshall Space Flight Center, Alabama

A mechanism enables the adjustment of the angular position of a set of Hall-effect devices that sense the instantaneous shaft angle of a brushless dc motor. The outputs of the sensors are fed to commutation circuitry. Measurement of the shaft angle is essential for commutation; that is, the application of voltage to the stator windings must be synchronized with the shaft angle. To obtain the correct angle measurement for commutation, the Hall-

effect angle sensors must be positioned at the proper reference angle.

The Hall-effect angle sensors are mounted on an annular board called, appropriately, the "commutation board." The commutation board is mounted on one end of the motor housing. Part of the rotor and shaft pass through the central hole of the commutation board. Heretofore, the angular position of the sensors was adjusted by turning off the motor, removing the end cap (which covers the commutation board), loosening the mounting screws that hold the commutation board, and manually rotating the commutation board by a small amount. The cap was then reinstalled and the motor was turned on, and the current drawn by the motor was measured. This procedure was repeated until an approximately minimum current reading was obtained. (A minimum current reading signifies maximum operating efficiency.)

The present mechanism (see figure) accelerates the adjustment procedure and makes it possible to obtain a more accurate indication of the minimum-current position because it provides for adjustment while the motor is running. The commutation board is held on the end of the housing by three mounting screws that are fitted with close tolerance to short circumferential slots in the board. Preload springs under the heads of the mounting screws prevent inadvertent rotation of the commutation board when the screws are loosened for an adjustment. A gear sector is mounted at a location on the periphery of the commutation board; this gear sector engages a pinion sector that turns on a pin attached to the housing. The pinion and gear sectors feature a zero-backlash design.

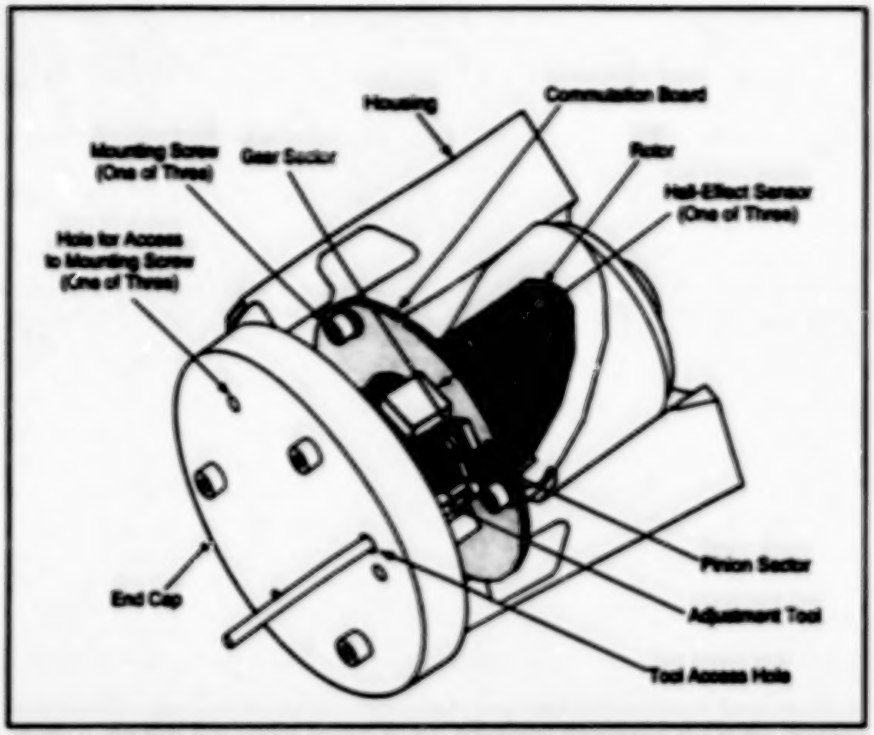

Holes in the End Cap provide access to the adjustment mechanism and to the mounting screws that hold the commutation board on the end of the housing.

A socket on the pinion receives an adjusting tool. To perform an adjustment, one inserts the tool in the socket via an access hole in the end cap. The tool is turned to rotate the pinion. By virtue of the gear ratio, this effects a fine angular adjustment of the commutation board. Once the adjustment yields a minimum current reading, the preload springs hold the board until the mounting screws are retightened.

This work was done by Richard E. Schaefer of United Technologies Hamilton Standard for Marshall Space Flight Center. Further information is contained in a TSP [see page 1].

This invention is owned by NASA, and a patent application has been filed. Inquiries concerning nonexclusive or exclusive license for its commercial development should be addressed to the Patent Counsel, Marshall Space Flight Center [see page 1]. Refer to MFS-28958.

Modular Track System for Positioning Mobile Robots

A manipulator could reach desired positions more quickly and easily.

NASA's Jet Propulsion Laboratory, Pasadena, California

A conceptual system for positioning mobile robotic manipulators on a large main structure would include modular tracks and ancillary structures that could be assembled easily along with the main structure. The system, called the "tracked robotic location system" (TROLS), was originally intended for application to platforms in outer space, but the TROLS concept might also prove useful on Earth; for example, to position robots in factories and warehouses.

The design of the TROLS would inherently solve some of the problems commonly encountered in positioning and orienting mobile robots. The surfaces of the main structure would be covered with the

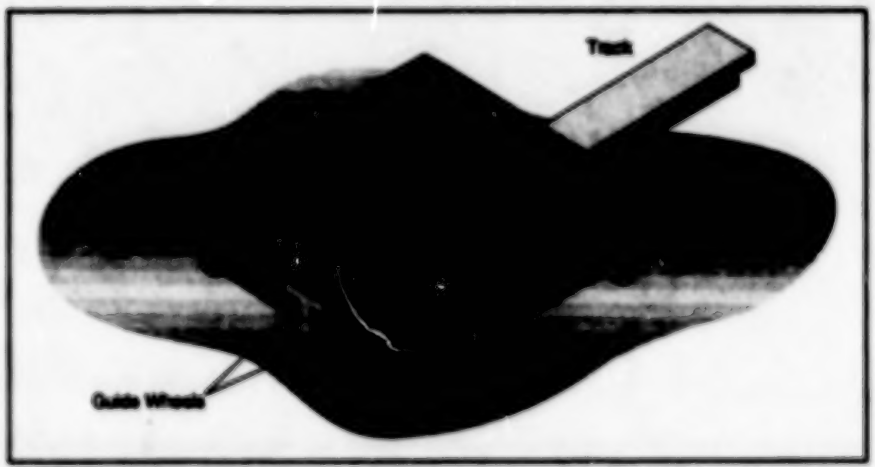

A T-Cross-Section Rail would keep a mobile robot on its track. Bar codes would mark locations along the track.

tracks, enabling the robots to reach all areas of interest. The contact between a robot and its tracks would automatically enforce the correct orientation. The main structure or the ancillary structures adjacent to the tracks would be marked with bar codes. Each robot would be equipped with bar-code-recognizing circuitry so that it could quickly find its way to its assigned location.

The tracks of the TROLS could be in the form of rails (see figure), grooves, or channels. The tracks would be built with standard dimensions and spacing so any module could be aligned with any adjacent module. The tracks would be located to enable robots to reach any object with which robots were required to interact.

This work was done by Jeff Miller of Caltech for NASA's Jet Propulsion Laboratory. Further information is contained in a TSP [see page 1].
NPO-19387

Calibration Valve With Built-In Test Port

A calibration valve includes a built-in test port for calibrating control-panel gauges in place, without having to remove them for calibration. The use of this valve reduces the number of plumbing parts and thus the number of potential leakage points. In addition, the application of the calibration valve saves time when calibrating the control-panel gauges or transducers and prevents damage or loss of the instruments by not having to remove them from the control panel for calibration.

This work was done by Carmine A. Pilchi of Rockwell International Corp. for Johnson Space Center. Further information is contained in a TSP [see page 1].
MSC-22410

Books and Reports

Alternative Habitats for First Lunar Outpost

A report describes an investigation of alternative design concepts for habitable structures at an outpost to be established on the Moon. Beginning with a baseline habitat concept derived from a habitat module of the Space Station *Freedom*, the investigation was directed toward modification of the baseline design to achieve five design goals. The first goal was better access by personnel to the surface of the Moon. For example, the airlock could be relocated under the habitat for easier access. Alternatively, the landing spacecraft could be modified to lower the habitat closer to the lunar surface so that the height for lifting objects would be reduced. The second goal was to provide for future expansion of the outpost by disconnecting the habitat module from the landing spacecraft and moving and connecting it to other modules at the outpost. Provisions for achieving these goals could include ramps, suspension cables, hoists, and equipping modules with limited capabilities as wheeled land vehicles. The third goal was increasing habitable volume. This could be done by redesign and by use of spent fuel tanks as enclosures for additional habitable space. The fourth goal was protection against radiation; no specific action toward this goal was proposed. The fifth goal was reduction of the overall mass. This could be accomplished by redesign, using lightweight materials like aluminum/lithium and metal-matrix composites.

This work was done by Charles R. Fowler, Kauser S. Imtiaz, Irwin E. Vas, and Gordon R. Woodcock of the Boeing Co. for Marshall Space Flight Center. To obtain a copy of the report, "Alternative Habitats for First Lunar Outpost," see TSP's [page 1].
MFS-28953

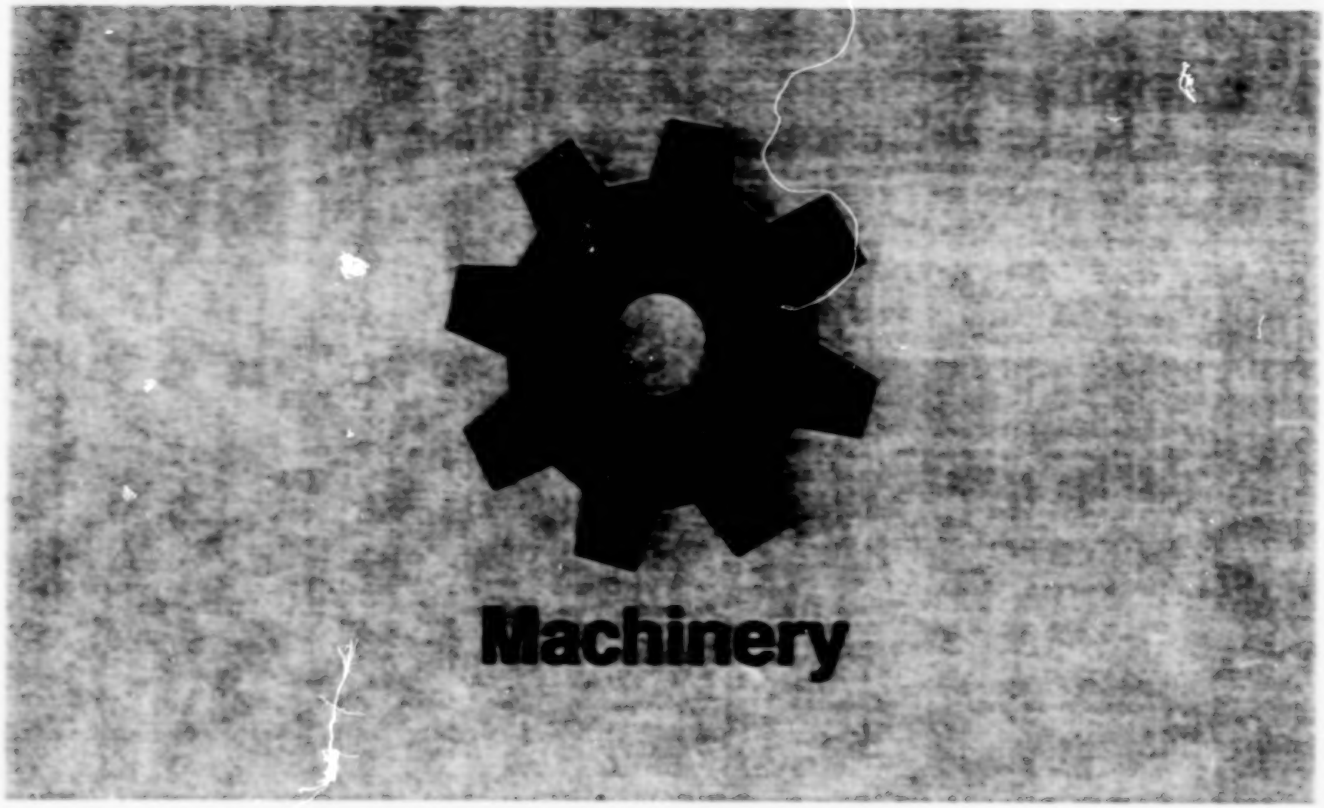

Hardware, Techniques, and Processes

BLANK PAGE

Inflatable Pole

This portable device extends reach up to 20 ft (6 m). *Lyndon B. Johnson Space Center, Houston, Texas*

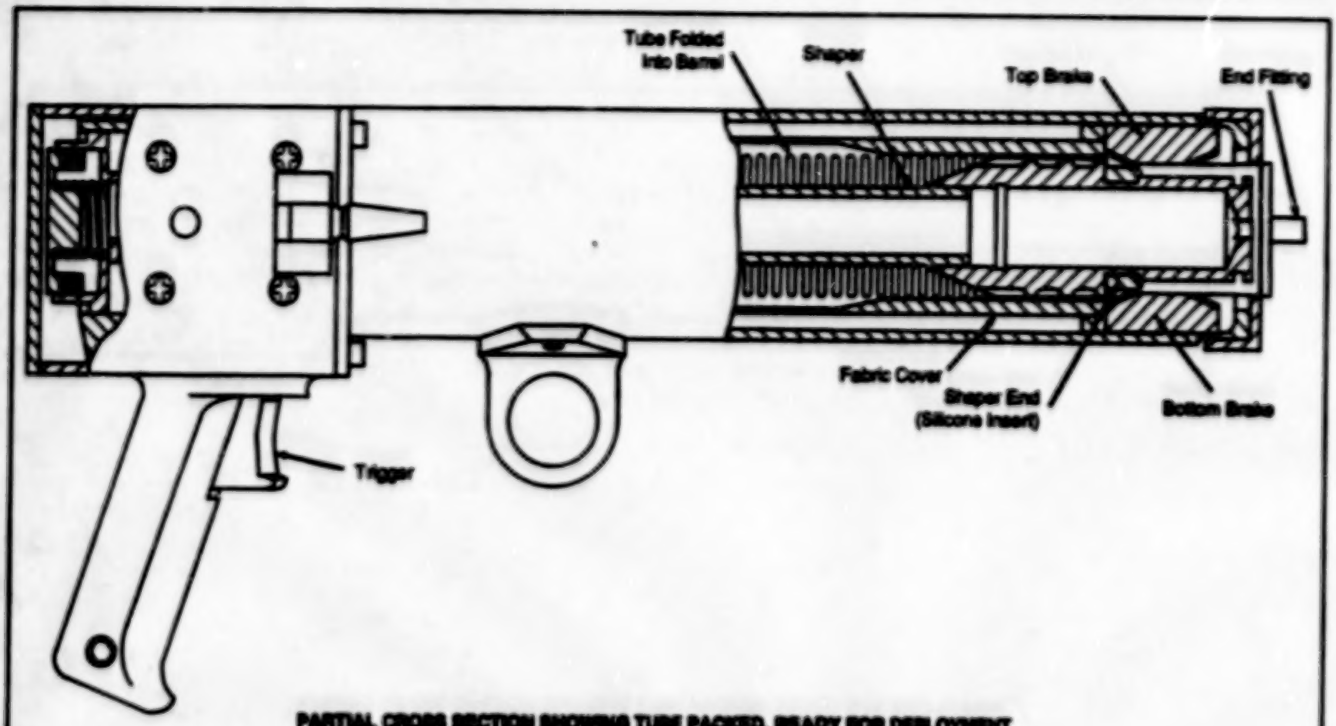

PARTIAL CROSS SECTION SHOWING TUBE PACKED, READY FOR DEPLOYMENT

INFLATABLE POLE IN USE

Before Deployment, the inflatable tube is neatly pleated in the space between the shaper tube and the fabric sheath. After deployment, it extends stiffly from the barrel of the gun.

An inflatable pole is a lightweight, portable tool for reaching an object at a height or across a gap. When not in use, the tool collapses to 3 to 5 percent of its inflated length. The pole was developed for use as a self-rescue device by an astronaut who becomes untethered outside a spacecraft: the astronaut would use the pole to reach a grapple on the spacecraft and pull to it. The pole might also be useful on Earth as a rescue device or in performing routine tasks like changing a high light bulb without a ladder.

The pole includes a 2-in.-diameter (10-cm-diameter) tube of urethane-coated Kevlar (or equivalent polyester) fabric. Before use, the tube is bunched on a shaper rod in a gas gun (see figure). To deploy it, a user presses the trigger of the gun releasing a regulated 30-psi (0.21-MPa) blast of nitrogen from a separate bottle. The gas inflates the tube. A fabric cover prevents snagging and ensures that the tube emerges straight.

The operator can stop deployment of the tube at any point up to its maximum 20-ft (6.1m) extension by releasing the trigger: this action applies the brakes on the gun barrel. The operator thus controls the length of the pole. Once deployed, the tube remains inflated and stiff while the operator uses it. The tube weighs only about 7 oz. (0.2 kg); thus, it has low inertia when extended, so that it can be maneuvered easily.

When the task with the inflatable pole has been completed, the operator opens a vent valve to deflate the tube. The operator then opens the gun, removes the fabric cover, and repacks the tube.

This work was done by Scott A. Swan of **Johnson Space Center**. *Further information is contained in a TSP [see page 1].*

This invention is owned by NASA, and a patent application has been filed. Inquiries concerning nonexclusive or exclusive license for its commercial development should be addressed to the Patent Counsel, Johnson Space Center [see page 1]. Refer to MSC-22244.

Shielded, Automated Umbilical Mechanism

Fluid and/or electrical connectors are protected against debris.

Lyndon B. Johnson Space Center, Houston, Texas

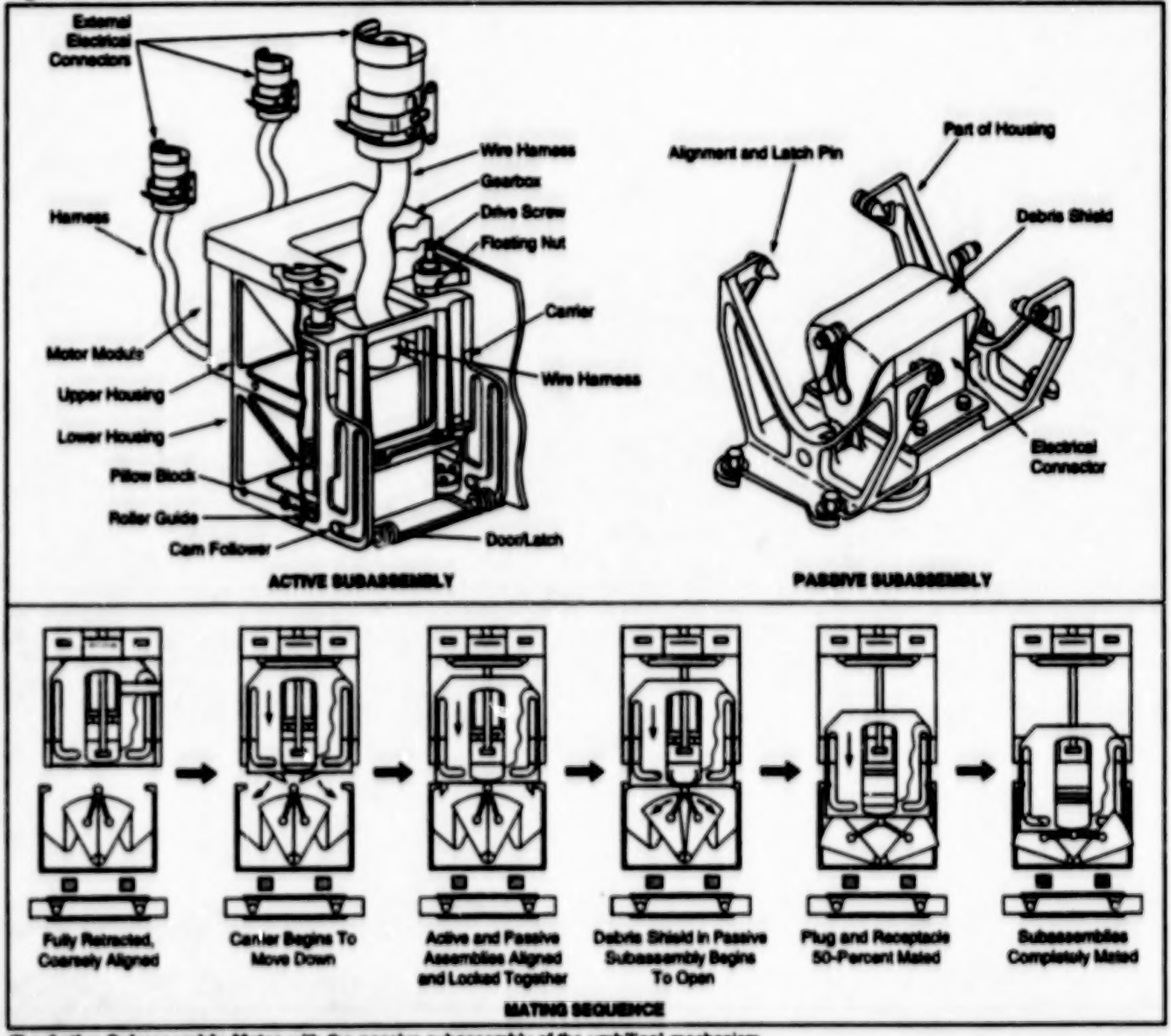

The Active Subassembly Mates with the passive subassembly of the umbilical mechanism.

An umbilical mechanism automatically connects and disconnects various fluid couplings and/or electrical contacts while shielding the mating parts from debris. The mechanism reacts mating and demating loads internally, without additional supporting structures.

The mechanism is designed for service in outer space, where its shields would protect against micrometeoroids, debris, ultraviolet radiation, and atomic oxygen. It could be used on Earth to connect or disconnect fluid or electrical utilities in harsh environments like those of nuclear powerplants or undersea construction sites, or in the presence of radioactive, chemical, or biological hazards, for example.

The mechanism consists of an active and a passive subassembly. It can accommodate an initial linear misalignment of 0.250 in. (6.35 mm) and angular misalignment of 2° between the subassemblies.

The mating sequence consists of the following steps (see figure):

1. The active subassembly with its connector retracted is coarsely aligned relative to the passive subassembly.
2. A carrier in the active subassembly begins to move a plug down as a cam action opens the debris shields in this subassembly.
3. The active and passive subassemblies are precisely aligned and locked together by a pin-and-drogue device.
4. Acting via a cam and linkage, the carrier in the active subassembly begins to open the debris shield of the passive subassembly.
5. When the debris shield in the passive subassembly is completely open, the plug attached to the active subassembly is 50-percent mated with a receptacle in the passive subassembly.
6. The carrier continues to extend the plug until it is completely mated with the receptacle.

All functions — extension of the plug, mating, and movement of the debris shields — are actuated by a single motor. If the mechanism jams or fails at any point in the sequence, an override feature in the drive train allows manual operation. The plug and receptacle in the mechanism can readily be changed between fluid-transfer and electrical applications.

This work was done by Daniel R. Barron, Brion F. Morrill, and Vytas Jasulaitis of McDonnell Douglas Corp. for **Johnson Space Center**. *Further information is contained in a TSP [see page 1].*

Title to this invention has been waived under the provisions of the National Aeronautics and Space Act [42 U.S.C. 2457 (f)] to McDonnell Douglas Corp. Inquiries concerning licenses for its commercial development should be addressed to

John Scholl, Counsel
McDonnell Douglas Corp.
5301 Bolsa Avenue
Huntington Beach, CA 92647
(714) 896-5999

Refer to MSC-22053, volume and number of this NASA Tech Briefs *issue, and the page number.*

Coordinated Control of Mobile Robotic Manipulators

A computationally efficient scheme is suitable for real-time implementation.

NASA's Jet Propulsion Laboratory, Pasadena, California

A computationally efficient scheme has been developed for on-line coordinated control of both manipulation and mobility of robots that include manipulator arms mounted on mobile bases. The scheme is applicable to a variety of mobile robotic manipulators, including robots that move along tracks (typically, painting and welding robots), robots mounted on gantries and capable of moving in all three dimensions, wheeled robots (see figure), and compound robots (consisting of robots mounted on other robots).

In the past, robots were typically mounted on stationary bases bolted to floors so that they could withstand the forces and torques applied to the bases when the robot arms carried payloads. However, there are significant advantages to placing robot arms on mobile bases. The mobility of a base extends the reach of the manipulator arm and increases the size of the robot workspace substantially at minimal cost. The additional movement of the base complicates the robot-control problem, but the availability of low-cost, high-performance computers makes it possible to achieve real-time control with computationally efficient algorithms like those of the present control scheme.

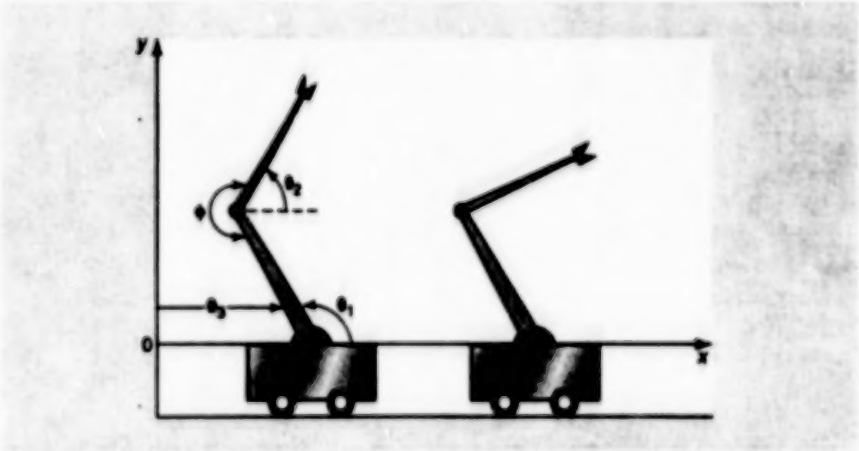

A Two-Link Robotic Manipulator Arm on a Wheeled Base has redundant degrees of freedom that can be exploited via a control method based on the configuration-control formalism.

In some prior approaches taken in the development of control schemes, the additional degrees of freedom in the mobility of the base would have been regarded unfavorably because of the additional complexity that they introduce. In the present approach, the additional degrees of freedom are turned to advantage by using them to accomplish additional tasks specified by the user. Furthermore, the on-line nature of the present method is enhanced by the ability of the user to change the specifications of tasks during operation, as described below.

The theoretical basis of the present method is the configuration-control formalism, which was discussed in several prior articles in *NASA Tech Briefs*, including "Increasing the Dexterity of Redundant Robots" (NPO-17801), Vol. 14, No. 10 (October, 1990), page 88; "Redundant Robot Can Avoid Obstacles" (NPO-17852), Vol. 15, No. 10 (October,

1991), page 86; "Configuration-Control Scheme Copes With Singularities" (NPO-18556), Vol. 17, No. 2 (February, 1993), page 81; and "More Uses for Configuration Control of Robots" (NPO-18607/NPO-18608), Vol. 17, No.10, (October, 1993), page 120. To recapitulate: A robot has n degrees of freedom. The basic task is to make the end effector (the hand at the tip of the manipulator arm) follow a prescribed trajectory in m-dimensional coordinates (where $m < n$). The $r = n-m$ redundant degrees of freedom are used simultaneously to perform an additional task.

Additional tasks could include (but are not limited to) reaching around obstacles, avoiding collisions with objects in the workspace, maintaining one or more links of the manipulator arm in a desired pose, and/or optimizing the overall kinematics in both the redundant and nonredundant degrees of freedom to enhance overall manipulability. The additional task is mathematically modeled by a set of kinematic functions that, in effect, define the trajectory in the redundant degrees of freedom. These functions are specified by the user.

In the present method, the degrees of mobility are simply combined with the degrees of manipulation into one set that contains both the redundant and nonredundant degrees of freedom, and all degrees of freedom are treated on an equal footing according to the computationally efficient configuration-control formalism. The user can assign weighting factors to individual degrees of mobility or manipulation as well as to each task specification. The user can also change task specifications and weighting factors during operation. Thus, overall, the present method is characterized by conceptual simplicity, computational efficiency, and flexibility — all advantageous for on-line, real-time control.

This work was done by Homayoun Seraji of Caltech for NASA's Jet Propulsion Laboratory. Further information is contained in a TSP [see page 1].

This invention is owned by NASA, and a patent application has been filed. Inquiries concerning nonexclusive or exclusive license for its commercial development should be addressed to the Patent Counsel, NASA Resident Office-JPL [see page 1]. Refer to NPO-19109.

Tuneable Auxiliary Control Mechanisms for RUM Actuators

Scan amplitudes could be maximized and/or power consumption minimized under changing conditions.

Marshall Space Flight Center, Alabama

Tuneable auxiliary control mechanisms for rotating unbalanced-mass (RUM) actuators are used to maximize scan amplitudes and/or minimize power consumption during changing conditions. This type of mechanism is a more sophisticated version of the type of mechanism described in "Auxiliary Control Mechanisms for RUM Actuators" (MFS-28817), *NASA Tech Briefs*, Vol. 19, No. 8 (August, 1995), page 62.

To give meaning to an explanation of the tuneable version, it is necessary to repeat most of the description of the simpler version from the noted prior article. Figure 1 illustrates schematically a scientific instrument equipped with a pair of RUM actuators for oscillation about a single axis to produce a line scan, plus an auxiliary control mechanism that would establish and maintain a constant center-of-scan position and/or vary the center-of-scan at a rate much less than that of the scan itself. The basic components of this mechanism would be a stepping motor, a speed-reducing (torque-increasing) gear train, and an angular-position encoder. The stator of the stepping motor would be mounted on a stationary supporting structure, while the rotor would be connected to the low-torque input shaft of the gear train.

The high-torque output shaft of the gear train would lie on the axis about which the instrument was to be oscillated and would be connected to the instrument via a torsionally flexible coupling. The encoder would monitor the angular position of the high-torque shaft. Driven by a pair of RUM actuators, the instrument would oscillate torsionally, via the flexible coupling, about the angular position of the high-torque shaft. The holding torque of the stepping motor, amplified by the gear train, would suffice to prevent the slippage of the high-torque shaft out of

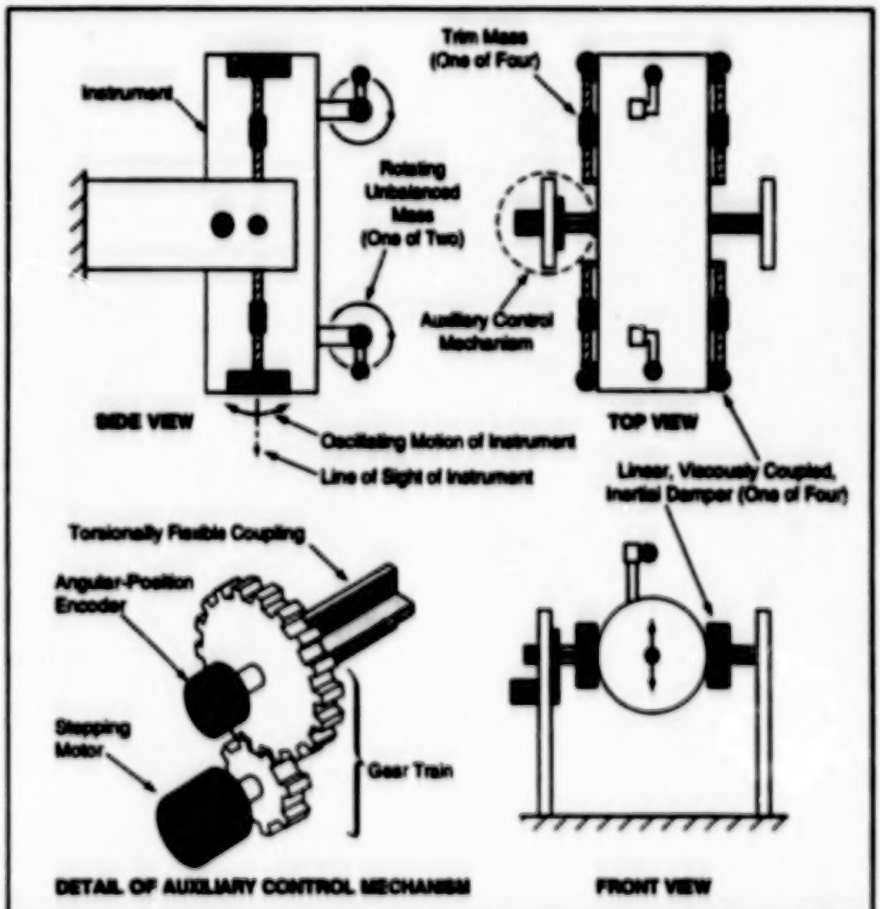

Figure 1. An Auxiliary Control Mechanism like this one would make it possible to design a relatively small, cheap, energy-efficient rotating unbalanced-mass actuator, but it could be adjusted to only a limited extent, if at all.

the commanded center-of-scan position.

In many if not most cases, it would be preferable to choose the torsional stiffness of the flexible coupling so that the resonant frequency of torsional oscillation would equal the frequency of the scan produced by the RUM actuators. Adjustable trim masses could be added to provide for some limited tuning to resonance, and dampers could be added for stability. The resonance would amplify the effect of the RUM actuators (the dampers would reduce the amplification somewhat) so that the same scanning motion could be achieved with smaller unbalanced masses. With smaller unbalanced masses, the RUM actuators would consume less power: numerical examples from representative design cases suggest that RUM actuators equipped with auxiliary control mechanisms of this type would consume as little as 1/100 the power of scanning mechanisms based on gimbal torque actuators. This completes the explanation of the simpler previous version.

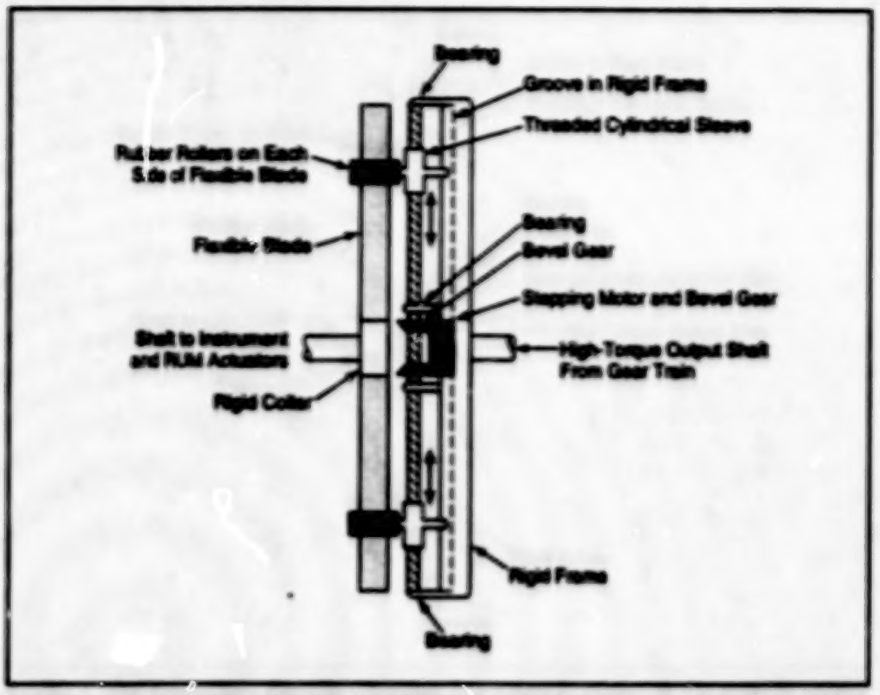

Figure 2. The Torsionally Flexible Coupling in a tuneable version of the auxiliary control mechanism of Figure 1 would be adjustable by use of a stepping-motor-driven worm-gear mechanism that would vary the bending length of a flexible blade.

In the more sophisticated tuneable version, the torsional stiffness of the torsionally flexible coupling would be made adjustable on command. As shown in Figure 2, the torsional flexibility would be provided by a nominally radially oriented flexible blade. A rigid collar would attach the blade to the shaft connected to the scanned instrument and its RUM actuators. Movable rubber rollers would establish the off-axis contact point for transmission of torsion between the instrument shaft and the high-torque output shaft. The torsional stiffness would be increased or decreased by moving the rollers in or out, respectively. The rollers would be mounted on sleeves that could slide in radial grooves in a rigid frame attached to the high-torque output shaft. Each sleeve would be internally threaded to engage a radially oriented worm gear driven via a bevel gear by a stepping motor. Thus, the radial position of the collars and, with it, the torsional stiffness of the coupling, would be varied by use of the stepping motor.

The adjustability would provide enhanced tuning at any time; the mechanism could be tuned to a resonant or nonresonant condition as needed, even in real time during a scan. Thus, the same mechanism could be adjusted as needed to accommodate various instruments with widely different moments of inertia, adjusted to change the amplitudes of scans in real time, and/or adjusted in real time to respond to changes in the inertial properties of the scanned instrument.

A combination of a pair of RUM actuators and an auxiliary control mechanism more complicated than that shown in the figure could be used to produce a two-dimensional (e.g., elliptical or raster) scan. By making its torsional stiffnesses adjustable, one could adjust the amplitudes and other parameters of the scans in real time. For example, in the case of an elliptical scan, one could change the major and/or minor axis of the ellipse, compensate for the effect of gravitation on the major and/or minor axis to obtain a circular scan, or compensate for differences between moments of inertia about the two scan axes to obtain a circular scan.

This work was done by Michael E. Pollas and Dean C. Alhorn of Marshall Space Flight Center. Further information is contained in a TSP [see page 1].

This invention is owned by NASA, and a patent application has been filed. Inquiries concerning nonexclusive or exclusive license for its commercial development should be addressed to the Patent Counsel, Marshall Space Flight Center [see page 1]. Refer to MFS-28930.

Estimating Vibrational Powers of Parts in Fluid Machinery

Vibrations of components are taken to be governed by local physics of flow.

Lewis Research Center, Cleveland, Ohio

In a new method of estimating the vibrational power associated with a component of a fluid-machinery system, the physics of flow through (or in the vicinity of) the component is regarded as governing the vibrations. The method was devised to generate scaling estimates for the design of new parts of rocket engines (e.g., pumps, combustors, nozzles) but is also applicable to terrestrial pumps, turbines, and other machinery in which turbulent flows and vibrations caused by such flows are significant.

The new method stands in contrast to several prior methods in which the vibrational powers associated with the components were estimated by scaling from global variables (e.g., engine thrust or exhaust velocity). In the new method, it is assumed that the scaling law is

$$\frac{G^2_{new}}{P_{s_{new}}} = \frac{G^2_{ref}}{P_{s_{ref}}}$$

where G^2 denotes the mean-square local vibrational power, P_s denotes the specific power (that is, the power per unit mass) of the pump or other component, the subscript "new" denotes the new component for which the estimate is sought, and the subscript "ref" denotes a similar preexisting reference component (e.g., a pump of similar, but not identical design), the vibrations of which have been measured.

The specific power of a pump or other component for use in equation is given by

$$P_s = \frac{KQ^3}{M}$$

where K is a lumped parameter that summarizes the effects of the flow geometry in or about the component, Q is the volumetric flow rate, and M is the mass of the component. The lumped parameter is given by

$$K = \frac{\int_{x=0}^{x=x_f} \left[\frac{1}{A(x)}\right]^3 \frac{1}{L(x)}\,dx}{x_f}$$

where $A(x)$ = the local cross-sectional area presented to the flow at position x, $L(x)$ = the local characteristic length in the plane of $A(x)$ (e.g., separation between a pump impeller and pump housing) perpendicular to the flow, and x_f = the length of the flow path through the component.

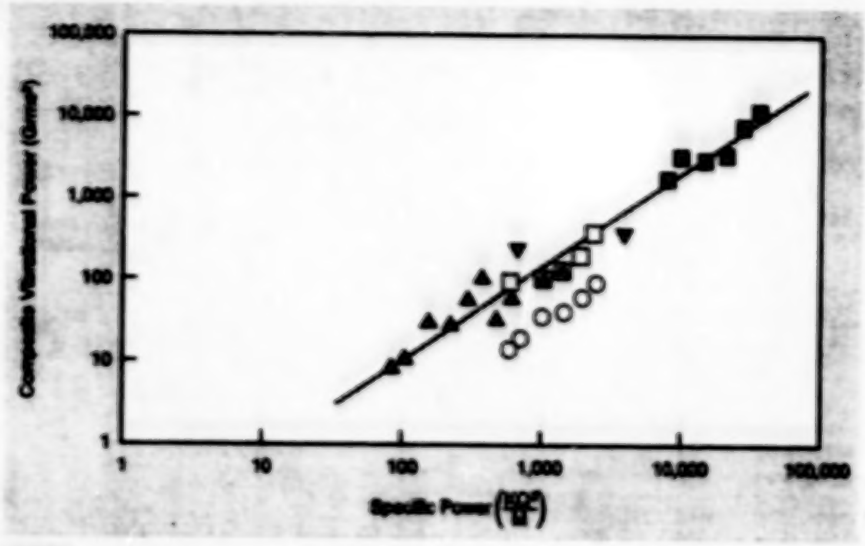

LEGEND

▼	ELV	Mark 3 Turbopump
▲	SSME	Low Pressure Oxidizer Turbopump (LTOTP)
□	SSME	High Pressure Oxidizer Turbopump (HPOTP)
■	SSME	Low Pressure Fuel Turbopump (LPFTP)
○	SSME	High Pressure Fuel Turbopump (HPFTP)

ELV – Expendable Launch Vehicle
SSME – Space Shuttle Main Engine

Data Pertaining to Five Turbopumps under various operating conditions cluster around a line that approximates the new scaling law.

Of course, this method of scaling is only approximate: strictly speaking, the use of K is valid only if the fluid has constant density (is incompressible). The validity of the method also depends on the assumption that the fluid flows quasi-steadily and that the flow gives rise to uncorrelated acoustic powers in different parts of the pump. Despite these limitations, when the method was applied to data from five different rocket-engine turbopumps, the processed data all lay near one straight line on a logarithmic plot (see figure).

This work was done by S. A. Harvey and L. C. Kwok of Rockwell International Corp. for **Lewis Research Center.** *Further information is contained in a TSP [see page 1].*
LEW-15194

Testing and Analysis of Rubbing of Turbine-Blade Tips

A combination of established techniques has been applied to a modern design problem.

Marshall Space Flight Center, Alabama

A unique combination of established techniques of experimentation and theoretical analysis has been devised to study the stresses induced in turbine blades by intermittent or periodic rubbing of the tips of the blades in turbine housings. Rubbing is an inevitable consequence of modern high-speed, high-efficiency turbine designs, which call for blade-tip clearances to be as small as possible; this is because thermal and centrifugal growth of blade-tip radii during operation sometimes reduces the already small blade-tip clearances to zero. It is necessary to quantify the stresses caused by rubbing in order to predict the fatigue lives of the blades.

In the initial application, the theoretical analysis involved time-domain numerical simulation of the responses of the blade to various rubbing excitations. For this purpose, the blade was represented by a conventional, linearly responding finite-element mathematical model. The simulated rubbing excitation was a once-per-revolution half sine pulse of tangential force at the blade-tip/housing seal interface, with a duration equal to the tip/housing contact time. Between excitatory pulses the simulated tangential force on the tip was zero.

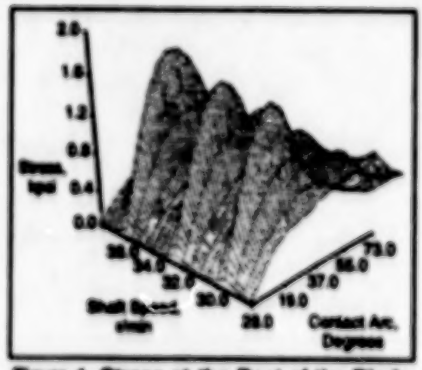

Figure 1. Stress at the Root of the Blade Shank was computed as a function of speed and contact arc in a parametric numerical-simulation study of the dynamic response.

In a parametric study, these computations were performed to map the response of the blade as a function of the length of the rubbing-contact arc and the speed of rotation of the turbine shaft. For each pair of values of these parameters, the simulation of dynamic response was continued until a steady-state dynamic motion was reached — typically in 30 to 40 revolutions. Figure 1

shows some of the results of this parametric study.

The experimental part of the effort involved the construction of a unique testing apparatus (see Figure 2). A turbine rotor was instrumented with strain gauges on its blades, and slip rings were used to pass the outputs of the gauges to external tape recorders. A simulated tip-seal segment of a housing was connected to a hydraulic actuator coupled with a control system and a displacement transducer. The motion of the tip-seal segment could thus be controlled precisely. In the tests, the turbine was driven at speeds up to 32,700 r/min, and the tip-seal segment was moved in to effect rubbing contact for short periods of time. The results of tests verified analytical predictions that the dynamic behavior consists of once-per-revolution rubs alternating with periods of free vibrations.

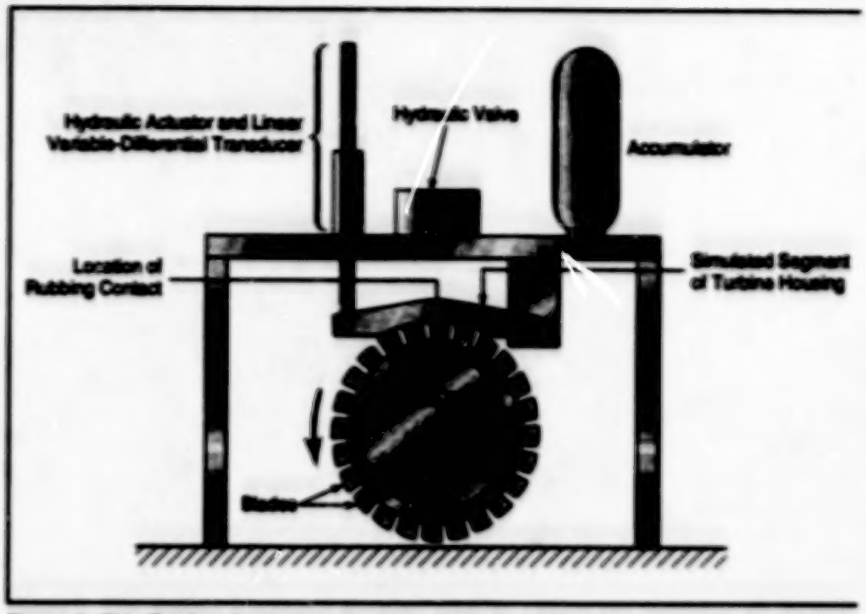

Figure 2. This Testing Apparatus simulates blade-tip rubbing and measures the dynamic responses of the blades.

This work was done by Gary A. Davis and Ray C. Clough of Rockwell International Corp. for Marshall Space Flight Center. Further information is contained in a TSP [see page 1].

Inquiries concerning rights for the commercial use of this invention should be addressed to the Patent Counsel, Marshall Space Flight Center [see page 1]. Refer to MFS-29981.

Wet/Dry Vacuum Cleaner

A hydrophobic bag with an absorbent pad retains water and dust.

Lyndon B. Johnson Space Center, Houston, Texas

The vacuum cleaner collects and retains dust, wet debris, and liquids. Designed for housekeeping on Space Station *Freedom*, it functions equally well in normal Earth gravity or in microgravity. It generates acoustic noise at comfortably low levels and includes circuitry that reduces electromagnetic interference to other electronic equipment.

The vacuum cleaner (see figure) draws materials into a bag made of a hydrophobic sheet with layers of hydrophilic superabsorbing pads at the downstream end material. The hydrophobic sheet lets air, but not liquid, leave the bag, while the hydrophilic material gels the liquid to retain it after the vacuum cleaner has been turned off. The hydrophilic material can gel many times its own weight of liquid. The bag holds dust particles larger than 40 mm and absorbs up to 48 oz (1.42 L) of liquid.

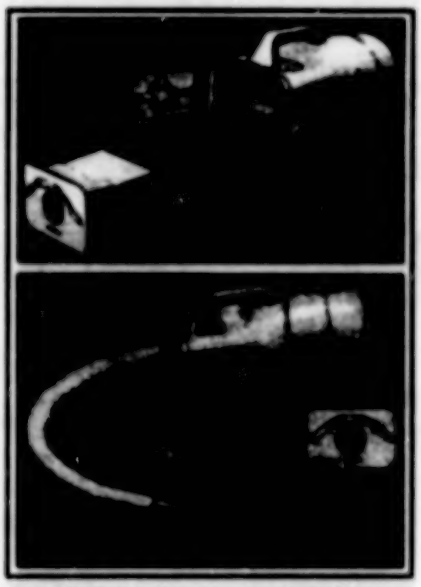

The Molded Polycarbonate Case Houses the other components of the vacuum cleaner. The hose is made of silicone rubber covered with Nomex fabric.

Suction is developed by a two-stage blower driven by a modified commercial 120-Vdc motor. The two stages help to keep noise low. The blower also provides a secondary airflow to cool its electronic components.

This work was done by Harold Reimers of Johnson Space Center and Jay Andampour, Craig Kunitser, and Ike Thomas of Lockheed Engineering & Sciences Co. No further documentation is available.
MSC-22044

BLANK PAGE

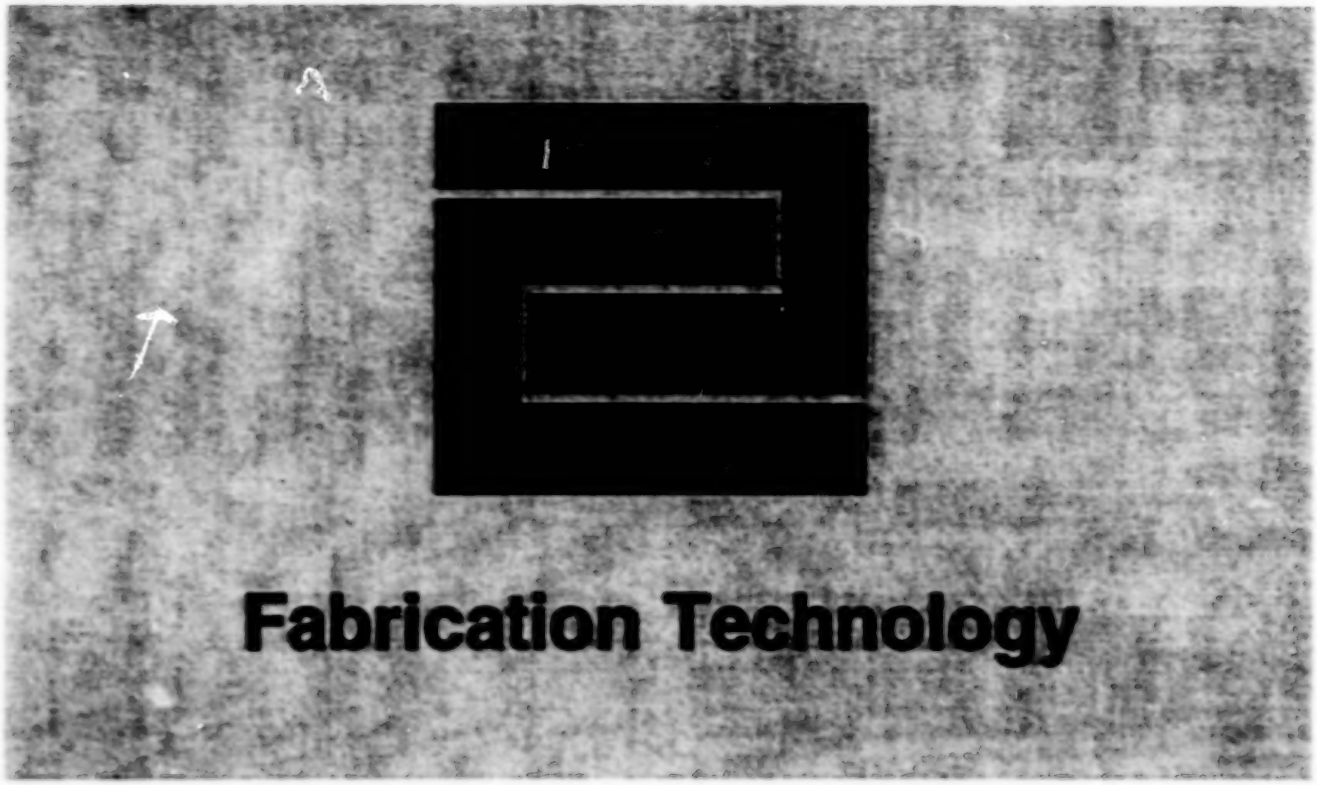

Fabrication Technology

Hardware, Techniques, and Processes

BLANK PAGE

Wax Reinforces Honeycomb During Machining

Wax-filled honeycomb can be cut to a precise contour on a lathe.

Langley Research Center, Hampton, Virginia

A method of machining on a conventional metal lathe has been devised for precise cutting of axisymmetric contours on honeycomb cores made of composite (matrix/fiber) materials. The method was devised because, heretofore, the fragility of these materials in their as-manufactured, unrestrained condition has made contouring difficult.

Composite honeycomb core materials exhibit high stiffnesses at low densities. Their composition and properties often make them the materials of choice for sandwich constructions in which composite face sheets are used. Some applications of these materials involve rigorous geometric tolerances. An example of such an application is as a core material in a precise composite reflector panel.

Machining of honeycomb materials on multiaxis milling machines is possible, but achievable surface accuracies are limited by the lower positioning accuracies generally associated with milling machines as compared with those of metal lathes. Also, corrections for tool geometries must be made as functions of cutting angles. Lathe turning generally provides accuracies higher than those obtained with milling machines, because of the smaller number of axes on which the cutting tool of a lathe must move. Also, the simple point geometry of the lathe cutting tool eliminates the need for geometric correction for the cutting angle.

The innovative method of machining on a lathe involves a preparation in which the honeycomb is placed in an appropriate fixture and the fixture is then filled with a molten water-soluble wax. A number of different waxes have been tried. Saunders Yellow™ water-soluble wax was found to work well; others may also work. (The identity of this particular wax is given for completeness only and does not constitute an endorsement, expressed or implied, by the NASA Langley Research Center.)

During filling of the fixture, the upper surface of the wax should be kept fluid and allowed to solidify last to reduce the formation of voids: this can be done by occasional application of heat to the surface with a hot-air gun. Shrinkage associated with the solidification of the wax causes additional molten wax from the top to be drawn down into the cells of the honeycomb. The wax serves both to fasten the honeycomb to the fixture and to support the individual honeycomb cells during the machining process.

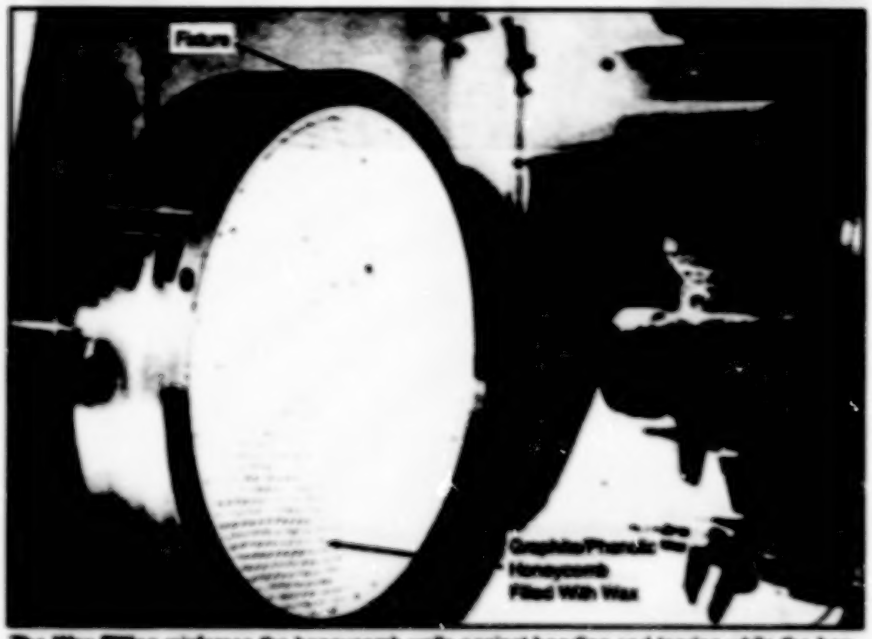

The Wax Filling reinforces the honeycomb walls against bending and tearing while the honeycomb is being contoured on a lathe.

The figure shows a wax-filled low-density graphite/phenolic honeycomb in a fixture positioned on a numerically controlled lathe for machining of a paraboloidal contour. A computer program was written to generate coordinates along the desired parabolic contour based on the focal length of the paraboloid. The fixture that contains the wax-filled honeycomb is rotated, and the parabolic contour is cut with a tungsten carbide tool.

The fixture consists of an aluminum sleeve 15 in. (38.1 cm) in diameter mounted on a backplate. The backplate includes a mount for attachment to the lathe. The sleeve is symmetric about its midplane and can be reversed and remounted to the backplate during an interruption of the machining process. In this way, convex and concave parabolic contours are machined on either side of the honeycomb. To ensure that the resulting parabolic contours remain concentric and parallel, the backplate is not removed during the machining process. The metal lathe shown in the figure has a specified machining accuracy of ±0.0005 in. (about ±0.01 mm).

After machining, the wax-filled honeycomb is sawn from the aluminum fixture, then placed in hot water to remove the wax, then rinsed for 10 min in dilute (0.5 weight percent) hydrochloric acid at room temperature. The honeycomb is then washed with deionized water and dried.

This work was done by Timothy W. Towell, David T. Fahringer, Peter Vasquez, and Alan P. Schaedegger of **Langley Research Center.** *No further documentation is available.*

LAR-14927

Sinterless Fabrication of Contact Pads on InP Devices

Carefully chosen contact materials are used.

Lewis Research Center, Cleveland, Ohio

Research has shown that with a proper choice of material, low-resistance contact pads can be deposited on solar cells and other devices by an improved technique that does not involve sintering. Until now, sintering has been used and has often proven destructive to the devices being fabricated.

To make low-resistance electrical contact to an InP semiconductor device according to the prior technique, contact metal is deposited on the semiconductor,

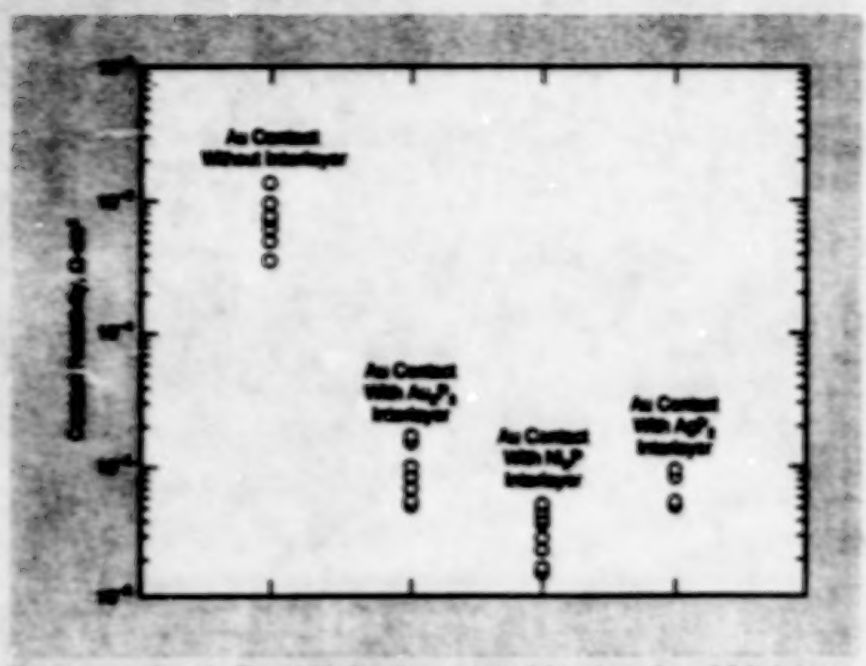

The Incorporation of a Phosphide Interlayer substantially reduces the resistivity between a gold current-carrying layer and an indium phosphide substrate.

than the contact metal must be sintered at high temperature. Although the sintering step desirably reduces the contact resistance, it also undesirably induces substantial interdiffusion between the metal and the InP substrate. Unless carefully controlled by imposition of diffusion barriers or by use of such techniques as rapid thermal processing, this interdiffusion can quickly degrade or destroy the device. Such shallow-junction devices as junction field-effect transistors and solar cells are particularly susceptible to damage during formation of contacts.

Research directed at understanding the mechanisms involved in the contact-sintering process has resulted in the identification of a special group of materials that includes the phosphides of gold, silver, and nickel; specifically, Au_2P_3, AgP_2, and NiP. The introduction of one of these materials between an underlying n-doped InP semiconductor and an overlying current-carrying metal layer results in low contact resistance. Further research has indicated that only a very thin interlayer of any of these compounds is needed to obtain low contact resistance, without having to subject the contact to the destructive sintering process.

Phosphide layers with thicknesses of the order of 20 to 30 Å on moderately doped InP are sufficient to make contact resistivities range downward to as little as 10^{-6} Ω-cm^2 (see figure). These values are only slightly greater than those obtained by use of the destructive sintering process.

This work was done by Victor G. Weizer of Lewis Research Center, Navid S. Fatemi of Sverdrup Technology, Inc., and Andras L. Korenyi-Both of Calspan Corp. Further information may be found in NASA TM-105870 [N92-24802/TB], "Sintertess Contacts to Shallow Junction InP Solar Cells."

Copies may be purchased [prepayment required] from the NASA Center for AeroSpace Information, User Services Division, Linthicum Heights, Maryland, Telephone No. (301) 621-0394. Rush orders may be placed for an extra fee by calling the same number.
LEW-15883

Improved Hermetic Feedthrough Seals for Optical Fibers

Inorganic sealing materials withstand widely ranging temperatures.

Lewis Research Center, Cleveland, Ohio

Improved hermetic feedthrough seals for optical fibers can withstand temperatures from as low as -325 °F (about -188 °C) to as high as 392 °F (about 200 °C) while maintaining a helium leak rate of below 10^{-11} cm^3/s. This feedthrough material was used in an optical connector design targeted to meet the specifications of the space shuttle main engine environment as well as the expected environment of space-based rocket engines. The seal was demonstrated to perform exceptionally through salt spray, sinusoidal and random vibrations (20 to 2000 Hz), mechanical shock (40 g's) thermal shock at the extreme temperatures, humidity, and radiation (neutron fluence, gamma, and ion) testing.

The figure depicts a simplification of a feedthrough of the improved type, for

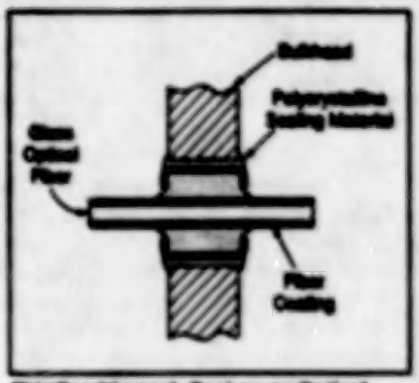

This Feedthrough Seal on an Optical Fiber can be made primarily or entirely of inorganic materials that withstand widely ranging temperatures.

illustrative purposes. Polyimide buffered glass/glass fibers are hermetically sealed to the feedthrough unit with the polycrystalline ceramic material. The sealing technology was demonstrated in two feedthrough types: a continuous fiber type as shown in the figure and a type where one end of the fiber is terminated with an SMA connector male. The latter type may be constructed with a standard MIL-C-38999 Series 3 or 4 bulkhead-mount, hermetically sealed receptacle.

Throughout the environmental testing, the optical signal passing through the units was monitored. The prototype feedthroughs passed the required tests with negligible insertion losses.

This work was done by Robert Jui-Un Fan of LiteCom, Inc., for Lewis Research Center. Further information is contained in a TSP [see page 1].
LEW-15417

Level Indicator on a Tubular Inside Micrometer

Leveling helps to ensure accurate measurements.

Marshall Space Flight Center, Alabama

A bubble-type level-indicating attachment on a tubular inside micrometer (see figure) helps a novice user obtain accurate measurements. The attachment can be helpful because in some situations that involve measurement of large, tight-tolerance inside dimensions, inside micrometers that are not held level between the contact point can give inaccurate readings.

A bubble-type level indicator is modified for use in this application by grinding it to a known length. The modified level indicator is then attached to the tubular inside micrometer by threading it into micrometer extensions that are attached to the graduated thimble of the micrometer.

The user adjusts the position and orientation of the micrometer and verifies that it is level by observing the bubble in the level indicator. Upon feeling the correct drag between the micrometer tips and the workpiece, the user can be confident that the tool is being used correctly and an accurate measurement has been obtained.

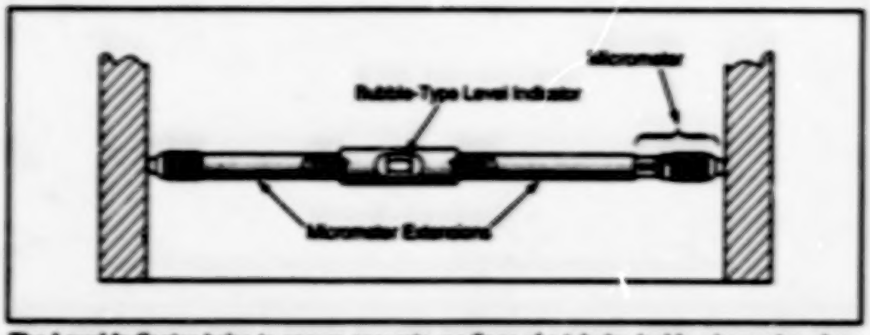

The Level Indicator helps to ensure accurate readings of a tubular inside micrometer when accuracy depends on keeping the micrometer horizontal.

This work was done by R. Michael Malinzak and Gary N. Booth of Rockwell International Corp. for Marshall Space Flight Center. No further documentation is available.

MFS-30026

Pressurized Bladder To Secure a Tile During Bonding

An apparatus for use in installing tiles with adhesive includes an inflatable bladder that holds a tile in place while the adhesive cures. Once the tile is placed in the desired position, the pressurized bladder is pressed against the tile with increasing force until the pressure in the bladder equals the desired tile bond pressure. A pressure gauge that can be monitored easily from a distance is used to ensure that the tile is being held with the proper force during curing.

This work was done by John M. Hutchinson of Lockheed Space Operations Co. for Kennedy Space Center. Further information is contained in a TSP [see page 1].

KSC-11662

BLANK PAGE

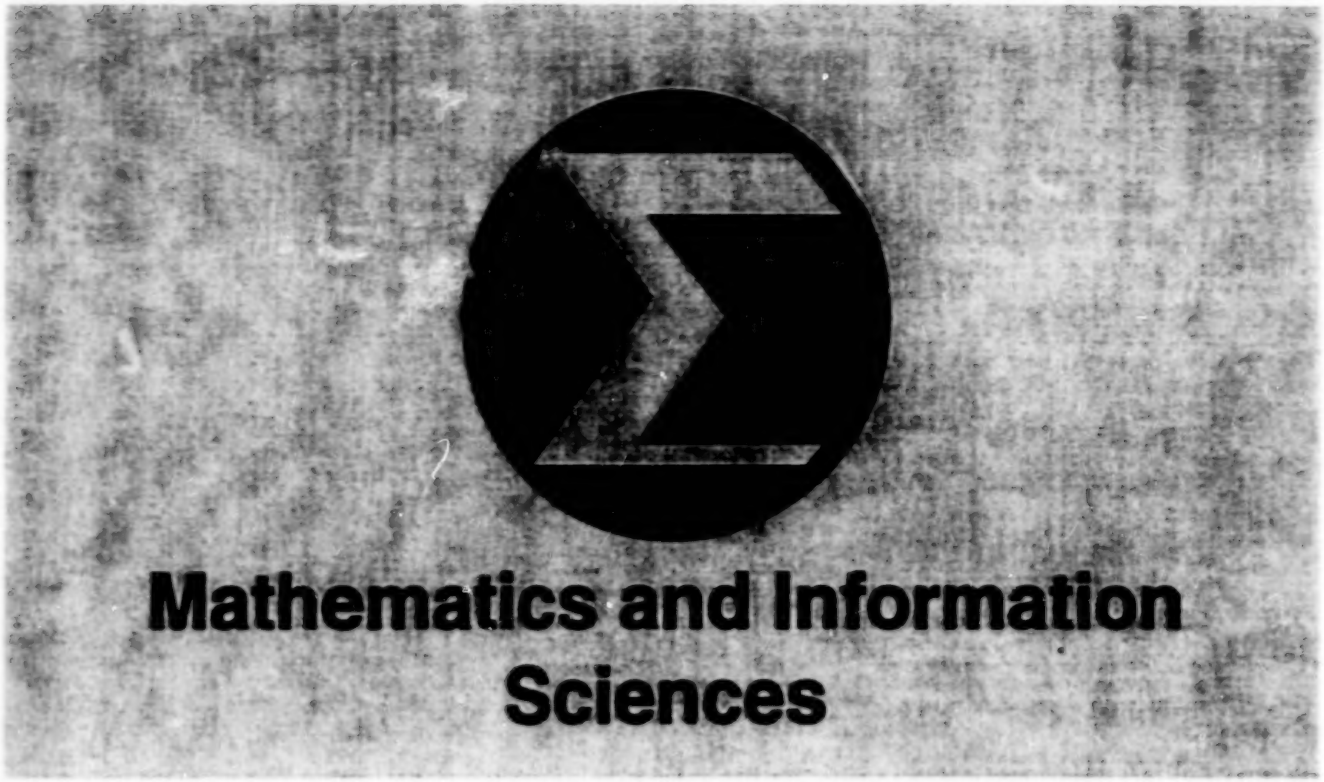

Mathematics and Information Sciences

Hardware, Techniques, and Processes

Books and Reports

Discrete Gabor Filters for Binocular Disparity Measurement

Binocular disparities would be determined from phases of discretized Gabor transforms.

Lyndon B. Johnson Space Center, Houston, Texas

Discrete Gabor filters have been proposed for use in determining the binocular disparity — the difference between the positions of the same feature or object depicted in stereoscopic images produced by two side-by-side cameras aimed in parallel. The magnitude of the binocular disparity can be used to estimate the distance from the cameras to the feature or object. In one potential application, the cameras would be charge-coupled-device video cameras in a robotic vision system, and binocular disparities and the distance estimates would be used as control inputs — for example, to control approaches to objects to be manipulated or to maintain safe distances from obstacles.

The major problem in determining the binocular disparity is to match corresponding features in the two images. Typical prior solutions have been computationally intensive and have often included explicit (and sometimes error-prone) feature-matching processes. In the proposed solution, no attempt is made to identify or match features explicitly. Instead, one matches features implicitly and obtains the binocular disparity by computing complex Gabor transforms (see Figure 1) of corresponding neighborhoods in the two images, then taking advantage of the fact that the phase shift between the Gabor transforms is proportional to the local binocular disparity in approximately the same way in which a phase shift in a Fourier transform of the entire image is proportional to a uniform lateral shift in the entire image. Characterizing this approach from another perspective, the local binocular disparity is computed directly from a locally computed parameter of the pair of images, and no formal matching process is needed.

In practice, it is necessary to compute the Gabor transforms by use of relatively coarse-grained two-dimensional filters or masks, each pixel of which approximates the value of the even or odd Gabor function at its position (see Figure 2). The size of the filter is optimized at 8 × 8 pixels on the basis of several conflicting considerations that include the need to obtain adequate resolution consistent with the pixel spacing, minimize the amount of computation, and minimize ambiguity in interpreting the output of the filter.

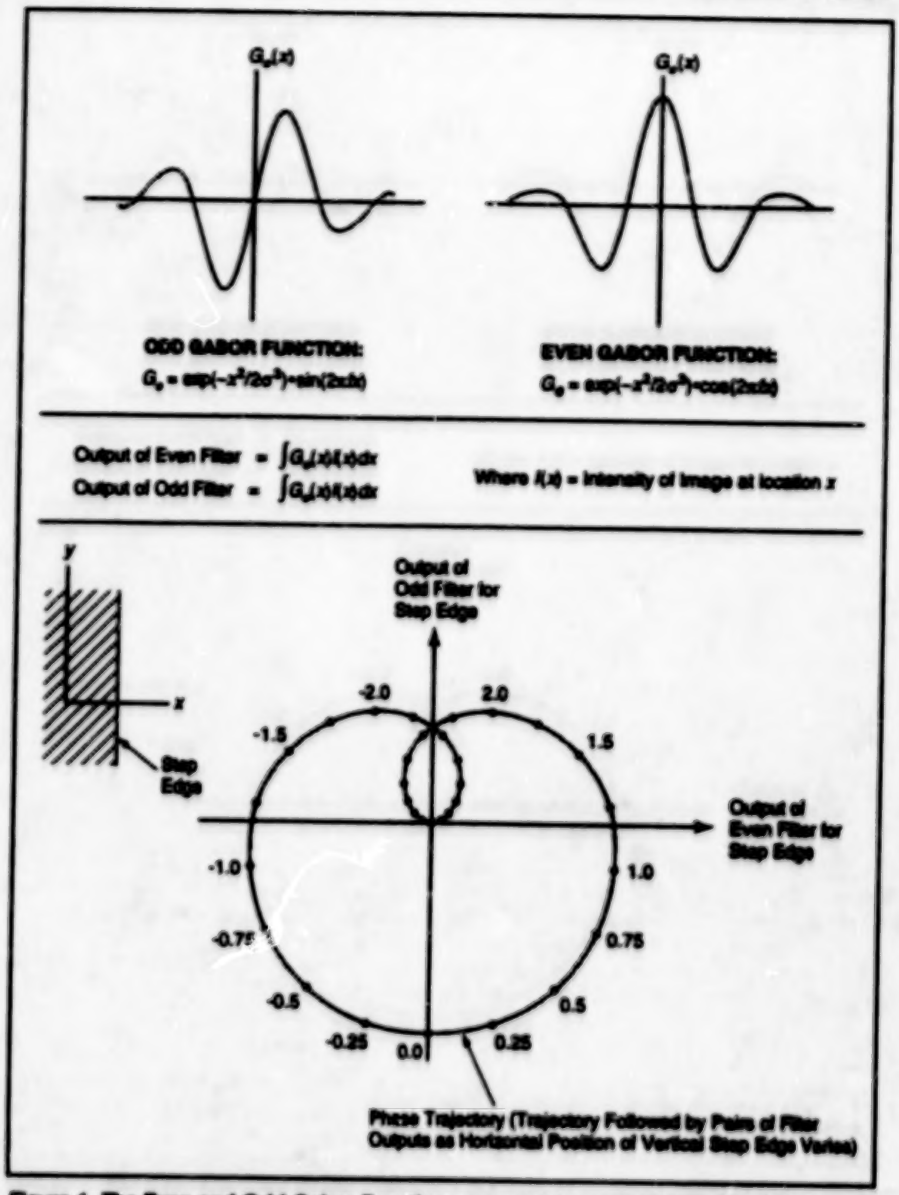

Figure 1. The Even and Odd Gabor Functions are used to compute complex Gabor transforms. The location of a feature (in this case, a step edge) can be determined from the phase of its complex Gabor transform.

The filters are applied as follows. The two images are divided into corresponding windows of 8 × 8 pixels each. The even Gabor filter is overlaid on each window. The brightness at each pixel is multiplied by the filter value at that pixel. The sum of the brightness-filter products of the window is a single number and constitutes the filter output for that window. The odd Gabor filter is then overlaid on each window, and the process is repeated. The phase of the approximate Gabor transform of each window can then be obtained easily from the relative values of the even- and odd-filter outputs, and the phases of the transforms of the corresponding windows in the two images can be compared to obtain the phase shift and, hence, the local binocular disparity.

0	2	-4	-5	5	4	2	0
2	5	-8	-10	10	8	5	-2
4	8	-12	-16	16	12	8	-4
5	10	-16	-21	21	16	10	-5
5	10	-16	-21	21	16	10	-5
4	8	-12	-16	16	12	8	-4
2	5	-8	-10	10	8	5	-2
0	2	-4	-5	5	4	2	0

Odd

0	-2	-4	5	5	-4	-2	0
2	-5	-8	10	10	-8	-5	2
4	-8	-12	16	16	-12	-8	4
5	-10	-16	21	21	-16	-10	5
5	-10	-16	21	21	-16	-10	5
4	-8	-12	16	16	-12	-8	4
2	-5	-8	10	10	-8	-5	2
0	-2	-4	5	5	-4	-2	0

Even

8X8 DISCRETE GABOR FILTERS SENSITIVE TO VERTICAL EDGES

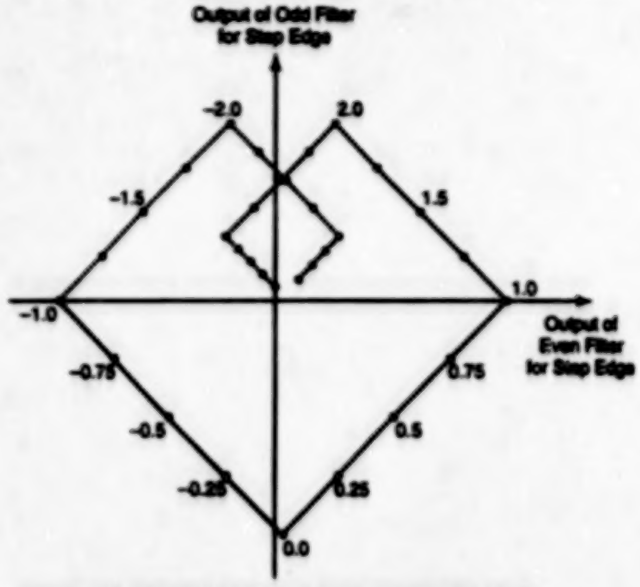

PHASE TRAJECTORY FOR STEP EDGE COMPUTED WITH 8X8 DISCRETE GABOR FILTER

Figure 2. The Gabor Functions Are Approximated by 8 x 8-pixel filters. The phase trajectory shown here is of the complex Gabor transform of a step edge, except that here it is computed approximately by use of the discrete filter instead of exactly as in Figure 1. The numbers and dots on the trajectory denote horizontal (x) position of the step edge in pixel units. Note that subpixel resolution is achieved readily.

This approach involves less computation than do prior approaches based on convolution. In this approach, each 8 × 8 filter is applied only once to each 4 × 4 pixel neighborhood; in a convolution-based approach with a filter of equal size, it would be necessary to apply that filter to each 4 × 4 pixel neighborhood 16 times. This makes possible a considerable reduction in computation time and/or a reduction in the complexity of image-processing circuitry — important considerations in robotic systems.

This work was done by Carl F. R. Weiman of Transitions Research Corp. for Johnson Space Center. Further information is contained in a TSP [see page 1].
MSC-22094

Books and Reports

More About Spurious Numerical Solutions of DEs

Reliability of the time-dependent approach to steady-state solutions is discussed.

A paper discusses the reliability of the time-dependent approach to numerical solution of nonlinear differential equations (DEs) that describe steady-state behaviors of physical systems. The time-dependent approach was followed in the related study described in the following article, "Spurious Numerical Solutions of Differential Equations" (ARC-13209). In the time-dependent approach, an approximate numerical solution for the steady state is obtained by numerically solving a time- or pseudotime-dependent version of the discretized counterpart(s) of the applicable ordinary or partial differential equation(s) and approaching the steady state asymptotically. The asymptotic results can sometimes converge or fail to converge to the true solutions, or converge to erroneous solutions that satisfy the discretized counterparts but not the underlying differential equations.

The paper notes that nonlinear dynamics and local and global bifurcation theory can be used to analyze and explain much of the asymptotic behavior of the discretized counterparts. These concepts were applied in a theoretical and computational study to reveal some of the spurious behavior of asymptotic numerical solutions of the viscous Burgers' equation

$$\frac{\partial u}{\partial t}+\frac{1}{2}\frac{\partial\left(u^2\right)}{\partial x}=\varepsilon\frac{\partial^2 u}{\partial x^2}, \qquad \varepsilon>0$$

where $u(x,t)$ is the desired solution, x is a spatial coordinate, t is time, and ε is a constant. The spatial solutions were obtained by use of a three-point central-difference scheme; the temporal solutions were obtained by two types of Runge–Kutta methods.

One of the conclusions drawn from the results of this study and the study described in the preceding article is that the use of a time step smaller than the linearized stability limit does not necessarily result in a true approximation to the exact solution, even though the initial data might be physically relevant. In addition, the conventional belief that one obtains a divergent solution when using a time step greater than the linearized stability limit is not always correct, inasmuch as spurious asymptotes can occur. Consequently, when linearized stability limits are used to guide the con-

straint of time steps in solving highly coupled nonlinear differential equations, time steps might exceed the actual linearized stability limits of the nonlinear difference equations. In particular, when one tries to stretch the maximum limit of the linearized allowable time step for a system of highly coupled nonlinear partial differential equations, spurious asymptotes of all of the various types could occur in practice, depending on the initial conditions, the form of the equations, and the numerical solution scheme. This is compounded in a practical situation in which the exact linearized stability limit is not computed but rather a frozen-coefficient procedure at each time step with a fixed grid spacing is used to estimate the true stability of the solution algorithm.

The paper presents a comparison of the guidelines, assumptions, usage, and applicability of nonlinear, and of three methods of linear, stability analysis. It concludes, from the comparison, that nonlinear analysis uncovers many of the nonlinear phenomena that cannot be predicted by linearized analysis.

This work was done by H. C. Yee of **Ames Research Center** *and P. K. Sweby of the University of Reading. To obtain a copy of the report, "On Reliability of the Time-Dependent Approach to Obtaining Steady-State Numerical Solutions," see TSP's [page 1].*

This invention is owned by NASA, and a patent application has been filed. Inquiries concerning nonexclusive or exclusive license for its commercial development should be addressed to the Patent Counsel, Ames Research Center [see page 1]. Refer to ARC-13208.

Spurious Numerical Solutions of Differential Equations

A paper presents a detailed study of spurious steady-state numerical solutions of differential equations that contain nonlinear source terms. Such model equations, along with applicable boundary conditions, are used to represent a baseline study for phenomena such as chemically reacting flows (e.g., in combustion). The equations are often solved numerically by time-marching methods, and the numerical solutions can sometimes diverge, oscillate, or converge to erroneous solutions, depending on the spatial and temporal discretizations, initial conditions, and the numerical boundary conditions used in the numerical (e.g., finite-difference) schemes: the recognition of this fact has given rise to an interdisciplinary field of study that has been called "the dynamics of numerics and the numerics of dynamics."

The main objectives of this study are (1) to investigate how well numerical steady-state solutions of a model nonlinear reaction/convection boundary-value problem mimic the true steady-state solutions and (2) to relate the findings of this investigation to implications for the interpretation of numerical results from computational-fluid-dynamics algorithms and computer codes that have been used to simulate reacting flows. The one-dimensional model nonlinear reaction/convection problem posed in this study is

$$u_t + au_x = \alpha S(u) \quad 0 \le x \le 1$$

$$u(x,0) = u^0(x)$$

where t is time, x is position, the subscripts denote partial differentiation with respect to the indicated variables, a and α are positive parameters, and the source term $S(u) = -u(1 - u)(2 - u)$. The boundary condition is either nonperiodic in the form of

$$u(0,t) = u_0 \qquad t \ge 0$$

or else periodic in the form of

$$u(0,t) = u(1,t) \qquad t \ge 0$$

This problem is chosen partly because its exact steady-state solutions are known.

In a typical practical computational fluid dynamics computation, an approximate steady-state solution for the steady state is obtained by solving the time-dependent version of the problem and approaching the steady state asymptotically. This approach is followed to solve the model problem, and the possible sources of errors, slow convergence, and nonconvergence of the solutions are assessed. The results of this assessment can be summarized as follows:

- Stable and unstable spurious steady-state numerical solutions (numerically irrelevant solutions) can be introduced independently by spatial and temporal discretizations that satisfy the same boundary condition and initial data.
- The various numerical treatments of the reaction term can drastically affect the stability of the spurious as well as the exact steady-state solutions.
- The time discretization can destabilize the stable spurious steady-state numerical solutions that are introduced by the spatial discretizations or vice versa.
- For a given finite-difference method, the strength of the coefficient of the convection term and the stiffness of the nonlinear source term can strongly affect the permissibility of spurious steady-state numerical solutions.
- The possible cause of convergence to a spurious steady state is analyzed, and a suggestion on how to avoid spurious steady-state solutions is made on the basis of this analysis.
- The numerical phenomenon of incorrect speeds of propagation of discontinuities may be linked to the existence of some stable spurious steady-state numerical solutions.

This work was done by A. Lafon and H. C. Yee of **Ames Research Center.** *To obtain a copy of the report "Dynamical Approach Study of Spurious Steady-State Numerical Solutions of Nonlinear Differential Equations — III. The Effects of Nonlinear Source Terms and Boundary Conditions in Reaction-Convection Equations," see TSP's [page 1].*

Inquiries concerning rights for the commercial use of this invention should be addressed to the Patent Counsel, Ames Research Center [see page 1]. Refer to ARC-13209.

Automated Management of Documents

A report presents the main technical issues involved in computer-integrated documentation. The problems associated with the automation of management and maintenance of documents are analyzed from perspectives of artificial intelligence and human factors. Technologies that may prove useful in computer-integrated documentation are reviewed: these include conventional approaches to indexing and retrieval of information, the use of hypertext, and knowledge-based artificial-intelligence systems. A particular effort was made to provide an appropriate representation for contextual knowledge, including generation of contexts on hypertext links. Thus, it was found that indexing of documents in computer-integrated documentation is sensitive to contexts. Theoretical considerations of navigation in hyperspace, acquisition of indexing knowledge, and maintenance of large bodies of documentation are discussed.

This work was done by Guy Boy of Sterling Software for **Ames Research Center.** *To obtain a copy of the report, "Computer Integrated Documentation," see TSP's [page 1].*
ARC-13241

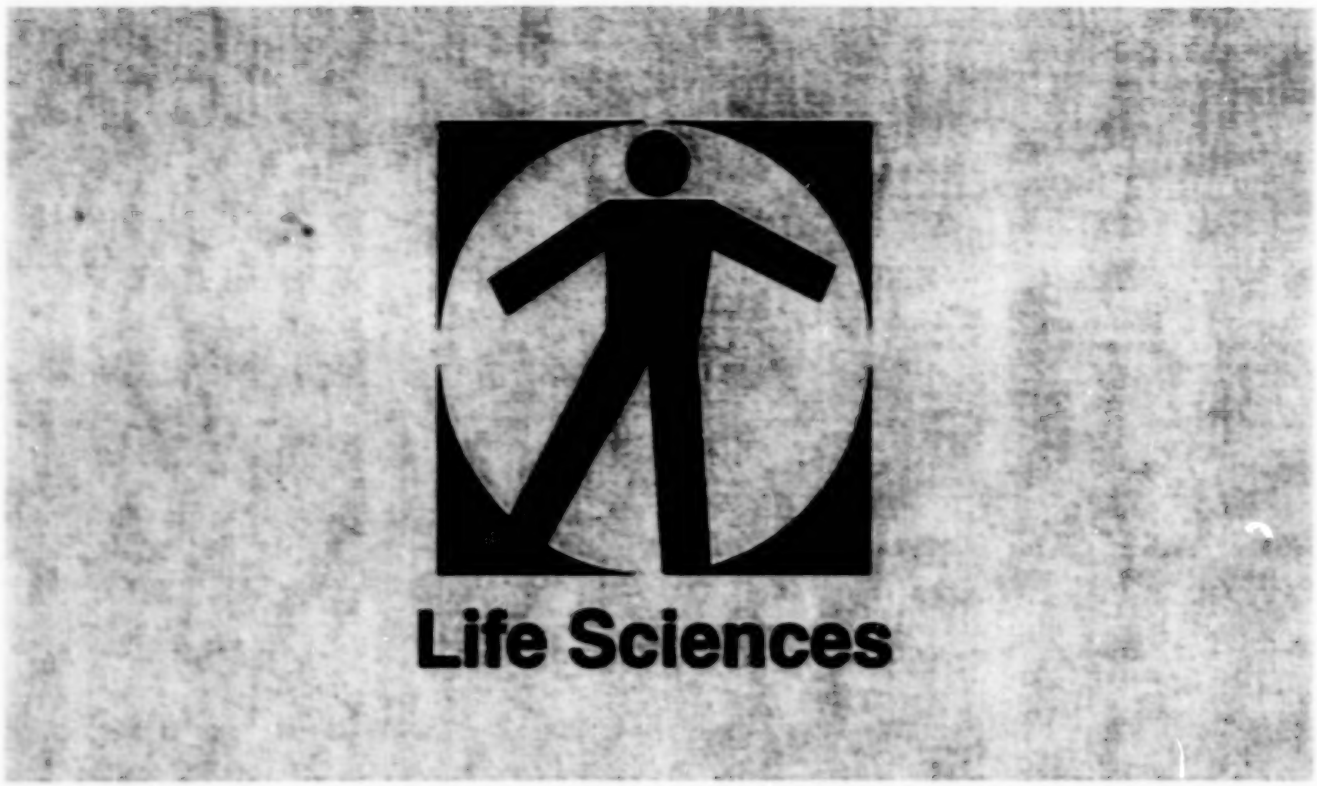

Life Sciences

Hardware, Techniques, and Processes

BLANK PAGE

Chamber Design for Slow Nucleation Protein Crystal Growth

New design provides gradation of nucleation and growth rates.

Marshall Space Flight Center, Alabama

A multiple-chamber dialysis apparatus (see figure) grows protein crystals on Earth or in microgravity with a minimum of intervention by a technician. The apparatus includes a reservoir and a series of sample chambers attached to one end of the reservoir. A dialysis membrane that passes low-molecular-weight solutes, but not high-molecular-weight solutes, is placed between the reservoir and the first chamber. Another such membrane is placed between each chamber and the succeeding or preceding chamber. Access to each chamber can be gained through a screw-in plug in its side. Sliding gate valves between the precipitant and growth chambers could be used to start the growth process. The use of multiple chambers provides a gradation of nucleation and growth rates.

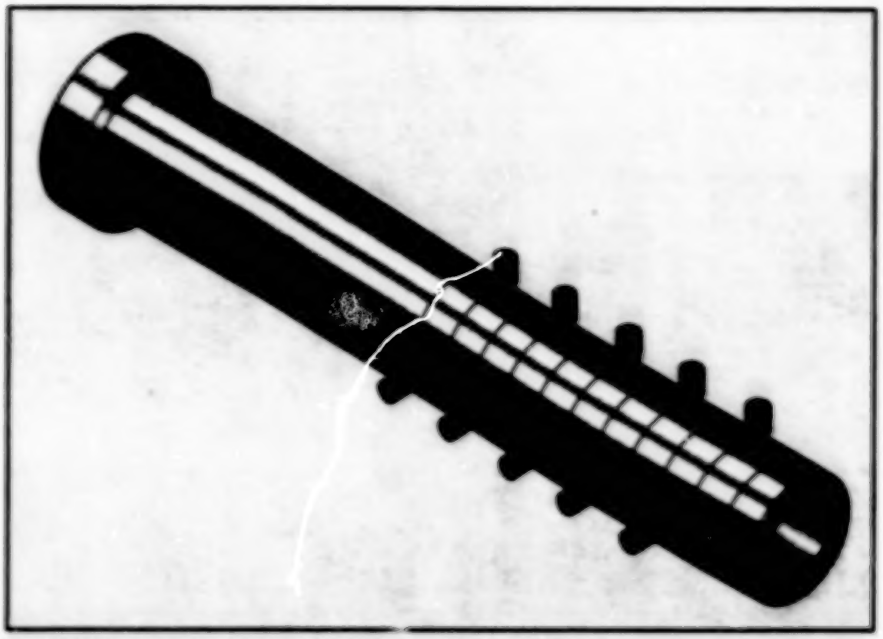

The Multiple-Chamber Dialysis Apparatus provides a gradation of nucleation and growth rates.

This work was done by Marc Lee Pusey for **Marshall Space Flight Center**. *To obtain a copy of the report, "Multiple Chamber Dialysis System for Protein Crystal Growth," see TSP's [page 1].*

Inquiries concerning rights for the commercial use of this invention should be addressed to the Patent Counsel, Marshall Space Flight Center [see page 1]. Refer to MFS-28967.

Predatory Microorganisms Would Help Reclaim Water

Pathogenic microorganisms would be removed from water without use of harsh chemicals, intense heat, or ionizing radiation.

Marshall Space Flight Center, Alabama

Wastewater-reclamation systems of a proposed type would use predatory, nonpathogenic microorganisms to consume pathogenic microorganisms. The predators in question are *Dictyostelium* amoebae, which consume bacteria (and presumably, could also be induced to eat microalgae, viruses, and protozoa). The *Dictyostelium* amoebae convert their prey into their own cell substance, which is largely cellulose. *Dictyostelium* is not harmful to humans, other macroscopic animals, or macroscopic plants. The cellulosic product could be subjected to further biodegradation or other treatment. Unlike some other wastewater-reclamation systems, these systems would not require the use of toxic chemicals, intense heat, or ionizing radiation (γ rays or ultraviolet) to destroy microorganisms.

Two apparatuses have been constructed to test the concept. One of them includes a growth chamber that contains an 18-in. (45.7-cm)-diameter rotating plate, on which petri dishes are placed. Each dish contains *Dictyostelium* growing on agar and a porous stainless-steel disk inoculated with bacteria and amoebae. The dishes are illuminated by two lamps, which provide constant simulated sunlight to induce growth of cellulosic *Dictyostelium* stalks. The plate is slowly rotated so that all samples are exposed equally to the light. The air in the growth chamber is kept at high humidity by circulating it between the growth chamber and an auxiliary chamber in which water is sprayed. No special equipment is needed to keep the temperature in the growth chamber within an acceptable range.

The other apparatus includes two connected 5-gal (19-L) plastic tanks, one of which serves as a reactor vessel, while the other serves as a holding tank. The reactor vessel contains a mixing paddle composed of four vertical panels. Tubes are mounted in the reactor vessel to take samples at four levels. An industrial wastewater-reclamation system is more likely to be based on this apparatus than on the first-mentioned apparatus.

This work was done by Morris A. Benjaminson of North Star Research, Inc., and Stanley Lehrer of Electro-Optics Devices Corp. for **Marshall Space Flight Center**. *Further information is contained in a TSP [see page 1].*

Inquiries concerning rights for the commercial use of this invention should be addressed to the Patent Counsel, Marshall Space Flight Center [see page 1]. Refer to MFS-26321.

Automated Diagnosis of Conditions in a Plant-Growth Chamber

Expert-system software advises nonexpert technicians about how to respond to malfunctions.

John F. Kennedy Space Center, Florida

The Biomass Production Chamber Operations Assistant software and hardware constitute an expert system that diagnoses mechanical failures in a controlled-environment hydroponic plant-growth chamber and recommends corrective actions to be taken by technicians. The plant-growth chamber and the expert system are subjects of continuing research directed toward the development of highly automated closed life-support systems aboard spacecraft to process animal (including human) and plant wastes into food and oxygen. The development of larger terrestrial biomass-production and -recycling systems might also benefit from this research.

The chamber and associated equipment (see figure) provide 200 ft^2 (18.6 m^2) of plant-growth area with controlled light levels, temperature, humidity, airflow, air composition, nutrient solution, temperature, pH, electrical conductivity, and chemical composition. Wheat, soybeans, lettuce, potatoes, and strawberries have been grown in the chamber. For purposes of this research, the knowledge base of the expert system concentrates on wheat crops. The knowledge base incorporates expertise from multiple expertise domains, including biology, electrical engineering, mechanical engineering, and chemistry. The knowledge base was developed by a group of experts in these fields and in information systems, using the techniques of knowledge engineering.

The system uses a Microsoft Windows interface to give technicians intuitive, efficient access to critical data. By selecting an icon on the Windows display, a technician can analyze a set of data, view operating equipment through closed-circuit television, cause the expert system to begin a diagnostic procedure, examine technicians' work schedules, or command the system to perform a computational simulation.

In the diagnostic mode, the system prompts a technician for information. For example, if a malfunction occurs in the nutrient-delivery system, the expert system asks for the time, location, and type of malfunction; the status of backup nutrient-delivery pumps; the type and the stage of growth of the crop; the visible amount of water in the plant trays; the ability to reduce the temperature; and the ability to turn lights on or off. When the expert system has enough information, it generates a recovery plan.

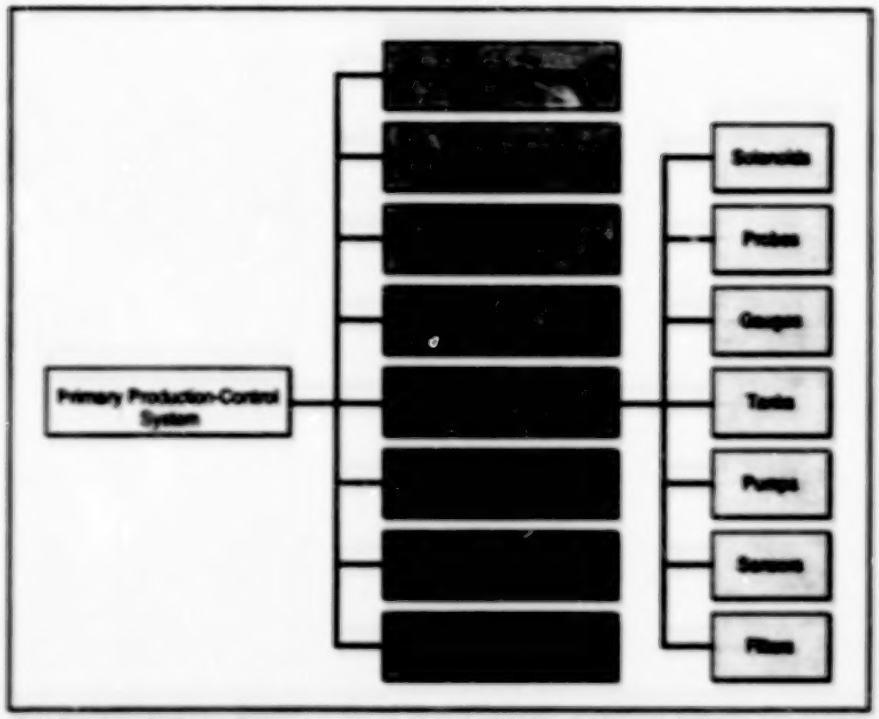

The Nutrient-Delivery System is one of several complex equipment systems that provide conditions favorable to the growth of plants. The expert system recommends responses to malfunctions in the nutrient-delivery system. Plans for the future call for extension of the expert system to respond to malfunctions in all the equipment systems.

The recovery plan not only gives instructions for how to correct the malfunction, but also indicates steps to minimize damage to the crop in the interim; this is an important feature because a malfunction can usually be diagnosed in a few minutes, but a few hours may be needed for repairs. For a nutrient-delivery failure, the expert system might advise such emergency measures as turning off lights, reducing the temperature of the air, and closing drains on plant trays to reduce the metabolic rate of the plants and conserve the remaining nutrient solution. For each measure, and for combined measures, the expert system estimates the time available before serious damage occurs. For a prolonged failure, the system may even advise that the crop be replanted.

This work was done by Barry R. Clinger and Alfred L. Damiano of McDonnell Douglas Corp. for **Kennedy Space Center.** *Further information is contained in a TSP [see page 1].*

Inquiries concerning rights for the commercial use of this invention should be addressed to the Patent Counsel, Kennedy Space Center [see page 1]. Refer to KSC-11761.

National Aeronautics and
Space Administration

END

12-22-99